UNIVERSITY OF GDAŃSK, Faculty of Chemistry

Sattibabu Merugu

Advancing transcriptomics-based and AOP-anchored predictive models for carbon nanotube inhalation: The case studies on acute phase signaling–driven inflammation

PhD Dissertation

Promotor:

Prof. dr hab. Tomasz Puzyn

Co-promotor:

Dr. Karolina Jagiełło

Doctoral thesis carried out at the Department of Environmental Chemistry and Radiochemistry in the Laboratory of Environmental Chemoinformatics

Gdańsk 2025

TABLE OF CONTENTS

ACKNOWLEDGEMENTS

This work was carried out at the **Laboratory of Environmental Chemoinformatics in the Faculty of Chemistry at the University of Gdańsk** between 2021 and 2025. I'm very grateful for the funding provided by the National Science Centre as part of the TransNANO project (UMO-2020/37/B/ST5/01894).

My PhD journey started in the Prof. Puzyn Lab, a place filled with inspiring people from all walks of life. I feel lucky to have been part of such a unique and supportive environment. This was only possible because of **Prof. dr hab. Tomasz Puzyn**, my supervisor, mentor, and constant source of encouragement. Thank you, Professor, for believing in me, guiding me, and supporting me through every stage. Your impact on my life goes far beyond science.

To **Dr. Karolina Jagiełło**, my co-promotor, thank you from the bottom of my heart. Your kindness, patience, and thoughtful advice helped me stay on track and shaped this dissertation in so many ways. I couldn't have done this without you.

To my collaborators, **Prof. Ulla Vogel** and **Dr. Sabina Halappanavar, thank you for** providing the experimental data that supported this dissertation and for your's guidance throughout the journey.

I also want to sincerely thank **Dr hab. Agnieszka Gajewicz-Skrętna** for your motivation and for introducing me to chemometrics through hands-on learning. You played a key role in my development, and I'm so grateful for that.

A special thanks to the senior researchers I had the privilege of learning from, **Prof. Leonid Gorb**, **Dr hab. Krzesimir Ciura**, **Dr. Alicja Mikołajczyk**, and **Dr. Anita Sosnowska**, your support, insights, and feedback meant a lot during my work.

To my dear friend **Michał Kałapus**, thank you for always being there, whether it was to share academic resources or just a good laugh in the lab. Your energy and positive attitude were a real gift during this journey. I'll always remember and appreciate your friendship.

To all my colleagues, **Viacheslav, Kabiruddin, Kamila, Natalia, Beata, Szymon Zdybel, Szymon, Kamil, Patrick, Martyna**, and **Pierre Bonnifessi**, thank you for making the lab such a great place to work. Each of you contributed something special to my time here.

A heartfelt thank you to **Katarzyna Dembowska**, who supported me like family. You looked after me, encouraged me, and stood by me in ways that go beyond words. Without you, these four years in Poland would have been much harder. You have a permanent place in my heart.

Most importantly, I want to thank my family. To my four brothers (**Nageswara Rao, Bandiyya, Kasubabu and Somu Naidu**), thank you for everything you've done to help me reach this point. Especially to my fourth brother, **Somu Naidu**, who gave up his own dreams so that I could chase mine. To my **mother**, whose strength and love have always lifted me up. And to my **father**, who left this world just before he could see this moment, I miss you, and I hope I've made you proud. More recently, I also lost my second brother (Bandiyya). I miss you deeply, brother, and carry your memory with me on this journey.

In closing, I believe that dreams, perseverance, and self-belief can take us farther than we imagine. Thank you to everyone who helped turn mine into reality.

ABBREVIATIONS

3R	Replacement, Reduction, and Refinement
AD	Domain of Applicability
AI	Artificial Intelligence
AO	Adverse Outcome
AOP	Adverse Outcome Pathway
BMD	Benchmark Dose
BMDL	Lower Bound of the Benchmark Dose
CARG	Compound Annual Growth Rate
Chemicals	Chemicals
CNTs	Carbon Nanotubes
CSS	Chemicals Strategy for Sustainability
CVD	Chemical Vapor Deposition
DEG	Differentially Expressed Gene
DT	Decision Tree
ECHA	European Chemicals Agency
ENMs	Engineered Nanomaterials
EPA	U.S. Environmental Protection Agency
FAIR	Findability, Accessibility, Interoperability and Reusability
FC	Fold Change
FDR	False Discovery Rate

GA	Genetic Algorithms
HCA	Hierarchical Cluster Analysis
IATA	Integrated Approaches for Testing and Assessment
JRC	European Commission Joint Research Centre
KE	Key Event
KwLPR	Kernel-weighted Local Polynomial Regression
LMO	Leave-Many-Out
LOAEL	Lowest Observed Adverse Effect Level
logFC	Fold Change Expressed
LOO	Leave-one-out
LVs	Latent Vectors
MIE	Molecular Initiating Event
ML	Machine Learning
MOA	Mechanism of Action
MWCNT	Multi-Walled Carbon Nanotube
NAM	New Approach Methodology
NGRA	Next-Generation Risk Assessment
NOAEL	No Observed Adverse Effect Level
OECD	Organization for Economic Co-operation and Development
PCA	Principal Component Analysis
PLS	Partial Least Squares

POD	Point of Departure
Q^2_{CV}	Cross-Validation Determination Coefficient
Q^2_{EXT}	External-Validation Coefficient
qAOP	Quantitative Adverse Outcome Pathway
QSAR	Quantitative Structure-Activity Relationships
R^2	Determination Coefficient
REACH	Registration, Evaluation, Authorisation and Restriction
RF	Random Forest
RMSCEXT	Root Mean Squared Error of Validation
RMSEC	Root Mean Squared Error of Calibration
ROS	Reactive Oxygen Species
SSbD	Safe and Sustainable by Design
SWCNTs	Single-Walled Carbon Nanotubes
TEM	Transmission Electron Microscope
WoE	Weight-of-Evidence

STRESZCZENIE

W niniejszej rozprawie zaprezentowano zintegrowane podejście, łączące dane omiczne oraz metody uczenia maszynowego (ML), w celu mechanistycznego zrozumienia toksyczności płucnej wywołanej przez nanorurki węglowe (CNT). Wobec rosnącej produkcji oraz szerokiego zakresu zastosowań jednościennych i wielościennych nanorurek węglowych (SWCNT i MWCNT), ocena ich bezpieczeństwa – szczególnie po ekspozycji drogą wziewną – stanowi istotny priorytet naukowy i regulacyjny. W celu wypełnienia tej luki badawczej połączono chemoinformatykę, transkryptomikę oraz modelowanie oparte na koncepcji ścieżek niekorzystnych skutków (Adverse Outcome Pathways, AOP), aby opracować modele ilościowych zależności struktura-aktywność specyficzne dla nanomateriałów (Nano-QSAR).

Główne pytanie badawcze dotyczyło możliwości integracji transkryptomiki i metod uczenia maszynowego w tworzeniu predykcyjnych modeli toksyczności płucnej wywołanej przez CNT, związanej z ostrą odpowiedzią zapalną po ekspozycji wziewnej. Postawiona hipoteza zakładała, że nanorurki o podobnych właściwościach fizykochemicznych i profilach transkryptomicznych wykazują zbliżone działania niepożądane w obrębie tkanki płucnej.

W celu weryfikacji tej hipotezy zrealizowano trzy zasadnicze cele badawcze. Po pierwsze, opracowano model Nano-QSAR oparty na koncepcji AOP, pozwalający na ilościowe powiązanie właściwości fizykochemicznych MWCNT z zaburzeniami transkrypcji w szlaku odpowiedzi ostrej fazy (ang. acute phase signalling, AR). Po drugie, przeprowadzono analizę porównawczą SWCNT i MWCNT w celu identyfikacji wspólnych i odmiennych cech strukturalnych wpływających na aktywację tego szlaku. Po trzecie, skonstruowano globalny model Nano-QSAR umożliwiający ocenę wpływu pozostałości metalicznych (takich jak Fe_2O_3 i CoO) na wczesne zmiany transkryptomiczne powiązane ze stanem zapalnym i włóknieniem płuc.Modele skutecznie identyfikowały kluczowe czynniki molekularne oraz wczesne zdarzenia kluczowe (ang. Key Events, KEs), wykazując wysoką wartość predykcyjną zgodną z zasadami walidacji modeli QSAR

według wytycznych OECD. Do najistotniejszych determinantów odpowiedzi zapalnej i włóknienia należały: stosunek długości do średnicy MWCNTs, powierzchnia właściwa i sposób funkcjonalizacji nanorurek, a także obecność określonych domieszek metali.

Zasadniczą innowacją przedstawionego podejścia jest integracja danych transkryptomicznych z modelowaniem Nano-QSAR. W przeciwieństwie do tradycyjnych modeli opartych na końcowych punktach apikalnych (np. histopatologia, toksyczność narządowa), proponowane rozwiązanie wykorzystuje genomowe profile ekspresji genów jako wskaźniki wczesnych odpowiedzi molekularnych i komórkowych w obrębie szlaku odpowiedzi ostrej fazy. Takie podejście zwiększa biologiczną interpretowalność modeli oraz poprawia ich trafność predykcyjną, umożliwiając precyzyjną identyfikację szlaków molekularnych zaburzanych przez konkretne właściwości strukturalne CNT. Ponadto, rozwiązanie to wpisuje się w aktualne trendy regulacyjne, promujące mechanistyczne podejście do oceny zagrożeń, oraz wspiera projektowanie bezpieczniejszych nanomateriałów zgodnie ze strategia "safer-by-design".

Podsumowując, niniejsza rozprawa ustanawia kompleksowe i innowacyjne ramy predykcyjnego modelowania toksyczności CNT, oparte na zintegrowanym podejściu molekularnym. Ukazuje wartość synergii pomiędzy chemoinformatyką, uczeniem maszynowym i biologią systemową w kontekście nowoczesnej toksykologii regulacyjnej oraz wspiera etyczny, wydajny i zrównoważony rozwój nanotechnologii.

SUMMARY

This dissertation presents an integrative omics and machine learning (ML) approach to the mechanistic understanding of carbon nanotube (CNT)-induced pulmonary toxicity. Considering the increasing production and diverse applications of single-walled and multi-walled CNTs (S- and MWCNTs), evaluating their safety, especially following inhalation exposure, has become a regulatory and scientific priority. To address this gap, the research bridges cheminformatics and transcriptomics and Adverse Outcome Pathway (AOP)-informed modeling to develop a predictive Nano-Quantitative-Structure-Activity-Relationship (Nano-QSAR) framework aligned with the principles of New Approach Methodologies (NAMs) and Next-Generation Risk Assessment (NGRA).

The central research question underpinning this work is**: *How can transcriptomics and machine learning be integrated to develop predictive models for CNT-induced acute phase-driven inflammation following inhalation exposure?*** The core hypothesis posits that CNTs with similar physicochemical characteristics and transcriptomic signatures are likely to induce comparable adverse effects in lung tissue. To investigate this, the study focused on the *acute phase response (AR) signaling pathway*, a well-established early marker of pulmonary inflammation and fibrosis.

To validate this hypothesis, the research pursued three primary objectives. First, an AOP-informed Nano-QSAR model was developed to quantitatively link the physicochemical properties of multi-walled CNTs (MWCNTs) with transcriptional perturbations in the AR pathway. Second, a comparative analysis of single-walled and multi-walled CNTs (SWCNTs and MWCNTs) was conducted to identify shared and distinct structural features that impact on acute phase response pathway. Third, the global Nano-QSAR model was developed to assess how residual metal impurities (such as Fe_2O_3 and CoO) contribute to early transcriptomic changes associated with lung inflammation and fibrosis.

These models successfully captured key molecular drivers and early key events (KEs), demonstrating strong predictive performance consistent with the OECD principles

for QSAR validation. Key physicochemical determinants, including aspect ratio, surface area/functionalization, and specific metal impurities, were identified as critical contributors of inflammatory and fibrotic responses.

A key innovation of this dissertation lies in the systematic integration of transcriptomic data into the Nano-QSAR modeling framework. Unlike traditional QSAR models that often rely on apical endpoints (e.g., histopathology or organ-level toxicity), this approach incorporates genome-wide gene expression profiles to capture early molecular and cellular responses within the acute phase pathway. This molecular-level integration enhances the biological interpretability and improves predictivity, enabling a more precise identification of pathways perturbed by specific physicochemical properties of CNTs. By anchoring transcriptomic responses to structural attributes, the strategy supports more nuanced and mechanistically grounded toxicity predictions. Moreover, it aligns with current regulatory trends emphazing mechanism-based hazard assessment and facilitates the development of safer-by-design (SbD) nanomaterials within the AOP and NAMs frameworks.

In summary, this dissertation establishes a comprehensive and innovative framework for the mechanistically informed prediction of CNT-induced toxicity. It demonstrates the value of combining cheminformatics, machine learning, and systems biology to advance regulatory toxicology and to support the ethical, efficient, and sustainable development of nanotechnology.

1. INTRODUCTION

1.1. DEFINITIONS AND STRUCTURES

Carbon nanotubes (CNTs) are a class of materials composed of carbon atoms, wherein neighbouring carbon atoms on the molecular scale are sp^2–hybridized into honeycombs, and these honeycomb lattices are then extended into overlapped sheets that form graphene. They have been under intensive and applied engineering since their discovery in the early 1900s. In 1991, Sumio Iijima published a landmark paper on multi-walled carbon nanotubes (MWCNTs).[1] Just two years later, researchers were able to synthesized single-walled carbon nanotubes (SWCNTs).[1] SWCNTs are typically 0.4–2 nm in diameter, while MWCNTs consist of multiple concentric shells and have diameters that can often exceed 100 nm (though most commonly below this). SWCNTs are essentially cylindrical structures formed from a single sheet of graphene, whereas MWCNTs consist of multiple concentric graphene cylinders, which may include two layers or more.[2,3]

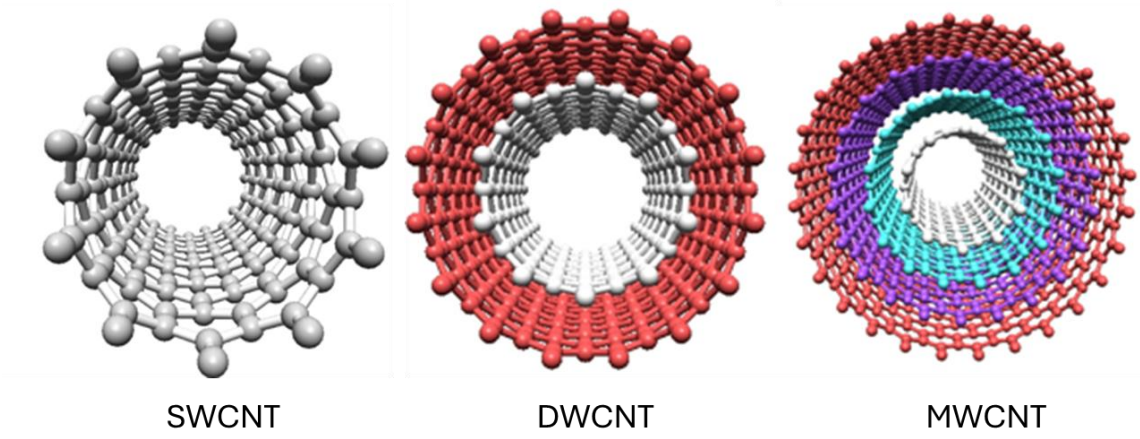

Figure 1. Illustrates the basic structures of single-walled, double-walled and multi-walled CNTs.

In both SWCNTs and MWCNTs, the fundamental atomic arrangement is based on a hexagonal graphene lattice. The way in which a graphene sheet is rolled, defined by the chiral vector (n-m), determines many of the CNTs properties, particularly their electronic behaviour. For instance, SWCNTs with an armchair configuration (n=m) exhibit metallic

conductivity, while those with a zigzag pattern (m = 0, or n = 0) or chiral arrangement (n≠m) may behave as semiconductors or metals, depending on the specific (n-m) relationship.

1.2. PHYSICOCHEMICAL PROPERTIES OF CNTS

1.2.1. CHIRALITY

The chirality of a CNT, defined by its (n, m) indices, governs its electronic behaviour and optical features. When both indices are equal, as in armchair nanotubes (n = m), the tube exhibits metallic conductivity. On the other hand, zigzag (n ≠ 0, m ≠ 0) and more general chiral forms (n ≠ m ≠ 0) may behave as either semiconductors or metals, depending on the arithmetic relationship between the indices (especially whether n-m is divisible by 3).[4,5]

1.2.2. MECHANICAL, ELECTRICAL, AND THERMAL PROPERTIES

Because of their diamond-hard sp^2 carbon lattice, CNTs are extremely strong electrically and thermally conductive, but except for this, they have been exceptionally strong as well. Consider, for instance, the tensile strength of one individual MWCNT was found to be 63 GPa (making it among the strongest known materials) (Yu et al., 2000).[4] Thermal conductivities as high as 3500 W/m·K have been measured for SWCNTs at room temperature[5], far exceeding almost all other materials (diamond is around 2200 W/m·K). Similarly, their electrical conductivity is also extraordinary, depending on chirality.[6] These high conductivities that nanotubes can facilitate electron transfer and perhaps catalyst redox reactions at biointerfaces. This inherent reactivity granted by intrinsic properties make nanotubes durable and, in some ways, unique at the nanoscale. On the other hand, extremely strong and low biodegradability also implies that CNTs (especially pristine ones) can be very biopersistent, resisting clearance and remaining in tissues for long periods, which poses long-term safety concerns.

1.2.3. SIZE AND ASPECT RATIO

The length and diameter of CNTs (and hence their aspect ratio) are crucial for their biological interactions and toxicity. Long, rigid CNTs act much like high-aspect-ratio fibers. When inhaled, long needle-like MWCNTs can penetrate deep into the lung and frustrate macrophage clearance, similar to asbestos fibers.[7–11] Such high aspect-ratio CNTs tend to persist in tissue and lead to chronic inflammation and fibrosis. In contrast, shorter or tangled CNTs are more easily cleared by cells and generally show less fibrosis. Thus, aspect ratio strongly affects the biopersistence and pathogenicity of these materials.

1.2.4. GRAPHENE WALL NUMBER AND STRUCTURAL RIGIDITY

Besides making carbon molecules a few nanometers in diameter, stronger and able to perform certain functions, how high the number of graphene layers (SWCNTs, DWCNTs and MWCNTs) is, changes CNTs rigidity and surface area. MWCNTs are mechanically stiffer and usually contain more impurities. Similarly, SWCNTs are highly flexible and hold a particularly large surface-to-volume ratio. An increased surface area may mean greater interaction with biomolecules. reactivity will be increased, thereby, through greater dispersion, once a functional group has been added to the surface.[12]

1.2.5. SURFACE CHEMISTRY AND FUNCTIONALIZATION

Surface chemistry of CNTs without any modification (i.e., pristine) is hydrophobic and tends to self-aggregate. This reduces their solubility both in water and biological fluids.[13] Such aggregates can trigger immune responses. CNTs are usually modified chemically in order to enhance their dispersibility and biocompatibility. Oxidative treatments (e.g. COOH or -OH functional groups) render CNTs more hydrophilic and reduce their cytotoxicity.[14] For example, one study showed that oxidized (–COOH) MWCNTs induced less cell death than pristine MWCNTs, although the oxidized tubes were tentatively somewhat more genotoxic. Covalently attaching polymers or biomolecules (e.g. polyethylene glycol) can further increase solubility and reduce direct membrane interactions. In a word, the covalent or noncovalent functionalization of CNT

surfaces changes them just as much in their dispersion, cellular uptake and ultimate toxicity.[14,15]

1.2.6. IMPURITIES AND RESIDUAL CATALYSTS

Most CNTs are produced by catalytic methods; chemical vapour deposition (CVD) is a typical example of this approach. It uses metal catalysts such as iron (Fe), cobalt (Co), or nickel (Ni) to start the growth process of carbon nanotubes. Some residual catalyst particles are embedded or attached to CNTs and cannot be removed. Leachate from these metal impurities can cause Fenton-type reactions, producing reactive oxygen species (ROS). Numerous research reports indicate that the generation of intracellular ROS by CNTs depends, in part, on the metal content.[16] Even commercial CNT samples often contain trace amounts of iron or other metals that contribute to oxidative stress in cells. Purification of these metals can reduce the effects, but it isn't easy to eliminate them. While the intrinsic fiber-like shape of CNTs is a primary factor in determining pathogenicity, metal impurities can magnify toxicity (especially oxidative stress) in certain conditions.[16]

1.3. APPLICATIONS AND MARKET IMPACT OF CARBON NANOTUBES

Using their unique properties, CNTs have been integrated into a wide array of industries.[17–22] Key application areas are detailed in Figure 2.

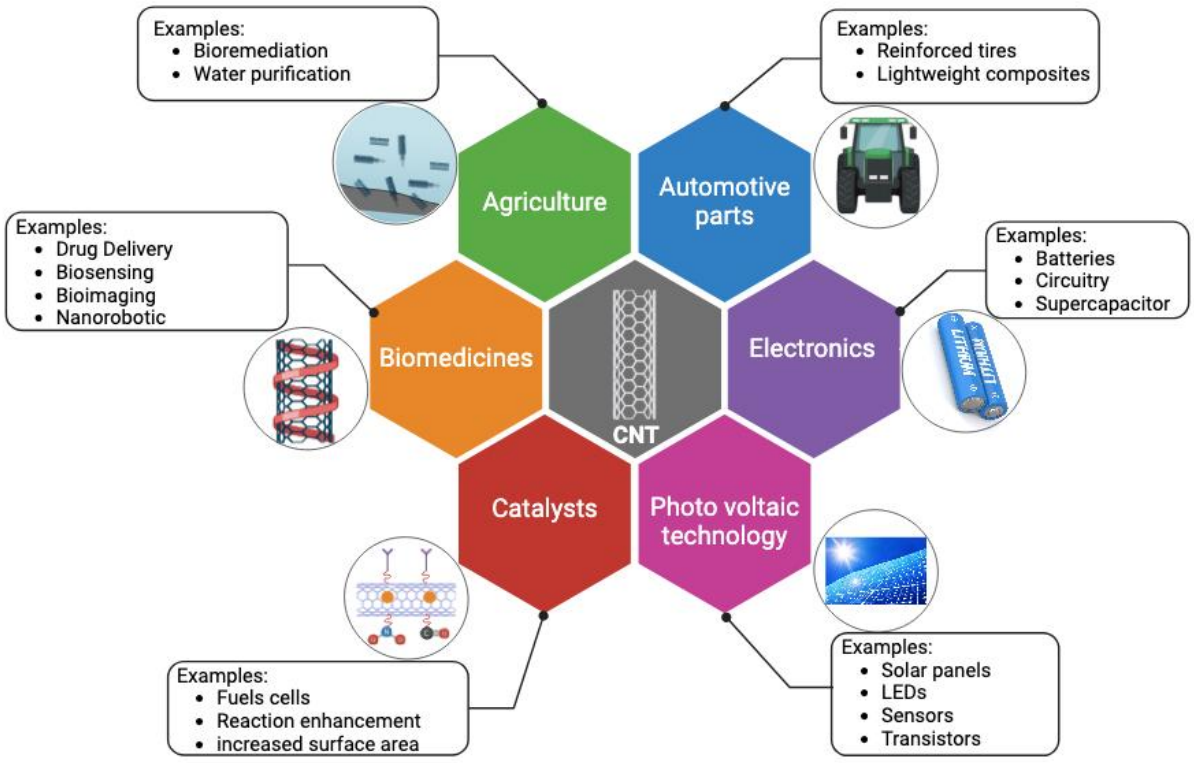

Figure 2. Overview of the main applications of carbon nanotubes across the industrial and biomedical sectors.

CNTs offer promising prospects due to their high electrical conductivity and nanometer-scale size. They have been applied to ultra-fast transistors, field-effect devices, bendable conductive films, transparent electrodes with nanoscale resolution, etc. CNTs can form the basis for ultra-fast Field-Effect Transistors (FETs) and carbon-based logic circuits, as well as for interconnects made of carbon fiber composite lines. They are also used in conductive thin films and inks for flexible displays.

CNTs play the role of conductive support and electrode additives in batteries (Li-ion or Li-S), supercapacitors and fuel cells. Their large specific area and excellent conductivity raise the efficiency of electron transfer in all cases. CNT-based composite materials are used in solar cells (as either transparent electrodes or active media to absorb light) and light-emitting diodes. This area is also being researched for catalysis in energy applications, such as the manufacture of hydrogen or as metal-carrier materials and electrolyte supports in fuel cells.

Since CNTs possess tremendous strength yet weigh next to nothing, they can be incorporated as reinforcement into composites that make aircraft and automobile components. CNT-reinforced plastics and fibers produce materials with superb strength-to-weight ratios. NASA and other organizations have studied CNT-based materials (US-COMP program).25 Automakers are using CNT-filled resins for lighter car panels, improved tire materials and electromagnetic shielding. In all these fields, CNT composites contribute to vehicles and aircraft that are lighter, stronger and more energy efficient.

CNTs serve as catalyst support (on account of their high specific area and good stability) and active materials for catalysis in purifying the environment. For example, they have been used to promote the catalytic oxidation of toxic chemicals, adsorb heavy metals or organic pollutants from water, and provide high-performance membranes used in filtrates. They can withstand horrible conditions and are conductive, so environmental sensors (detecting gases or toxins) are a good fit for them. Furthermore, CNT-based photocatalysts are being researched for their ability to decompose persistent pollutants under light irradiation.

CNTs work for drug delivery and gene introduction in biomedicine. Thanks to their small size, this material can penetrate cells. In recent years, engineers have developed means to make them functional so that they can carry drugs or DNA right past the cell membrane to its target location. They play a role as contrast agents in (eg photoacoustic) imaging and sensing devices for biologically important molecules such as DNA. CNT scaffolds are used in tissue engineering with the capability to conduct electricity, which enables skin cells to grow.

Crops that detect diseases quickly enough for humans to stop their spread mean at least ten times the yield. Nanowire biosensors fashioned on silicon have been tested in living plants by UC Davis plant pathologist Pamela Ronald. For ecological restoration purposes, a network of sensors could be installed inside an estuary to monitor its oxygen level, etc. Both examples demonstrate how experts in fringe areas have begun applying cellulose paper-based tubes, the highest cost component, in conjunction with other

materials such as glass fibres. The upshot is a cheaper fit for new types of sensors and further moisture-proofing.

The global market is progressing fast as it can fulfil many needs across various sectors. For example, a report released by Grand View Research estimates (2024) that the global market for CNT was estimated to be around USD 3.71 billion with a CAGR (Compound Annual Growth Rate) of approximately 14.1% through 2030.[23] According to another study, predicted growth from USD 5.0 billion in 2024 to USD 24.1 billion by 2034 (CAGR 17%).[24]

Table 1. The estimated market value of carbon nanotubes across various sectors, along with projected growth trends

Sector	2024 Market Value (Billion USD)	Future Value	Target Year	CAGR (%)
Electronics & Semiconductor	$3.7	Growing at 14.1% CAGR (2025–2030)	2030	14.10%
Energy Storage	$6.88	$18.67 (by 2032)	2032	13.30%
Automotive & Aerospace	$5.9 (2025)	$24.1 (2034)	2034	17%
Pharmaceutical & Biomedical	$6.45	$18.01 (by 2031)	2031	13.70%
Environmental (Water, Air Purification)	$1.31	$2.63 (by 2029)	2029	14.90%

In specific areas, such as medical/biomedical applications of CNTs, it is anticipated that the market will rise from its expected to grow of about USD 6.45 billion in 2023 to USD 18.01 billion by 2031(CAGR 13.7%).[25] Similarly, the CNT-based environmental technology market is projected to advance from USD 1.31 billion in 2024 to USD 2.63

billion by 2029 (CAGR 14.9%).[26] These values (Figure 2 and Table 1) illustrate the enormous potential for future growth of CNTs in electronics, energy, healthcare, and other fields.

Particularly, the global market for MWCNTs is currently dominated by this market, primarily due to their scalable production processes and relatively lower costs. Figure 3 shows a detailed comparison of S- and MWCNTs.[23–26]

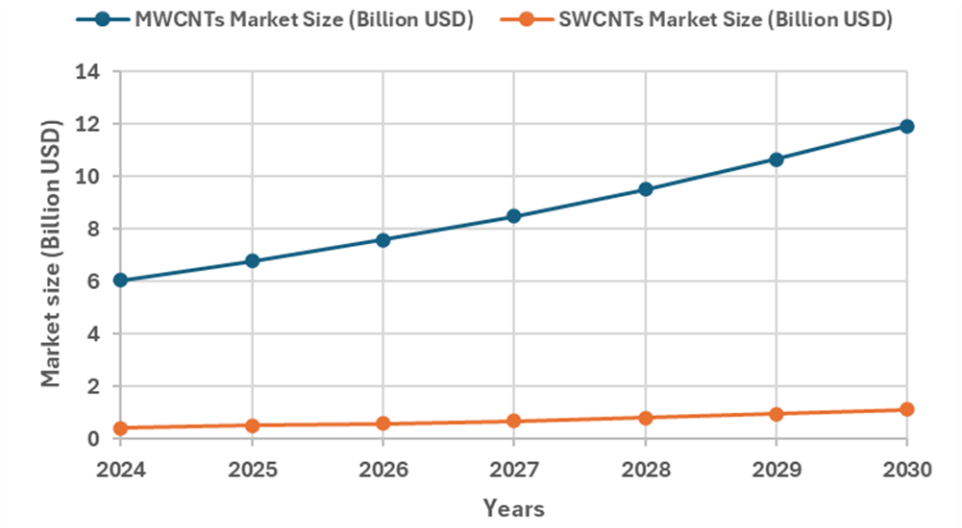

Figure 3. Market trends for CNTs distinguish between the single-walled and multi-walled carbon nanotube types across major application sectors.

1.4. MECHANISMS OF THE CNT-INDUCED TOXICITY

Carbon nanotubes have raised safety concerns due to their potential toxic effects, especially via inhalation. When CNTs are introduced into biological systems, they can lead to diverse effects on cells through several mechanisms (Figure 4).[27,28]

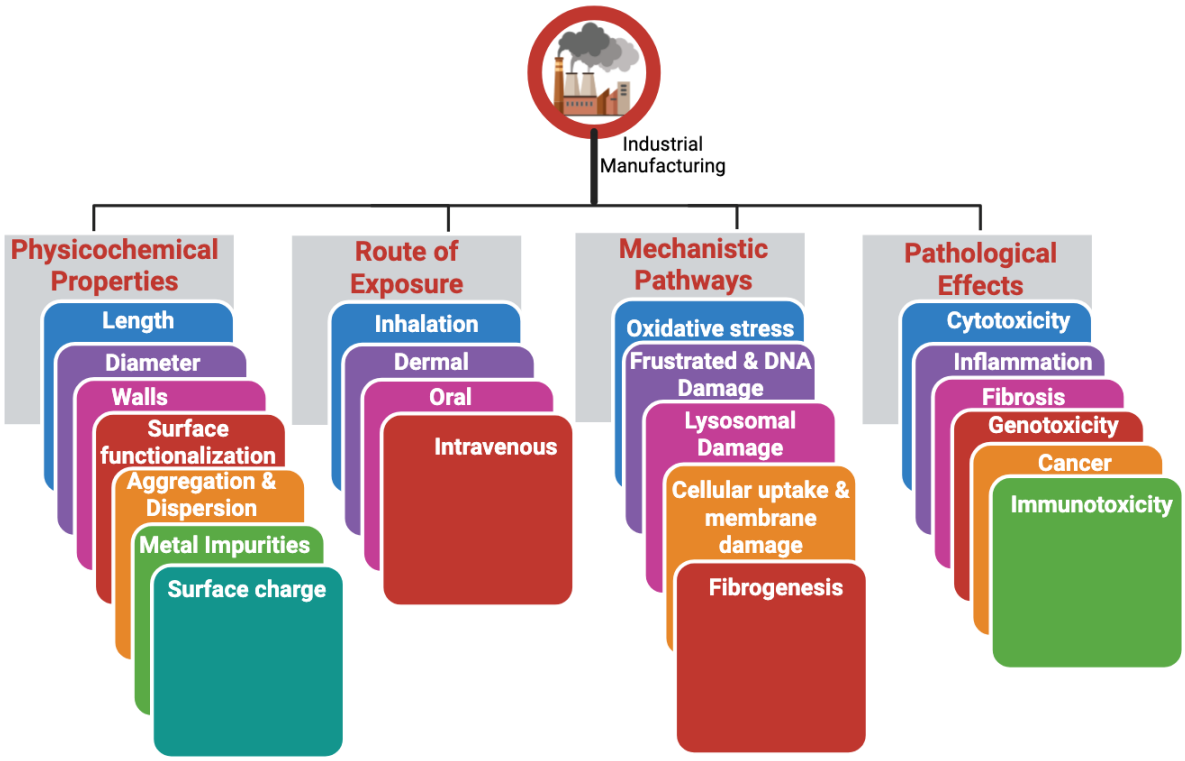

Figure 4. Physicochemical and biological factors influencing the toxicity of CNT. Nanotubes toxicity is determined both by intrinsic physicochemical properties (i.e., length, rigidity, surface chemistry and metal impurities) as well as key biological mechanisms such as oxidative stress and generation of ROS, frustrated phagocytosis, genotoxicity and DNA damage, lysosomal disruption and activation of inflammasome, cellular membrane damage and induced of pulmonary fibrosis.

1.4.1. OXIDATIVE STRESS AND ROS GENERATION

CNTs are known to penetrate the cell membranes and interact with intracellular components, leading to their persistent accumulation within organelles, such as the endoplasmic reticulum.[29] This localization is associated with the generation of reactive oxygen species (ROS), which lead to oxidative stress. Some studies have reported that even small doses of MWCNTs can induce high levels of intracellular ROS. It seems to be associated with solubilized metal contaminants present in MWCNTs (e.g., Fe, Co, Ni). Indeed, a correlation between intracellular ROS production and the metal content of CNTs has been frequently observed.[28] The ROS, such as superoxide anions and hydroxyl radicals, can damage cellular macromolecules, including lipids, proteins and DNA, leading to

inflammation, mitochondrial dysfunction, and cell death. While even metal-free CNTs can induce ROS generation through surface defects or activation of oxidative enzymes, metal-rich CNTs tend to elicit higher oxidative stress. Therefore, enhanced ROS production is considered a key mechanism underlying CNT-induced cytotoxicity and inflammation.[30]

1.4.2. FRUSTRATED PHAGOCYTOSIS AND PERSISTENT INFLAMMATION

Long, rigid CNT fibers are often too large for macrophages to fully engulf, leading to frustrated phagocytosis. This failure to clear the fiber results in chronic activation of immune cells. Macrophages attempting (and failing) to digest the CNTs release pro-inflammatory cytokines (e.g. TNF-α, IL-1β) and reactive species extracellularly, sustaining tissue inflammation. This mechanism mirrors the fiber-toxicity paradigm seen with asbestos. In fact, in animal studies, long MWCNTs instilled into body cavities induced asbestos-like pathological outcomes.[31] Overall, frustrated phagocytosis by long CNTs drives ongoing inflammation and secondary tissue damage.

1.4.3. GENOTOXICITY

The genotoxic effects of CNTs are typically mediated through oxidative stress mechanisms. This process may initiate with the generation of ROS via metal-catalysed such as Fenton chemistry involving iron, or through cellular accumulation of CNTs via phagocytosis. Subsequently, ROS production can be further amplified by the activation of NADPH oxidase.[32] The physicochemical characteristics of MWCNTs significantly influence their genotoxicity.[33,34] For example, in the study by Poulsen et al.,[33] a panel of 10 different MWCNTs was analyzed, suggesting that variations in parameters, such as length, rigidity and surface properties, directly affected the manifestation of genotoxicity effects in lung tissues. High-aspect-ratio CNTs (long, rigid tubes) have been shown to pose a greater genotoxic risk. This increased risk is likely attributed to their persistence in the biological system and higher ROS generation capacity.[35] Chronic exposure to such CNTs

may cause DNA damage[36] and impaired DNA repair, leading to mutations and increased carcinogenic potential over time.[37]

1.4.4. PULMONARY FIBROSIS

Pulmonary fibrosis is a well-documented long-term pathological outcome of CNT exposure, observed across numerous experimental animal models.[38–44] When CNTs enter the lungs, whether through inhalation, intratracheal instillation or pharyngeal aspiration, they trigger an immediate and robust inflammatory response. This acute phase is characterized by the recruitment and accumulation of immune cells such as neutrophils, macrophages, and lymphocytes, along with the release of pro-inflammatory and pro-fibrotic cytokines, chemokines and growth factors. Both type 1 (Th1/M1) and type 2 (Th2/M2) immune pathways are activated during this phase.

Fibrotic changes can begin as early as day 1 post-exposure, marked by the deposition of extracellular matrix (ECM) components in the alveolar septa begins to emerge. In the early stage, neutrophils and classically activated M1 macrophages dominate the immune response, sustaining inflammation and initiating tissue remodeling. As the response progresses, a shift toward a type 2 dominant microenvironment occurs. Th2 lymphocytes and alternatively activated M2 macrophages become more prevalent, releasing type 2 cytokines (e.g., IL-4, IL-13) that suppress acute inflammation while promoting fibrotic remodeling.

Fibroblasts and myofibroblasts, key effector cells in fibrosis, are activated and expanding during this process. They are responsible for producing and depositing collagen and other ECM components that contribute to tissue scarring. By around 28 days of post-exposure, chronic fibrotic phenotypes are typically fully established and can persist for months to a year. These long-term changes include interstitial fibrosis, thickening of alveolar septa, persistent inflammation and granuloma formation.

Importantly, prolonged fibrosis and unresolved chronic inflammation create a tissue environment that may contribute to carcinogenic progression.[45–48] Persistent fibroblast activation, immune dysregulation, and elevated oxidative stress can lead to DNA damage, impaired repair mechanisms, and cellular transformation.

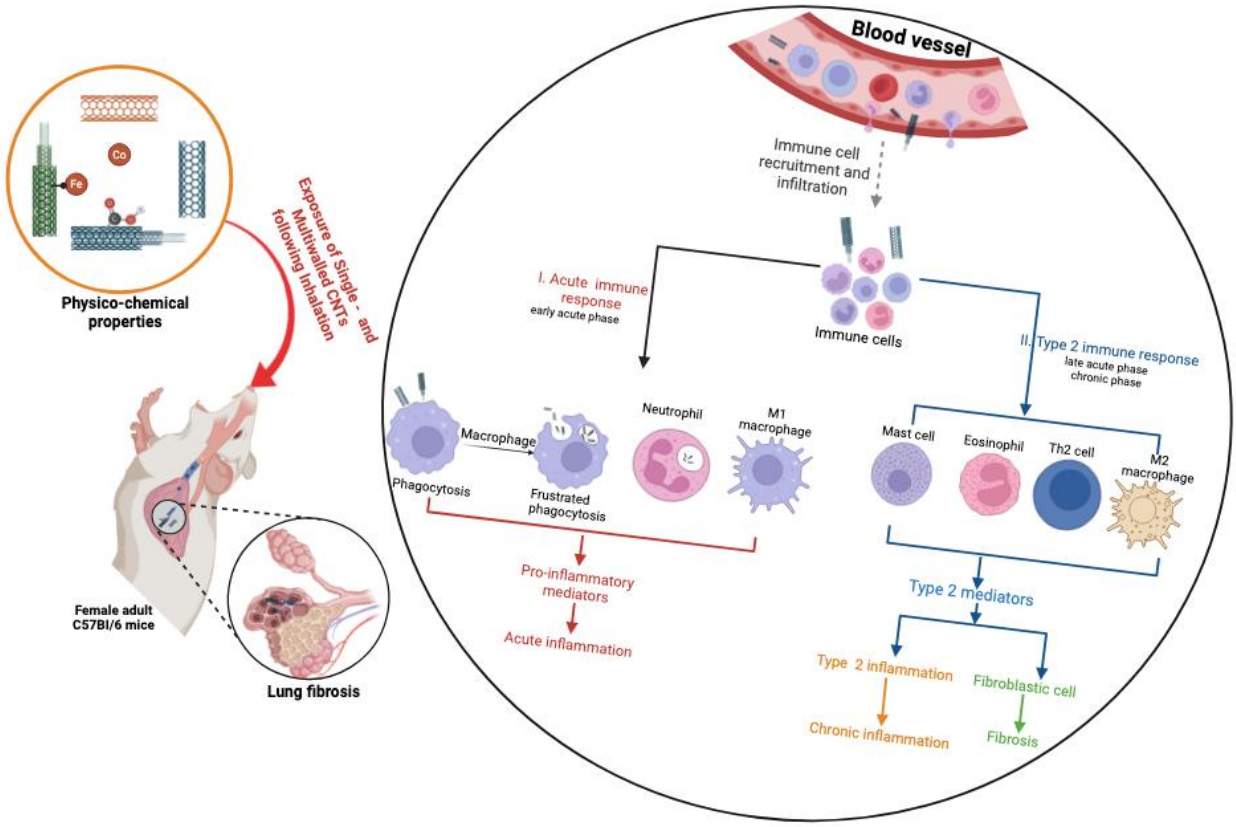

Figure 5. Overview of CNT-induced lung inflammation and fibrosis. Upon inhalation exposure to CNTs, various immune cells are recruited from the bloodstream and infiltrate the lung tissue. This immune activation is initiated by the release of cytokines, chemokines, reactive oxygen species (ROS), and alarmins, which arise through distinct mechanisms triggered by CNTs. During the early acute phase, neutrophils and pro-inflammatory M1 macrophages predominate, secreting mediators that drive acute inflammation. As the response progresses into the late acute phase, immune cells associated with type 2 immunity become dominant, releasing type 2 cytokines and mediators that promote type 2 inflammation. This shift facilitates the transition from acute to chronic inflammation, ultimately contributing to the development and progression of pulmonary fibrosis.[49]

The general mechanisms of CNT-induced pulmonary toxicity outlined in this dissertation provide a systematic conceptual framework. By focusing on lung inhalation exposure, which is the most relevant route for occupational and environmental exposure scenarios. This work emphasizes the significance of CNT-induced perturbations at the transcriptomic pathway level. Particularly, it addresses acute inflammation and fibrosis as described in the adverse outcome pathway (AOP 33). This mechanistic overview is both comprehensive and aligned with current regulatory priorities.

1.5. CURRENT PARADIGMS IN NANOMATERIALS SAFETY ASSESSMENT

1.5.1. TRADITIONAL PHENOTYPE-BASED ASSESSMENT

For decades, methods for the safety evaluation of compounds have mostly relied on toxicity tests conducted with live animals. These tests raise ethical issues, are time-consuming, and frequently yield results that cannot be easily translated into human terms because of the differences between species.[50,51] Not only is traditional toxicology an expensive and laborious process, but it also lacks a mechanistic understanding of exposure. It often fails to predict organismic responses to new toxicants and substances accurately. The approach used by regulatory bodies to evaluate safety constitutes a hazard-based paradigm, where toxic effects are identified at high doses, and then these findings are used to assess chemical safety risk to human health. Although this method has served as the backbone of basic understanding, especially of nanomaterials, which often exhibit behaviors not adequately captured by conventional testing designs. A more sophisticated approach is needed for safety assessment, and one which is both mechanistic- and human-relevant.[52]

1.5.2. FROM TRADITIONAL TO TRANSFORMATIVE: EMERGING PARADIGMS

Tox21 noted the limitations of traditional toxicology given how many complex compounds there are. Consequently, the scientific and regulatory communities are changing their reliance from traditional testing to new predictive, mechanism-based, and human-relevant models and methods. This change is being pursued based on concepts such as New Approach Methodologies (NAMs), Next-Generation Risk Assessment (NGRA), Integrated Approaches to Testing and Assessment (IATA) and Adverse Outcome Pathways (AOPs). The purpose of these paradigms is to improve the efficiency, ethical acceptability and scientific validity of toxicology.[53]

1.5.2.1. NEW APPROACH METHODOLOGIES (NAMs)

NAMs represent a step change for modern-day toxins expertise. They are comprised of non-animal approaches and methodologies utilized in harnessing data to inform safety evaluations of chemical compounds in regulatory submissions.[54,55] They involve *in silico* (computational), *in chemico* (reaction-based) and *in vitro* (cell-based) methods, and exposure assessment and biological tools, including systems biology, allow hazard prediction and risk assessment to move one step forward.[56,57] They also incorporate omic technologies (genomics, proteomics, metabolomics), organ-on-chip devices, and high-content screening platforms that offer mechanistic insights.

1.5.2.2. NEXT-GENERATION RISK ASSESSMENT (NGRA)

NGRA can be defined as an exposure-driven risk assessment approach that integrates NAMs. NGRA transforms risk assessment by shifting the focus away from traditional hazard-based models toward a more holistic understanding of risk that includes realistic exposure scenarios, biological relevance, and mechanistic insights.[58,59]

Key principles of NGRA include:

- **Human relevance**: Data used should be directly relevant to human biology.

- **Hypothesis-driven**: Assessments are guided by specific, testable hypotheses.
- **Exposure-led**: Exposure data inform the scope and design of toxicological testing.
- **NAM-based**: Preference is given to NAMs over traditional animal testing.
- **Fit-for-purpose**: The approach is tailored to the specific regulatory question.

Risk assessment with NGRA promotes transparency, reproducibility and efficiency. Given that its framework is capable of supporting a weight-of-evidence (WoE) approach that integrates omics analysis, computational models, traditional cell systems, and in vitro assays, NGRA also gives weight to this. The use of read-across and grouping strategies, especially valuable with structurally or functionally similar nanomaterials. Such an approach harmonizes well with international efforts to modernize chemical safety assessments.

1.5.2.3. INTEGRATED APPROACHES TO TESTING AND ASSESSMENT (IATA)

IATA (OECD 2024)[60] lists several hazardous response indicators, such as toxicological and ecological signs, that can be optimally combined to provide an acceptable basis for hazard identification and quantitative risk assessment. IATA was developed as a step-by-step method for the classification and prioritization of chemicals, leading to valid properties data inputs for summarizing existing knowledge in a format which is data-rich instead of data-poor and for harmonizing across different regulatory domains to make quantitative predictions of both short- and long-term effects more accurate. IATA often consists of the following steps:

- **Problem formulation**: Defining the regulatory context and assessment goals.
- **Data gathering**: Collecting existing data, including historical data and NAMs.
- **Data integration**: Using decision trees, logic frameworks, or WoE approaches to integrate data.

- **Uncertainty analysis**: Assessing the reliability and relevance of the data.

By applying IATA, the efficiency and effectiveness of risk assessment can be improved, data relevance enhanced, and unnecessary testing reduced. For example, with regard to nanoparticles where little information is available, IATA frames are especially useful with clustering and read-across[61,62], allowing data-poor substances to be assessed on the basis of similarities to better-characterized analogues. EU-funded projects like GRACIOUS, SUNSHINE, HARMLESS and PATROLS have played important roles in developing IATA for nanomaterials.

1.5.2.4. ADVERSE OUTCOME PATHWAYS (AOPs)

When a chemical stressor (e.g., internal or external factors) interacts with a molecular target (biological tissue or organ), it affects other molecular events in the target, which further may lead to response(s) at higher levels of biological organization and ultimately results in development impairment of other higher organism(s).[63]

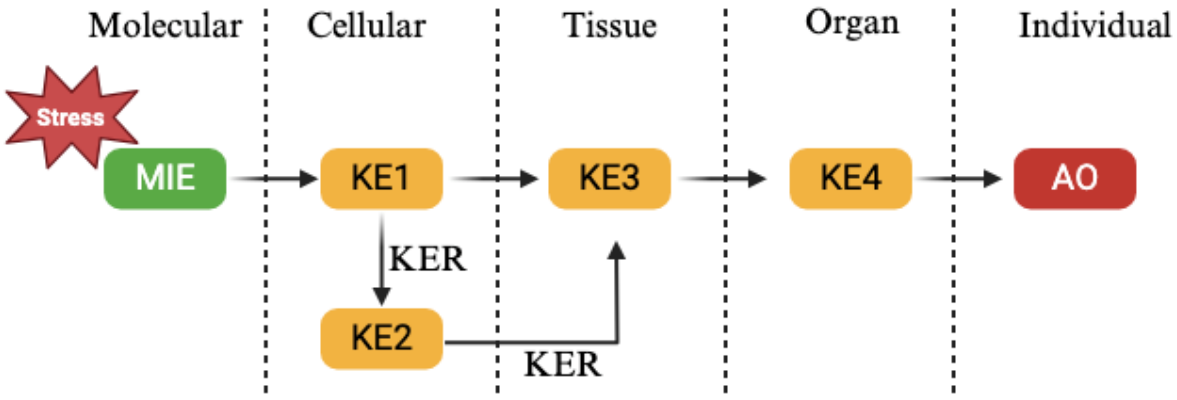

Figure 6. Schematic presentation of an adverse outcome pathway (AOP). The red stress sign box represents the stressor, which initiates the pathway. The green box denotes a molecular initiating event (MIE) – a biological interaction at the molecular level triggered by the stressor. While the orange boxes represent key events (KE) occurring at various levels of biological organization, progressing sequentially towards the adverse outcome (AO). Black arrows indicate the key event

relationships (KER), which define the causal and temporal connections between events within the pathway.

AOPs offer a theoretical construct to define toxicological interactions at different hierarchical levels of biological organization. MIEs to AOs on the individual and population scales. The AOPs are actually described as linear series of KEs that proceed in cascade along biological levels and strata. They provide a mechanistic explanation of how chemical exposure across living systems manifests as toxicities (Figure 6). A typical AOP consists of:

- **Molecular Initiating Event (MIE)**: The initial interaction between a chemical and a biological target.
- **Key Events (KEs)**: Measurable biological changes that occur downstream of the MIE.
- **Adverse Outcome (AO)**: The final toxicological effect of regulatory concern.
- **Key Event Relationships (KERs)**: Causal links between KEs and the AO.

AOPs facilitate knowledge integration across disciplines and data types, supporting the development of predictive models, NAMs, and IATA frameworks.[64,65] They are particularly useful in structuring complex biological information and in aligning experimental data with regulatory endpoints. The OECD has established the AOP Knowledge Base (aopwiki.org)[66] to promote the development and sharing of AOPs, and this resource is increasingly used in chemical and nanomaterial risk assessment. In nanotoxicology, AOPs are being developed to describe the development of adverse outcomes such as pulmonary fibrosis following exposure to nanomaterials.[67–69] By linking experimental data with established AOPs, researchers can more effectively assess the potential health effects of exposures to compounds over time. This structure demonstrates the knowledge base, so that NAMs will be accepted by regulatory authorities more easily, resulting in clearer and safer decision-making in the future.

In this unifying framework of NAMs, NGRA, IATA and AOPs, the era of traditional and complex chemical/material safety assessments has begun. As an alternative to the bat model for relevance to humans and mechanisms, if reflects a sensible plan forward for comprehensive assessment of safety of complex.

1.5.2.5. THE ROLE OF AOP-INFORMED NANO-QSAR MODELING

For decades, *in silico* models such as QSAR have played a pivotal role in the pharmaceutical and nanotechnology industries. They can elucidate structure-activity or structure-toxicity relationships. Thereby, they can support developing drugs and identifying whether substances are harmful. However, when applied to nanomaterials, the conventional QSAR models have required adaptation due to the complex and unique nature of nanoscale materials. The idea of Nano-QSAR was first formulated in 2009 by Puzyn et al. in a pioneering study that highlighted both the advances and challenges in its development.[70]

Nanomaterials are different from traditional small molecules. They have unique physicochemical properties such as size, shape, surface chemistry-related features (e.g, agglomeration/aggregation states) as well as environment, which can significantly influence their biological activity. Consequently, we cannot predict the biological responses of nanomaterials on the basis of solely molecular structure.[71,72]

Since the early days of its development, Nano-QSAR models have tried to address this complexity. It correlates the physicochemical descriptors with phenotypic outcomes (e.g., *in vitro* toxicity). While these models demonstrate the predictive power, they often lack mechanistic transparency. A critical limitation of early Nano-QSAR efforts was the empirical selection of descriptors without a particular underlying reason.

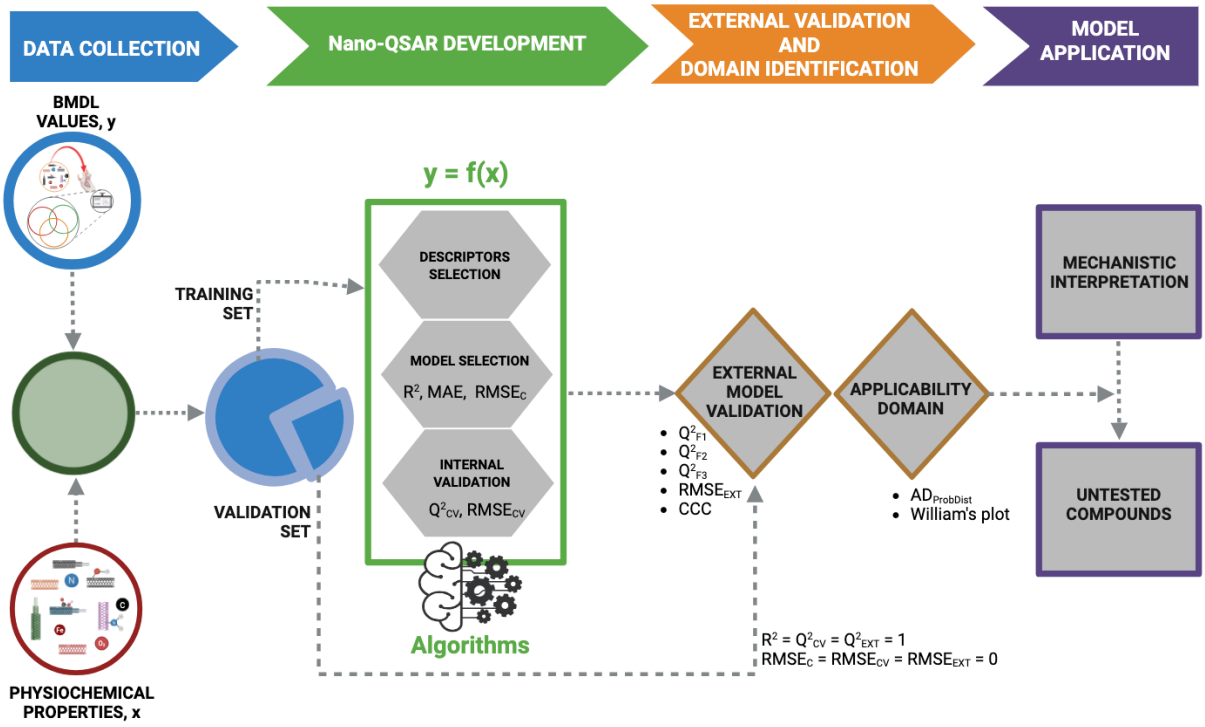

Figure 7. Workflow of AOP-informed nano-QSAR modeling aligned with OECD principles.

To bridge this gap, the concept of AOP-informed Nano-QSAR modelling has emerged. In 2021, the research group led by Dr. Karolina Jagiello introduced this approach as a major step forward in the field.[73] The paradigm aims to enhance the interpretability, regulatory applicability, and predictive robustness of Nano-QSAR models by aligning nanomaterial descriptors with biological pathways and key events (KEs) defined within the AOP framework, for example, pathways such as agranulocyte adhesion and diapedesis.

This dissertation builds upon that foundation by developing and demonstrating a proof-of-concept AOP-informed Nano-QSAR framework (see Figure 7). The objective is to strengthen the biological fidelity and mechanistic relevance of Nano-QSAR models, thereby contributing to the emergence of a modern, mechanism-driven paradigm in nanotoxicology and chemical risk assessment.

EXPERIMENTAL DATA

One of the most challenging steps in developing a QSAR model is obtaining proper experimental data. This process becomes more structured and biologically meaningful within an AOP context. AOP framework provides a manner to systematically collect and organize experimental data from various sources, which can help to identify key biological events that are both physiologically and chemically plausible.[74]

The reliability of any QSAR model is essentially determined by the consistency, quality and relevance of the input data. Therefore, data should be from peer-reviewed literature and reputable public repositories (such as aopwiki.com) or be commissioned from Good Laboratory Practice (GLP)-certified facilities. Another important thing is that the data was generated under standardised and reproducible conditions such as dose, duration, route of administration (e.g., inhalation), target organ or tissue (e.g., lungs) and analytical methods to minimize noise or bias that might occur in generated models. The representation of detailed metadata is equally important, as it provides essential context for understanding the experimental setup. The metadata should include exposure, biological models, analytical instrumentation and any deviations from the standard procedures.

The dataset must be rigorously quality controlled and statistically assessed for homogeneity and coherence before model development can ensue. Homogeneity refers to the dataset being consistent both in design (i.e., experiments should be conducted under the same conditions) and in toxicological significance. For example, mixing data from different sources that are truly heterogeneous (e.g., in vivo and in vitro) can give rise to an ambiguity of mechanism and so reduce model interpretability.

Standard data preprocessing steps such as normalisation, missing values imputation and outlier detection are crucial for improving data quality. For example, special attention should be given to the physicochemical properties of nanomaterials such as size, surface chemistry and residual metal traces, which can vary significantly depending on

experimental conditions. If these descriptors are assessed according to a standardised procedure, then enhance the reproducibility and predictive performance of the model.

In the case of CNT-induced lung fibrosis, AOP 33 (previously AOP 173), recently endorsed by the OECD, offers a mechanistic foundation highly relevant to high-aspect-ratio nanomaterials (HARNs). As demonstrated by Halappanavar and colleagues, this AOP outlines a clear sequence of key biological events associated with fibrotic outcomes, making it an ideal framework for guiding the selection of experimental data in AOP-informed Nano-QSAR model development.

DATASET SPLITTING (TRAINING/VALIDATION SETS)

The next critical step in Nano-QSAR modeling is the rational splitting of the dataset into training and validation sets. This process is essential for building robust, generalisable models and for assessing their predictive performance.

In the context of AOP-informed Nano-QSAR, the partitioning strategy must not only ensure statistical soundness but also preserve biological relevance. This is especially important when dealing with transcriptomics-derived pathway perturbation data linked to specific key events (KEs) in an AOP. A poorly partitioned dataset can lead to overfitting or underfitting, thereby undermining the biological insight and regulatory reliability of the model. Thus, several data splitting strategies can be employed, such as random, stratified and ratio-based methods.[75] In AOP-informed modelling, care must be taken to avoid data leakage, a scenario where mechanistically similar materials appear in both training and validation sets, artificially inflating performance metrics. One strategy to mitigate this risk is to group materials by mechanistic class or response type and ensure these groups are only present in one subset (e.g., training or validation) but not both. Additionally, external validation is encouraged by the OECD guidelines for QSAR model development. If possible, data from completely independent studies (e.g., different labs, exposure protocols, or transcriptomics platforms) should be used as an external test set. This provides the most stringent test of a model's generalisability and practical utility.

Finally, cross-validation techniques such as k-fold cross-validation, leave-one-out (LOO) may be implemented during model optimisation to reduce variability and ensure stability in the prediction outcomes. These approaches also help in the fine-tuning of hyperparameters and assessing model robustness in the absence of a large external test set.

DESCRIPTORS SELECTION

The descriptors used in nano-QSAR modeling can generally be derived from either experimental characterization or theoretical calculations. Experimental descriptors refer to empirically measurable properties such as initial particle size, aspect ratio, diameter, specific surface area, zeta potential, and elemental or compositional data.

In this dissertation, I exclusively use experimentally derived descriptors obtained from our collaborators. These descriptors are reliable for investigation, consistent across studies and have had their results validated by standardized experimental procedures and hence are highly reliable, reproducible and of regulatory significance. Once a comprehensive set of descriptors has been compiled, the next critical step is selecting the most meaningful variables to develop a robust and interpretable QSAR model. This process aims to identify a minimal subset of descriptors that contribute significantly to the model's predictive power, while avoiding redundancy due to high intercorrelation among variables.

Several approaches can be employed for variable selection:

- **Expert Knowledge Approach:** Leveraging domain expertise remains invaluable. Experienced QSAR modellers use their understanding of nanomaterial behaviour, biological mechanisms, and toxicological pathways to guide initial descriptor selection. This approach benefits from literature reviews and prior empirical evidence, helping to focus on descriptors most likely to influence the endpoint.
- **Statistical and Correlation Analysis:** Variable reduction often involves a two-step process. First, a preliminary pre-reduction filters descriptors based solely on their statistical properties (e.g., removing variables with low variance or high

collinearity), without considering the endpoint (dependent variable, Y). Next, a more focused selection incorporates response data, identifying variables that show strong correlations with the endpoint and improve model performance.

- **Genetic Algorithms (GA):** GAs are powerful heuristic search methods that iteratively optimize descriptor subsets based on model fitness criteria. Their ability to efficiently explore large descriptor spaces makes them widely used in QSAR modeling, especially when dealing with complex nanomaterial datasets.
- **Principal Component Analysis (PCA):** PCA reduces dimensionality by transforming correlated descriptors into uncorrelated principal components that capture the majority of variance in the data. Selecting descriptors based on PCA loadings can help retain the most informative structural features while minimizing noise.

The choice of variable selection method should be aligned with the quality and size of the dataset, as well as the specific endpoint being modelled. A key consideration in QSAR development is maintaining a suitable ratio between the number of observations and variables to avoid overfitting and ensure generalizability. It is widely demonstrated that ratios should be as large as possible. By carefully selecting a set of descriptors, the Nano-QSAR models can achieve greater predictive accuracy and interpretability.

MODEL DEVELOPMENT

The next critical step in developing AOP-informed Nano-QSAR model is to ensure alignment with the OECD principles, which are essential for establishing model quality and regulatory acceptance.[76–81] For validation, the developed QSAR model must satisfy five key OECD principles:

1. **A Defined Endpoint** – The biological or toxicological endpoint that the model predicts must be clearly defined.

2. **An Unambiguous Algorithm** – The computational method must be transparent, reproducible, and fully documented.
3. **A Defined Domain of Applicability (AD)** – The chemical space where the model can reliably make predictions must be clearly characterized.
4. **Appropriate Performance Metrics** – The model's goodness-of-fit, robustness, and predictive ability must be properly assessed.
5. **Mechanistic Interpretation, If Possible** – The model should provide insights into the biological mechanisms underlying the predicted effects.

OECD Principle 1 – A Defined Endpoint

The first principle is based on data quality (data curation), to ensure that the endpoint being predicted, whether toxicity or physicochemical property, is clearly defined and homogeneously measured. This is crucial because endpoints may vary depending on experimental protocols or conditions applied, which variability will affect the reliability of the model.[80]

OECD Principle 2 – An Unambiguous Algorithm

Principle 2 emphasizes transparency in the model's mathematical or computational approach. All details about molecular descriptors, algorithms, and calculation procedures must be thoroughly documented so that any user can reproduce the predictions. Following recommendations by the European Commission Joint Research Centre (JRC), QSAR models should be reported using standardized formats such as QMRF (QSAR Model Reporting Format) and QPRF (QSAR Prediction Reporting Format), which are necessary for regulatory registration (e.g., under REACH). This principle ensures the model's reproducibility and clarity.[78]

OECD Principle 3 – A Defined Domain of Applicability

The applicability domain (AD) defines the boundaries within which the model's predictions are reliable. Since QSAR models are calibrated on a finite set of compounds,

their accuracy depends heavily on the structural similarity of new compounds to those in the training set. Predictions made within the AD (i.e., by interpolation) are more trustworthy, while those outsides are less reliable.[82,83]

In this dissertation, two AD methods are applied:

Williams Plot: This widely used technique plots standardized residuals against leverage values. Leverage (h_i) measures the distance of a compound's descriptor vector from the training set centroid and is calculated as:

$$h_i = x_i^T (X^T X)^{-1} x_i \quad (1)$$

Where Xi is a row vector of descriptors for (i^{th}) chemical compounds, and X is a matrix of descriptors from the training set.

The threshold for leverage is defined as:

$$h^* = \frac{3(p+1)}{n} \quad (2)$$

Where p is the number of descriptors used in the model and n is the number of chemical compounds in the training set.

Model limitations with respect to the response space (y-axis) are generally constrained within boundaries defined by ±3 standard deviations of the standardized residuals.

As a practical guideline, only predictions falling within a defined applicability domain, often visualized as a square area bounded by the critical leverage value (h*) on the x-axis and ±3 standard deviation units on the y-axis are considered reliable.

Table 2. Statistical information about the Nano-QSAR models[80,84–87]

	Statistical metrics	Formula	Criteria
Goodness of fit	Determination coefficient	$R^2 = 1 - \frac{\sum_{i=1}^{n_T}\left(y_i^{exp} - y_i^{pred}\right)^2}{\sum_{i=1}^{n_T}\left(y_i^{exp} - \bar{y}_i^{exp}\right)^2}$	$R^2 > 0.7$
	Root mean square error for calibration	$RMSE_c = \sqrt{\sum_{i=1}^{n}\frac{\left(y_i^{exp} - y_i^{pred}\right)^2}{n}}$	RMSEc as low as possible
Internal validation	Cross-validation coefficient	$Q2CV = 1 - \frac{\sum_{i=1}^{n}(y_i^{exp} - y_i^{predcv})^2}{\sum_{i=1}^{n}(y_i^{exp} - y_i^{\sim exp})^2}$	$Q^2_{CV} > 0.6$
	Cross-validation Root mean square error for calibration	$RMSEcv = \sqrt{\frac{\sum_{i=1}^{n}(y_i^{exp} - y_i^{predcv})^2}{n}}$	RMSEc as low as possible
External Validation	External validation coefficient Q^2_{F1}	$Q^2_{F1} = 1 - \frac{\sum_{i=1}^{n_T}\left(y_i^{exp} - y_i^{pred}\right)^2}{\sum_{i=1}^{n_{EXT}}\left(y_i^{exp} - \bar{y}_T^{exp}\right)^2}$	$Q^2F1 > 0.6$
	External validation coefficient Q^2_{F2}	$Q^2_{F2} = 1 - \frac{\sum_{i=1}^{n_{EXT}}\left(y_i^{exp} - y_i^{pred}\right)^2}{\sum_{i=1}^{n_{EXT}}\left(y_i^{exp} - \bar{y}_{EXT}^{exp}\right)^2}$	$Q^2F2 > 0.6$
	External validation coefficient Q^2_{F3}	$Q^2_{F3} = 1 - \frac{[\sum_{i=1}^{n_{EXT}}(y_{i=1}^{n_{EXT}} - y_i^{pred})^2]/n_{EXT}}{[\sum_{i=1}^{n_T}(y_i^{exp} - y_{EXT}^{-exp})^2]/n_T}$	Q2F3 > 0.6
	Concordance correlation coefficient	$CCC = \frac{2\sum_{i=1}^{n_{EXT}}(y_i^{exp} - \bar{y}_{EXT}^{exp})(y_i^{pred} - \bar{y}_{EXT}^{pred})}{\sum_{i=1}^{n_{EXT}}(y_i^{exp} - \bar{y}_{EXT}^{exp})^2 + \sum_{i=1}^{n_{EXT}}(y_i^{pred} - \bar{y}_{EXT}^{pred})^2 + n_{EXT}(\bar{y}_{EXT}^{exp} - \bar{y}_{EXT}^{pred})^2}$	CCC > 0.8
	Root mean square error for prediction	$RMSE_p = \sqrt{\frac{\sum_{i=1}^{n_{EXT}}\left(y_i^{exp} - y_i^{pred}\right)^2}{n_{EXT}}}$	RMSEp as low as possible
Uncertainty of prediction	Average absolute error	$AAE = \frac{1}{n}\sum_{i=1}^{n}\left\lvert y_i^{exp} - y_i^{pred}\right\rvert$	AAE as low as possible

Where y_i^{exp} – the experimental value of the structural property for the ith compound; y_i^{pred} – the predicted value of the property for the ith compound; $\bar{y}_i^{exp}$ – the mean experimental value of the property; $\bar{y}_i^{pred}$ – the mean predicted value of the property; n_T – the number of source compounds in the training set; n_{EXT} – the number of the source compounds in the validation.

The leverage approach assesses the structural similarity of each compound relative to the training set by calculating a distance measure within the descriptor space. This method helps identify influential observations (those with high leverage), structural outliers (compounds structurally distinct from the training set), and response outliers (predictions that deviate significantly from observed values). Identifying these points is crucial for evaluating the model's applicability domain and ensuring trustworthy predictions

Probability-Oriented Distance-Based Approach (ADProbDist): This graphical method defines the AD based on average Euclidean distances between new compounds and the training set in descriptor space, combined with standardized residuals to account for endpoint prediction errors. It provides confidence regions (e.g., 95% or 99%) to evaluate if new compounds fall within the model's reliable prediction domain.

OECD Principle 4 – Appropriate Measures of Goodness-of-Fit, Robustness, and Predictivity

Model performance must be validated statistically through:

- **Goodness-of-Fit:** Measures how well the model fits training data, assessed via the coefficient of determination (R^2) and root mean square error of calibration (RMSEc). High R^2 and low RMSEc indicate good training performance.
- **Internal Validation:** Evaluates model stability using cross-validation methods like Leave-One-Out (LOO), Leave-Many-Out (LMO), or bootstrap. Key metrics include cross-validation coefficient (Q^2_{CV}) and $RMSE_{CV}$. These tests ensure the model is not overfitted to training data.
- **External Validation:** Tests predictive accuracy on an independent validation set not used during training. Metrics such as external validation coefficient (Q^2_{EXT}) and root mean square error of prediction ($RMSE_{EXT}$) measure how well the model generalizes. Additional parameters, including Q^2_{F1}, Q^2_{F2}, Q^2_{F3}, Concordance

Correlation Coefficient (CCC), and Average Absolute Error (AAE), further characterize external predictivity.

A well-performing model will have comparable R^2, Q^2_{CV}, and Q^2_{EXT} values close to 1, with consistent and low RMSE values. Large discrepancies, especially if R^2 and Q^2_{CV} exceed Q^2_{EXT} substantially, suggest overfitting and poor predictive power.[84–87]

OECD Principle 5 – Mechanistic Interpretation, If Possible

The final OECD principle emphasizes that QSAR models should ideally provide mechanistic insight by linking descriptors to the biological endpoint. This ensures that a model offers more than statistical associations by revealing how specific structural or physicochemical features influence toxicity or bioactivity. However, conventional QSAR models often prioritize structure–activity correlations without directly mapping chemical/material features to molecular initiating events MIEs within an AOP framework. To address this gap, Jagiełło et al.[73] (2020) proposed a transcriptomic-based, AOP-informed Nano-QSAR approach that integrates mechanistic biological data into model development.

1.6. MACHINE LEARNING METHODS IN DATA-DRIVEN MODELING APPROACH

Machine learning (ML) methods used in this work are divided mainly by their analytical goals: unsupervised and supervised learning.

Unsupervised learning identifies data intrinsic patterns or groupings without relying on predefined labels or outcomes. These methods are useful for exploring the underlying structure of data, clustering similar nanoforms or detecting hidden patterns. Common unsupervised techniques include hierarchical cluster analysis (HCA), principal component analysis (PCA) and k-means clustering. In this dissertation, HCA and PCA were employed to group nanotubes based on their physicochemical properties and associated biological

responses. The theoretical assumptions of these methods will be presented later in the work (Section 1.6.1).

On the other hand, supervised learning involves modeling the relationships between input variables (features or descriptors) and a known outcome (labelled response). This approach is essential for selecting significant descriptors that influence endpoints and for building predictive models. Supervised techniques include both linear and non-linear regression, such as Kernel-weight Local Polynomial Regression (KwLPR), Decision Trees (DT), Random forests (RF), Gradient Boosting and XGBoost. These methods have been widely applied in nanotoxicology to correlate the physicochemical properties of CNTs with their observed biological effects. Effective feature selection is crucial in supervised learning to improve model interpretability, reduce overfitting and ensure robustness. The theoretical assumptions of these methods will be presented later in the work (Sections 1.6.2, 1.6.3, and 1.6.4).

1.6.1. HIERARCHICAL CLUSTERING ANALYSIS METHOD (HCA)

Hierarchical clustering analysis (HCA) is a multivariate statistical method that facilitates the exploration of complex datasets by identifying similarities and differences between objects based on their characteristics in a multidimensional space. The main assumption of this method is that the similarity between objects can be assessed using distance metrics. The smaller the distance, the more similar the objects; larger distances indicate greater dissimilarity. There are several distance measures are commonly used in HCA, and the choice of selection often depends on the specific objectives of the analysis:

- **Euclidean distance**: Measures the geometric distance between objects in feature specific.
- **Squared Euclidean distance**: Gives more weight to the difference between objects.
- **Chebyshev distance**: Based on the maximum difference among all features, thus highlighting extreme dissimilarities.
- **Manhattan distance:** Based on the sum of absolute differences between features.

Once the distances between all objects are calculated, the next step involves grouping them into clusters using a selected linkage method, which determines how clusters are merged:

- **Single linkage**: Merges clusters based on the smallest distance between their nearest members, emphasizing object similarity.
- **Complete linkage:** Uses the largest distance between the members of different clusters, emphasizing dissimilarity.
- **Group average:** Calculates the average distance between all pairs of objects from different clusters, providing a balanced approach.
- **Ward's method:** Minimizes the total within-cluster variance (sum of squared deviations) often leading to compact and spherical clusters.

The outcome of the HCA is typically visualized as a **dendrogram**, a tree-like diagram that illustrates the hierarchical relationships among the analyzed objects.

1.6.2. PRINCIPAL COMPONENT ANALYSIS (PCA)

Principal Component Analysis (PCA) is a powerful technique for analazying multidimensional data. It serves two main purposes: (i) uncovering hidden relationships among variables, and (ii) reducing the dataset's dimensionality while retaining most of its original information.

The assumptions of the PCA method are based on transforming the original dataset of correlated variables into a new set of uncorrelated (orthogonal) variables called principal components (PCs). These components are linear combinations of the original variables and are constructed to capture as much variability as possible. The first principal component (PC1) accounts for the highest variance, while subsequent components (PC2, PC3, etc.) explain progressively smaller portions. Importantly, the total variance in the dataset remains constant after transformation; it is simply redistributed across the new principal components. The explained variance percentage of each component, calculated from its eigenvalue, indicates how much of the dataset's variability it captures.

Each original variable contributes to the principal components through factor loadings, the coefficients in the linear combinations. Variables with higher absolute loading values have a stronger influence on that component, helping to interpret which features drive specific patterns in the data. By projecting the dataset into the space defined by the first few components (e.g. PC1 and PC2), PCA creates a linear map that makes it easier to visualize similarities, groupings and outliers in the data. This dimensionality reduction not only simplifies analysis but also enhances interpretability in complex datasets.

1.6.3. KERNEL-WEIGHT LOCAL POLYNOMIAL REGRESSION (KwLPR)

The kernel-weighted local polynomial regression (KwLPR) is a nonlinear, locally adaptive regression method that falls under the category of lazy supervised learning algorithms. It employs locally weighted least squares (LWLS) to estimate the regression function m(x), allowing for flexible modelling of complex, nonlinear relationships between predictors and response variables in the context of Nano-QSAR modelling.

KwLPR operates by fitting a polynomial of degree p within a local neighborhood of a query point (x_0), the method minimizes the following weighted least square's function:

$$min_{\beta_j} \sum_{i=1}^{n} \left\{ Y_i - \sum_{j=0}^{p} \beta_j \, (x_i - x_0)^j \right\}^2 K \left(\frac{x_i - x_0}{h} \right) \quad (3)$$

Where: X represents the design matrix centered around the query point (x_0), Y is the response variable (e.g., biological or toxicological endpoint), p is degree of the polynomial, K is the kernel function (which defines the neighbourhood shape and assigns weights to data points based on their proximity to x_0), h is the bandwidth (smoothing parameter) that determines the size of the local neighborhood, n is the number of independent variables or data points, b - vector of regression coefficients.

The regression coefficients (b) are obtained by solving the weighted least squares Equation:

$$\hat{\beta} = (X^T W X)^{-1} X^T W y \quad (4)$$

Where: W is a diagonal matrix representing the weights derived from the kernel function.

The kernel assigns higher weights to observations closer to x_0, gradually reducing the influence of points as their distance increases. This localized weighting mechanism makes KwLPR particularly effective for handling heterogeneous or nonlinear datasets. Especially, to address the challenges posed by small and limited datasets.

In contrast, KwLPR offers a locally adaptive and interpretable modelling framework, which is particularly suitable for nanomaterials with diverse physicochemical profiles and complex dose response relationships. In this dissertation, KwLPR was applied to MWCNTs-induced toxicological responses, providing improved predictive accuracy and mechanistic insights compared to conventional modelling methods. These results, which have been previously published as part of my research (section 4.1), underscore the utility of KwLPR in advancing a mechanism-based, AOP-informed predictive toxicology framework.

1.6.4. TREE-BASED LEARNING METHODS

Tree-based algorithms constitute a class of supervised machine learning methods that are particularly effective for modelling complex, nonlinear relationships, ranking feature importance and performing classification/regression tasks. In this study, regression tree (RT) approaches were applied to investigate the relationship between the physicochemical properties of CNTs and their toxicological effects. These models not only facilitated the prediction of biological responses but also enabled the identification and priotitization of key descriptors most strongly influencing the modeled endpoints.

To comprehensively investigate the structure–activity relationships (SARs) underlying CNT-induced toxicity, multiple tree-based machine learning models were employed, including Decision Tree (DT), Random Forest (RF), Gradient Boosting (GB), and eXtreme Gradient Boosting (XGBoost). These models were selected for their strengths in model interpretability, predictive accuracy, and feature selection efficiency. A detailed

account of the model development process, hyperparameter optimization strategies, and validation procedures is provided in Section 4.3.

2. RESEARCH PROBLEM, HYPOTHESIS AND OBJECTIVES

2.1. RESEARCH PROBLEM AND MAIN HYPOTHESIS

The increasing production and use of CNTs presents new opportunities and raises significant safety concerns, posing critical challenges. As production scales up, so does the risk of unintentional release into the environment or occupational settings. This is particularly concerning given the current limitations in our understanding of CNTs potential impact on human health and ecological systems.

Conventional *in silico* toxicity testing methods (e.g., QSAR) often fail in providing mechanistic insights into hazard potential. These models typically rely on simplistic correlations with phenotype-based endpoints and lack of integration with biologically meaningful or mechanistically relevant outcomes (e.g., pathway-specific AOs). Therefore, they provide limited mechanistic interpretation and predictive relevance.

toxicology is undergoing a paradigm shift in chemical/advanced material risk assessment, developing towards the NGRA framework. This approach incorporates NAMs within IATAs and is aligned with the AOP concept. Collectively, these strategies aim to streamline testing, reduce animal use, and enhance the mechanistic relevance of hazard assessment. They are together promoting the 3Rs principles: Replacement, Reduction, and Refinement of animal testing.

Within this framework, data-rich approaches combining transcriptomics, chemoinformatics, bioinformatics, artificial intelligence (AI), and machine learning (ML) offer a promising avenue for mechanistic hazard prediction.

In this work, the central premise is based on a systems toxicology framework, integrating machine learning and Transcriptomic-level data integration to unravel the complex mechanisms underlying CNT-induced pulmonary inflammation, with a focus on the acute phase response (AR) pathway. Building upon the proof-of-concept study proposed by K. Jagiello et al.[73] (2021), the author investigated a key inflammatory pathway, particularly the “agranulocyte adhesion and diapedesis” pathway, which serves as an early indicator of inflammation and tissue damage.

In this dissertation, I hypothesize that carbon nanotubes with similar physicochemical properties and transcriptomic signatures may trigger similar molecular initiating events (MIEs) within the acute phase response (AR) signaling pathway, **leading to similar downstream adverse outcomes at the tissue level**. These tissue-level similarities suggest that structural determinants, such as aspect ratio, surface area and presence of metal impurities, play a mechanistically causal role in pathway-level toxicity as outlined in AOP 33 (lung fibrosis) and AOP 237 (atherosclerosis). To explore this hypothesis, the research guided by the following key questions:

- What physicochemical features of MWCNTs are associated with pulmoanry and cardiovascular pathologies mediated by acute inflammation?
- How do the physicochemical features influence the differences in mechanisms between single- and multi-walled carbon nanotubes (S- and MWCNTs) in the acute phase response following inhalation exposure?
- Can we quantitatively link specific metal impurities in carbon nanotubes to their transcriptomic impact and the modulation of acute inflammatory responses?

By addressing these questions, this research aims to understand the role of intrinsic CNT properties in driving adverse outcomes. These insights form the foundation of this research and justify the development of the study's overarching hypothesis and objectives.

2.2. DETAILED RESEARCH HYPOTHESIS

The research hypothesis assumes that the physicochemical properties of S- and MWCNTs influence their toxicity by perturbing specific molecular pathways associated with early key events (KEs) in identified AOPs, ultimately leading to adverse outcomes such as lung inflammation, fibrosis and/or atherosclerosis. This assumption is tested through the following three hypotheses for CNT-driven risk assessment.

HYPOTHESIS 1.

I hypothesized that the structural properties of multi-walled carbon nanotubes (MWCNTs) are significantly associated with perturbations in the acute phase response signaling (AR) pathway in mouse lungs following inhalation exposure. These perturbations can be modeled using an AOP-informed Nano-QSAR approach to predict molecular-level inflammatory responses that may lead to lung fibrosis and/or cardiovascular pathologies.

HYPOTHESIS 2.

Single-walled and multi-walled CNTs (S- and MWCNTs) with similar structural features can exhibit comparable transcriptomic changes in the acute phase response signaling pathway. These shared structural characteristics are hypothesized to underlie common mechanisms contributing to pulmonary and cardiovascular toxicity.

HYPOTHESIS 3.

I hypothesize that metal impurities present in CNTs can act as critical drivers of transcriptomic disruptions, leading to inflammation and fibrosis following inhalation exposure. Specific metal contaminants can be quantitatively linked to early upstream key events (KEs) in the acute phase response signaling pathway through global AOP-informed Nano-QSAR models.

2.3. DETAILED RESEARCH OBJECTIVES

The research hypotheses will be tested by achieving the following objectives:

OBJECTIVE 1.

To identify the structural properties of multi-walled carbon nanotubes (MWCNTs) that perturb the acute phase response signaling (AR) pathway in the lungs of mice exposed via inhalation to a panel of 14 MWCNTs. This objective aims to support the development of a new AOP-anchored Nano-QSAR model capable of predicting molecular-level

responses associated with inflammation that may lead to lung fibrosis and/or cardiovascular pathologies.

OBJECTIVE 2.

To quantitatively compare S- and MWCNTs in terms of their structural properties and associated impact on the acute phase response signaling pathway, with the aim of identifying shared structural characteristics and gene expression profiles that may help explain their similar modes of action (MoA) related to pulmonary and cardiovascular pathologies.

OBJECTIVE 3.

To investigate the role of metal impurities in CNTs as potential contributors to transcriptomic disturbances that drive inflammation and fibrosis mechanisms following inhalation exposure. This objective aims to develop a global AOP-informed Nano-QSAR model that quantitatively links specific metal contaminants in CNTs to gene expression changes, particularly within the acute phase response signaling pathway. The model will focus on early upstream key events (KEs) associated with pro-inflammatory responses and enable the prediction of lung and cardiovascular pathologies induced by metal-containing CNTs.

3. RESEARCH METHODOLOGY

3.1. CONCEPT AND WORK PLAN

In my dissertation, particular emphasis is placed on the "acute phase response (AR) signaling" pathway. This pathway represents an early upstream event in the inflammatory cascade and is initiated during neutrophil influx through the release of acute phase reactants. These mediators trigger the synthesis and secretion of pro-inflammatory cytokines and chemokines, as well as the recruitment of immune cells into lung tissue. Critically, these events can promote fibroblast and myofibroblast proliferation and differentiation, thereby contributing to extracellular matrix (ECM) deposition and remodeling, key features of lung fibrosis.

Moreover, nanomaterial-induced activation of the acute phase response pathway has been implicated in linking inhalation exposure to broader health risks, including inflammation, fibrosis, cancer, and cardiovascular disease, as recognized in AOP 237. Notably, the acute phase protein Serum Amyloid A (SAA) has been shown to drive plaque progression in murine models of atherosclerosis, illustrating the systemic consequences of local pulmonary inflammation.

Part I. (section 4.1): Nano-QSAR modelling of MWCNTs

In this part of the study, I aimed to explore how specific structural features of MWCNTs influence the activation of the acute phase response (AR) signaling pathway in the lungs of mice. To do this, I used data from 14 commercially available MWCNTs administered at a high single dose of 54 μg/per mouse following inhalation, with lung tissue examined one day post-exposure in female C57BL/6.

The main goal was to determine which physicochemical properties of the MWCNTs were most strongly linked to the activation of the AR pathway, and their potential role in triggering early inflammatory responses. I developed a Nano-QSAR model aligned with an AOP framework. The model is designed to predict early molecular events driven by specific structural features of carbon nanotubes that may eventually lead to adverse health effects, such as lung fibrosis or cardiovascular diseases.

This newly developed data-driven model adds to the growing set of transcriptomic-based, AOP-informed Nano-QSAR models and may serve as an in silico NAM to support the safety assessment of MWCNTs using a weight of evidence approach. Ultimately, I hope to improve current risk assessment strategies and contribute to the safer design and application of nanomaterials in the future.

Part II. (section 4.2): Grouping of S- and MWCNTs based on toxicity mechanisms

In this section, the goal was to compare S- and MWCNTs in terms of their structural properties and their impact on the acute phase response signaling pathway. By conducting a quantitative comparison, I aimed to identify shared structural features and similar biological responses, particularly in the gene expression profiles, that could explain common mechanisms of toxicity.

Understanding whether S- and MWCNTs with similar characteristics trigger the same toxicological pathway is important for grouping them based on their mode of action (MoA). This approach may help clarify how both types of CNTs contribute to inflammation-related outcomes, such as lung injury and cardiovascular complications. Grouping them in this way could also support more efficient hazard assessments and inform the development of predictive models for nanomaterials for nanomaterial safety.

Part III. (section 4.3.): Global Nano-QSAR model development

In this part of the study, I focused on understanding the role of metal impurities in CNTs as potential contributors to adverse biological effects following inhalation exposure. The aim was to investigate how these metal impurities may influence gene expression profiles related to inflammation and fibrosis.

To achieve this, I developed a global Nano-QSAR model based on the AOP framework. This model was designed to quantitatively link specific metal contaminants in CNTs to changes in gene expression with a particular focus on the acute phase response signalling (AR) pathway. By capturing early upstream key events (KEs) related to the

activation of pro-inflammatory immune responses, this model helps predict CNTs-induced inflammation, which may eventually lead to lung fibrosis.

3.2. EXPERIMENTAL DATA USED

In my research work, I relied on the results of experimental studies conducted by the collaborating institutions:

- The animal studies were performed by **Prof. Ulla Vogel** at the National Research Centre for Working Environmental Copenhagen DK-2100, Denmark.
- The transcriptomics studies were conducted by **Dr. Sabina Halappanavr** at the Environmental Health Science and Research Bureau, Health Canada, Ottawa, Ontario K1A 0K9, Canada.

3.3. APPLIED MACHINE LEARNING METHODS USED

In this dissertation, I developed machine learning methods to align with research objectives. These methods are categorized into supervised, unsupervised and ensemble machine learning techniques based on their functionality.

Objective 1: I developed a quantitative Nano-QSAR model to predict the relationship between key structural descriptors of multi-walled carbon nanotubes (MWCNTs) and the acute phase response (BMDL values) using the kernel-weighted local polynomial regression (KwLPR) algorithm.

Objective 2: I compared the structural properties of single-walled and multi-walled CNTs (S- and MWCNTs) and assessed their impact on the acute phase response signaling pathway by using a combination of statistical and multivariate analysis techniques aimed at identifying shared characteristics that could explain their similar mode of toxicological action.

- Radar plots were used to visualize Pearson correlation coefficients (r) between physicochemical properties of S- and MWCNTs and the transcriptional benchmark dose

lower limit (BMDL) values associated with the acute phase response pathway. This allows for a comparative overview of key property-response relationships.

- Hierarchical Cluster Analysis (HCA) and Principal Component Analysis (PCA) were applied to explore and visualize the similarities and differences among CNT types in the multidimensional space. These unsupervised methods helped uncover grouping patterns and variability in both structural descriptors and inflammation-related gene expressions.

Objective 3: I developed global Nano-QSAR models to predict the relationship between the presence of metal impurities in CNTs and both acute phase response (BMDL values) as well as gene expression profiles (PC1/PC2), utilising the random forest (RF) algorithm.

3.4. SOFTWARES USED FOR THE STUDY CONDUCTED

For data-driven models development and applicability domain in this study were performed in Python (3.12.7)[88] and R (4.2.3)[89] scripts written in the following libraries:

Python libraries:

Numpy (1.24.0).[88]

Pandas (1.5.3).[90]

Seaborn (0.11.2).[91]

Matplotlib (3.6.3).[92]

Scikit-learn (1.1.3).[93]

SciPy (1.9.3).[94]

R libraries:

Stats (4.4.0).[95]

Dplyr (1.1.4).[96]

Reshape2 (1.4.4).[97]

Ggplots (3.5.1).[98]

Caret (7.0-1).[99]

4. RESULTS AND DISCUSSIONS

4.1. The Impact of MWCNTs Properties on Lung Pathologies and Atherosclerosis Through Acute Inflammation: A New AOP-anchored *In silico* NAM

4.1.1. SPECIFIC OBJECTIVE AND SUBJECT OF RESEARCH

In line with the first objective of this research (see section 2.3), the specific goal of this part of the study is defined as follows:

OBJECTIVE 1.

To identify the structural properties of multi-walled carbon nanotubes (MWCNTs) that perturb the acute phase response signaling (AR) pathway in the lungs of mice exposed to a panel of 14 MWCNTs. This objective supports the development of a new AOP-anchored Nano-QSAR model designed to predict molecular-level inflammatory responses that may lead to lung fibrosis and/or atherosclerosis pathologies.

4.1.2. EXPERIMENTAL DATA

The machine learning models developed in this study relied on experimental data (Table 3) provided by collaborating research groups. Dr. Ulla Vogel at the National Research Centre for the Working Environment (NRCWE) was delivered the physicochemical property data for a panel of 14 multi-walled carbon nanotubes (MWCNTs)[100–104] Dr. Sabina Halappanavar at Health Canada contributed transcriptomic benchmark dose lower confidence limit (BMDL) values.[105,106]

The dataset included key physicochemical descriptors, such as aspect ratio, length, diameter, surface area, and surface functionalization, which reflect the intrinsic characteristics of each nanomaterial. Corresponding BMDL values, derived from previous transcriptomic dose–response analyses, quantified pathway-level biological responses

relevant to acute-phase signaling and aligned with adverse outcome pathways (AOPs). These BMDLs served as transcriptomic indicators of toxicological potency.

Table 3. Structural properties of MWCNTs and their $BMDL_{AR}$ values

Experimental data									
CNT	Physicochemical properties of the MWCNTs								Endpoint
	Pristine	OH	COOH	NH_2	Length [nm]	Diameter [nm]	Specific surface area [m^2/g]	Aspect ratio	$BMDL_{AR}$[µg/mouse]
NM-401	1	0	0	0	4050.0	67.0	18	60	0.17
NRCWE-026	1	0	0	0	850.0	11.0	246	77	0.58
NRCWE-048	1	0	0	0	1604.0	15.1	185	106	4.29
NRCWE-006	1	0	0	0	5700.0	65.0	26	88	5
NRCWE-047	1	0	0	0	532.5	13.0	216	41	8.91
NRCWE-049	1	0	0	0	731.1	13.9	199	53	9.34
NRCWE-043	1	0	0	0	771.3	26.7	82	29	8.57
NRCWE-046	1	0	0	0	717.2	17.2	223	42	10.76
NRCWE-045	1	0	0	0	1553.0	28.1	119	55	9.52
NRCWE-062	1	0	0	0	468.0	8.8	443	53	11.24
NRCWE-061	0	0	0	1	730.9	16.4	170	45	4.91
NRCWE-044	0	1	0	0	1330.0	32.6	74	41	14.46
NRCWE-064	0	0	1	0	213.6	7.5	445	29	14.85
NRCWE-063	0	1	0	0	345.4	14.2	426	24	15.46

Pristine – 1 means the absence of surface coatings, while 0 is the presence of functional groups, length/diameter – measured by SEM, surface area – measured according to the Brunauer-Emmet-Teller method, OH and COOH – the amount of functionality measured by CEA (assuming that all oxygen was OH- or COOH-group), $BMDL_{AR}$ – BMDL values for Acute phase signaling response pathway.

By combined dataset was used to develop QSAR models capable of predicting the biological impact of MWCNTs based on their physicochemical profiles.

4.1.3. METHODOLOGY USED

To develop the Nano-QSAR model, I employed the kernel-weighted local polynomial regression (KwLPR) method, which is particularly designed for reliable modeling with small datasets. The KwLPR approach is based on the assumption that the underlying function at any point in the dataset can be approximated by a low-degree polynomial, with the kernel function (k) determining the assigned weights to data points, giving importance to those closer to the target point (x_0), while weight decrease with increasing distance. By combining the simplicity of linear regression with the flexibility of nonlinear regression modeling, the KwLPR method builds a locally weighted linear model at each data point.[107] It focuses on observations within the nearest neighborhood, defined by the kernel function (K) and the smoothing parameter (bandwidth, h). The theoretical basis and detailed implementation of the KwLPR method are discussed in section 1.6.3

This Nano-QSAR model quantitatively links the structural features of 14 multi-walled carbon nanotubes (MWCNTs) to their biological activity, specifically targeting the acute phase response signaling pathway. Among the available descriptors, the model identified aspect ratio and specific surface area as the most predictive features. These were used as independent variables (X), while the transcriptomic BMDL values ($BMDL_{AR}$) served as the response variable (Y) to predict lung inflammation potential.

To prepare the dataset, I first ranked the MWCNTs in ascending order based on their $BMDL_{AR}$ values. This ranked dataset was then split into a training set (80%) and a validation set (20%) using a ratio-based approach.[108] Eleven MWCNTs were assigned to the training set for model development, while the remaining three were reserved for external validation. I performed this split manually to ensure that both subsets reflected the overall variability in the data, thereby supporting a more balanced and robust modeling process.

During model training, I evaluated several kernel types and tuned key parameters controlling the local neighborhoods to enhance the flexibility and performance of the KwLPR algorithm. Extensive modeling on the training data revealed that the best results

were obtained using an Epanechnikov kernel, a fixed bandwidth, and a non-zero constant polynomial degree. These hyperparameters were optimized using a leave-one-out cross-validation approach.

As the dataset does not cover the full diversity of carbon nanotubes, it is critical to verify whether a given material falls within the model's applicability domain before applying the model to novel CNTs. This step ensures that the predictions are both reliable and relevant for new materials.

Table 4. The detailed splitting data into the training and validation sets for the obtained KwLPR-based ten Nano-QSAR-AOP-anchored models.

MWCNTs	Splitting									
	M1	**M2**	**M3**	**M4**	**M5**	**M6**	**M7**	**M8**	**M9**	**M10**
NM-401	T	T	T	T	T	T	T	T	T	T
NRCWE-026	T	T	T	T	T	T	T	T	V	T
NRCWE-048	V	V	V	V	V	V	V	V	T	T
NRCWE-061	T	T	T	T	T	T	T	T	T	T
NRCWE-006	T	T	T	T	T	T	T	T	T	V
NRCWE-043	T	T	T	T	T	T	T	T	V	T
NRCWE-047	V	V	T	T	V	V	T	T	T	V
NRCWE-049	T	T	T	V	T	V	V	T	T	T
NRCWE-045	T	T	V	T	T	T	T	V	T	T
NRCWE-046	T	V	T	T	T	T	T	T	V	T
NRCWE-062	T	T	T	T	T	T	T	T	T	T
NRCWE-044	T	T	T	T	T	T	T	T	T	T
NRCWE-064	V	T	T	T	T	T	V	V	T	T
NRCWE-063	T	T	V	V	V	T	T	T	T	V

T = training set, V = validation set, M = number of models

I undertook several measures to ensure the robustness of the modeling results. These steps were designed to minimize the risk of random correlations and to ensure the findings were

not dependent on a single division of the dataset into training and test sets but rather reflect an overall trend in the data. To support the validity of aspect ratio and specific surface area as key predictors of acute inflammatory responses, I developed 10 individual Nano-QSAR models, each using different training and test set compositions. The full details of these models are provided in Tables 4, 5 and 6.

Furthermore, to evaluate the reliability of the non-linear regression model, I applied a distance-based probability ($AD_{ProbDist}$) applicability domain (AD) to assess the model prediction uncertainty (refer to section 1.5.2.5). In addition, I used a more straightforward approach, partial dependence plots (PDPs), to interpret feature importance in the developed Nano-QSAR model.

4.1.4. RESULTS AND DISCUSSION

An AOP-informed Nano-QSAR model was developed using the KwLPR algorithm to quantitatively link the physicochemical properties of 14 MWCNTs with the BMDL values associated with the **'**acute phase response signaling' pathway, a key indicator of pulmonary inflammation. The characteristics of these MWCNTs are summarized in Table 3 and include length (nm), diameter (nm), specific surface area (m^2/g), and aspect ratio (length-to-diameter ratio).

Additionally, a few of the nanotubes also have different surface-modified functional groups (surface was modified by -COOH, $-NH_2$, and -OH), which might alter their surface properties and interactions with biological systems, which can enhance or reduce the toxicity of MWCNTs.[109] In addition to their core properties, several MWCNTs in the dataset featured surface modifications with functional groups such as -COOH, $-NH_2$, and -OH**,** which are known to influence surface reactivity and biological interactions. These modifications may enhance or mitigate the toxic potential of MWCNTs by altering their bioavailability and cellular uptake.

While the study is limited to a panel of 14 MWCNTs, one should be aware that this small dataset does not capture the full diversity of carbon nanotube structures and

properties. However, the data-driven model developed in this study is based on currently available and experimentally consistent datasets for these 14 MWCNTs. It is important to emphasize that the reliability and predictive accuracy of data-driven models depend heavily on the consistency and quality of the input data. All data should be measured using the same standardized protocols to minimize bias and variability. Incorporating data from various sources can introduce inconsistencies that may challenge the model's robustness. Therefore, I prioritized developing a model that meets strict criteria, even though this approach may limit the size of the studied nanotubes.

To maximize variability within the dataset, I included both pristine and functionalized MWCNTs, with various groups, such as -OH, -COOH, and -NH2. Additionally, nanotubes were selected to differ in critical parameters (including aspect ratio and surface area) to ensure that the dataset captured a representation range of relevant properties, despite its limited sample size. Considering the significance of aspect ratio as a crucial structural property influencing MWCNT-induced lung inflammation, it was pre-selected as a key descriptor in the model. Alongside aspect ratio, the specific surface area (BET) was identified as the relevant descriptor based on both literature evidence and expert knowledge.[73] These two descriptors were ultimately used to build the final Nano-QSAR model.

Building on the selection of aspect ratio and specific surface area as key descriptors, the resulting models demonstrated consistently strong statistical performance. Goodness-of-fit values (R^2) ranged from 0.87 to 0.94, while predictive performance metrics (Q^2_{F1} = 0.76 - 0.92, Q^2_{F2} = 0.72 - 0.94, and Q^2_{F3} = 0.75 - 0.97) confirmed the model's predictive reliability. This rigorous approach reinforces the robustness of our findings and confirms that the observed trends are generalizable across different data splits. Details of the individual models, along with the models' quality metrics, are provided in Table 6.[76,77] The modeling strategy adopted also appears to be an optimal solution for analyzing variance in performance estimation, particularly given the sensitivity of classical cross-validation approaches when applied to small training dataset sizes. It is important to note that the

removal of a few data points, or even a single data point, as in the leave-many-out or leave-one-out cross-validation procedures, does not necessarily lead to a consistent estimate of the model. This is especially true when the size of the training dataset is limited.

Table 5. The best Nano-QSAR model experimental versus predicted BMDL values

CNTs	Aspect ratio	Specific surface area	Experimental $BMDL_{AR}$	Predicted $BMDL_{AR}$	Set
NM-401	60.45	18	0.17	1.56	T
NRCWE-026	77.27	245.8	0.58	0.58	T
NRCWE-061	44.5	170.4	4.91	6.56	T
NRCWE-006	87.69	26	5	3.61	T
NRCWE-043	28.86	82	8.57	11.15	T
NRCWE-049	52.79	199	9.34	8.60	T
NRCWE-045	55.33	119	9.52	9.64	T
NRCWE-046	41.65	223	10.76	10.19	T
NRCWE-062	53.07	443.2	11.24	12.23	T
NRCWE-044	40.86	74	14.46	11.66	T
NRCWE-063	24.36	426.4	15.46	14.47	T
NRCWE-048	106.37	185	4.29	5.00	V
NRCWE-047	41.09	216	8.91	9.89	V
NRCWE-064	28.62	445.2	14.85	13.43	V

Table 6. The detailed statistics of the obtained KwLPR-based predicted ten Nano-QSAR-AOP-anchored models

No.	R^2	MAE	RMSEc	Q^2_{F1}	Q^2_{F2}	Q^2_{F3}	CCC	$RMSE_p$	AAE
Model-1	0.91	1.20	1.47	0.94	0.94	0.95	0.92	1.08	1.04
Model-2	0.89	1.55	1.79	0.88	0.88	0.97	0.91	0.95	0.90
Model-3	0.94	0.76	1.17	0.89	0.87	0.88	0.86	1.63	1.50
Model-4	0.92	0.92	1.34	0.86	0.84	0.85	0.83	1.81	1.53
Model-5	0.90	1.25	1.51	0.89	0.87	0.88	0.86	1.62	1.46
Model-6	0.94	0.30	0.59	0.85	0.82	0.96	0.79	0.98	0.96
Model-7	0.91	1.18	1.45	0.82	0.81	0.84	0.81	1.90	1.58
Model-8	0.92	1.07	1.37	0.78	0.76	0.80	0.78	2.13	1.89
Model-9	0.87	1.65	1.75	0.78	0.72	0.75	0.69	2.33	2.18
Model-10	0.92	1.00	1.39	0.76	0.72	0.77	0.85	2.27	1.85

R^2 = goodness of fit (determination coefficient), Q^2_{F1}, Q^2_{F2}, Q^2_{F3} = predictive ability (external validation coefficient), CCC = concordance correlation coefficient, MAE = mean absolute error, RMSE = root mean square error for the training set (RMSEc), and the validation set ($RMSE_p$), AAE = average absolute error.

To assess the predictivity and reliability of the Nano-QSAR model by the principles outlined by the OECD, I conducted a thorough examination using various internal and external validation metrics for the selected model with the best statistics. These metrics encompass measures of goodness-of-fit, external predictive power, and error-based indicators, as referred to in Table 6. According to the OECD principles for the validation of QSAR models, the developed model was of acceptable quality, as demonstrated by Table 6 metrics and the scatter plot (Figure 8) of the experimental versus predicted values. The training set and validation set data points were clustered around the trend line, indicating that the model was successful in its predictions.

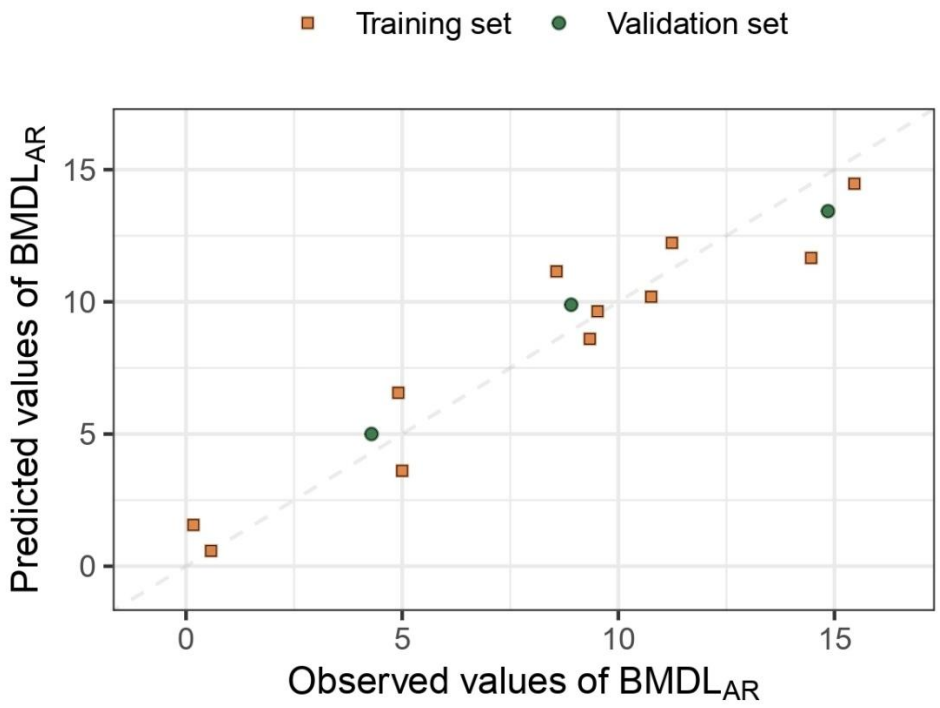

Figure 8. A scatter plot of the experimental observed versus predicted $BMDL_{AR}$ values for training and validation compounds using the Nano-QSAR model based on the structural properties, including aspect ratio and specific surface area. Usually, the color code is measured, green – training set, orange – validation set, for model calibration and validation.

The predictive uncertainty of the KwLPR-based model was further evaluated using the $AD_{ProbDist}$ approach to assess its applicability domain.[110] The analysis (Figure 9) demonstrated that all the compounds studied fell within the optimal prediction space (i.e., the green zone). Based on these observations, the KwLPR-based Nano-QSAR model is highly applicable for predicting lung inflammation associated with the 'acute phase response signaling' pathway perturbed following exposure to MWCNTs investigated in the study.

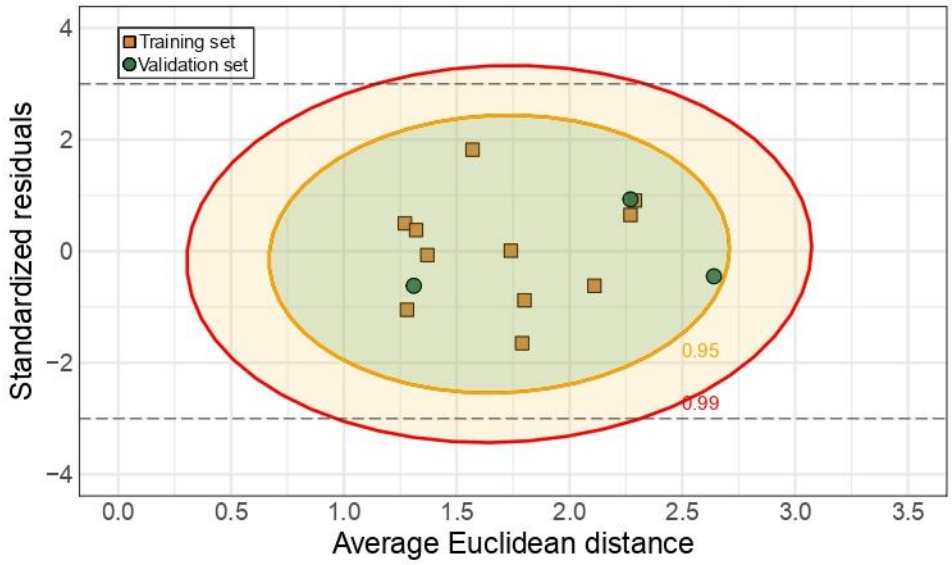

Figure 9. The applicability domain of the Nano-QSAR model is estimated by the probability-oriented distance-based approach ($AD_{probDist}$).

Significance of selected descriptors in the modeled response

According to OECD principle 5, providing a mechanistic interpretation of QSAR model predictions is essential whenever possible. However, in the case of KwLPR method, do not provide the cause-effect relation equation for a quantitative understanding of model descriptors and response activity. Thus, I adopted a partial dependence plot (PDPs), Figure 10.[111] The PDP plot visualizes the relationship between a specific explanatory feature (i.e. aspect ratio and surface area) and the predicted outcome of the model (here: $BMDL_{AR}$) while marginalizing over the other features. This approach enables us to understand the individual contribution of each feature to the model prediction and to determine whether the relationship between the target response and feature is linear or more complex. In this plot, the Y-axis represents the mean predicted response (in our case, $BMDL_{AR}$), while the X-axis denotes the range of the values for the given descriptor.

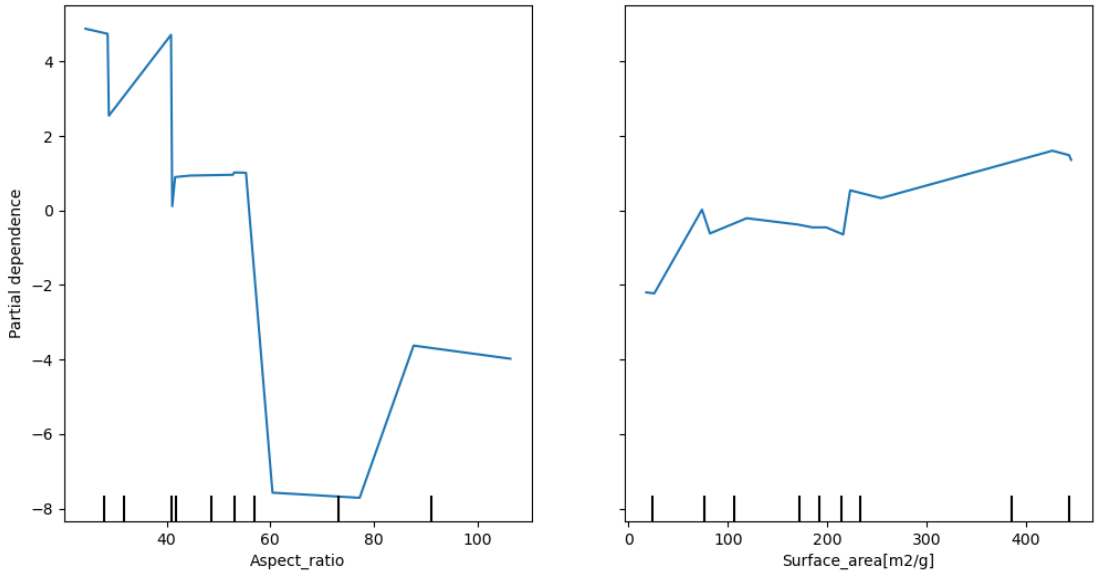

Figure 10. A) Illustrates the PDP for the aspect ratio of MWCNTs. B) Illustrates the PDP for the surface area of MWCNTs. The x-axis represents the feature (A - surface area, B - aspect ratio), while the y-axis shows the partial dependence of the predicted $BMDL_{AR}$ values.

As shown in Figures 10A and 10B, the magnitude of changes in the model prediction associated with aspect ratio is substantially greater than that observed for surface area. Therefore, I conclude that the aspect ratio strongly influences $BMDL_{AR}$. Previous studies support this finding, suggesting that the aspect ratio might be a significant factor in CNT-induced pulmonary toxicity. Aspect ratio affects the ability of carbon nanotubes to penetrate cells, tissues, and organelles, thereby increasing their potential to cause cellular damage and trigger inflammatory responses.[112,113]

Further straightforward analysis is that the relationship between the aspect ratio of the set of 14 MWCNTs and their effect on the acute phase response signaling pathway suggests that nanotubes with lower aspect ratios have less impact (i.e., higher BMDL values are required to induce perturbation in the pathway) compared to those with high-aspect-ratio nanotubes. This trend, at least, is evident when comparing MWCNTs with an aspect ratio less the 60 to those between 60 and 80 length-to-diameter ratios. As shown in Figure 11, this pattern is clearly visible $BMDL_{AR}$ values against aspect ratio. For instance,

NRCWE-063, NRWE-064, and NRWE-044, these carbon nanotubes have the lowest aspect ratios, which require the highest doses to disrupt the pathway. In contrast, NM 401 and NRCWE-026, which have aspect ratios of 60.45 and 77.27, respectively, are the most toxic.

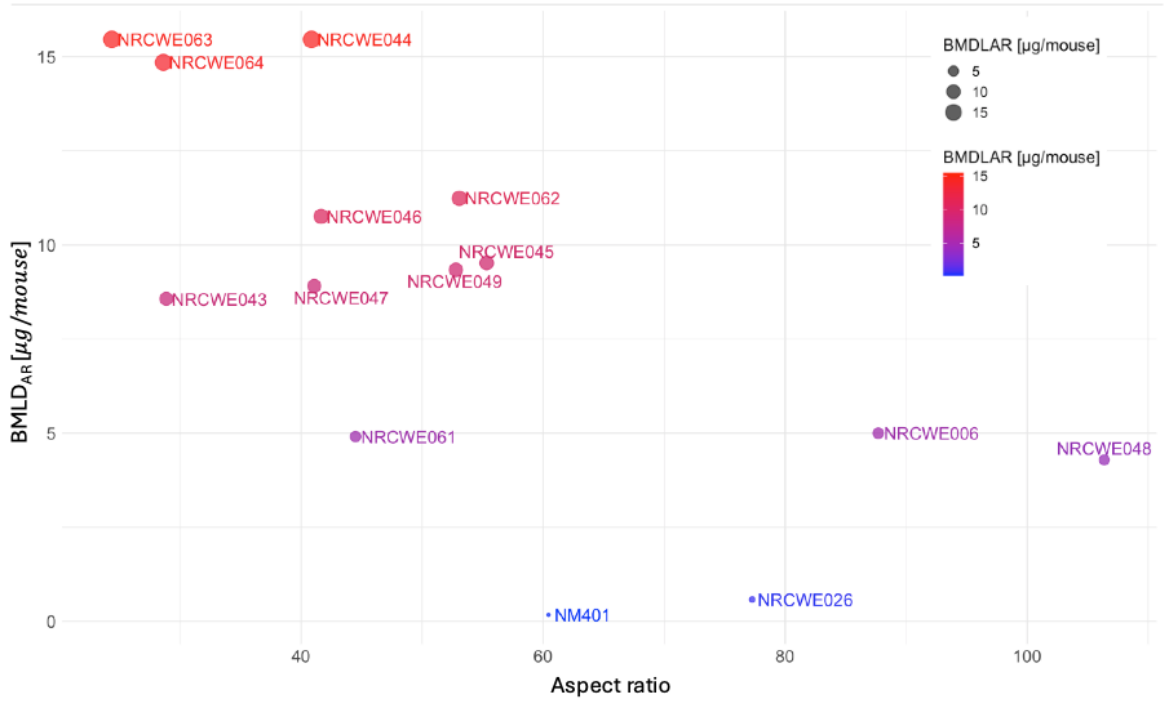

Figure 11. Exploring the impact of aspect ratio characterizing multi-walled carbon nanotubes on acute phase response (AR) pathway ($BMDL_{AR}$). The size and color of the dots correspond to $BMDL_{AR}$: the biggest red dots refer to the highest doses (less toxic), while the smallest blue dots refer to the lowest doses (high toxic).

While the PDP plots highlight that the aspect ratio is of primary importance concerning the effects of the studied MWCNTs on the acute phase response signaling pathway, the surface area also has an influence. The machine learning-driven analysis, as shown in Figure 10B supported by Figure 12, suggests, however, that this relationship is not straightforward. This contrasts with earlier findings based on the Pearson correlation coefficient, where the BET surface area was strongly associated with the acute phase signaling pathway. One possible reason for this discrepancy is the difference in how the acute phase response was defined. In Danielsen et al.'s study[104], toxicity was assessed based

on SAA3 protein levels, whereas our analysis used BMDL values derived from the set of genes associated with the pathway. Interestingly, there are nanotubes with very different specific surface areas that show similar effects on the pathway. For example, NM 401 and NRCWE-026 both exhibit the lowest $BMDL_{AR}$ values, 0.17 µg/mouse and 0.58 µg/mouse, respectively, indicating high toxicity. Yet, NM-401 has the smallest BET surface area (18.0 m^2/g) among the studied materials, while NRCWE-026 has one of the largest BET surface areas (245.8 m^2/g). This suggests that specific surface area alone does not explain the observed toxic effects. Other factors such as rigidity, surface functionalization and surface chemistry may significantly influence the toxicity of MWCNTs.

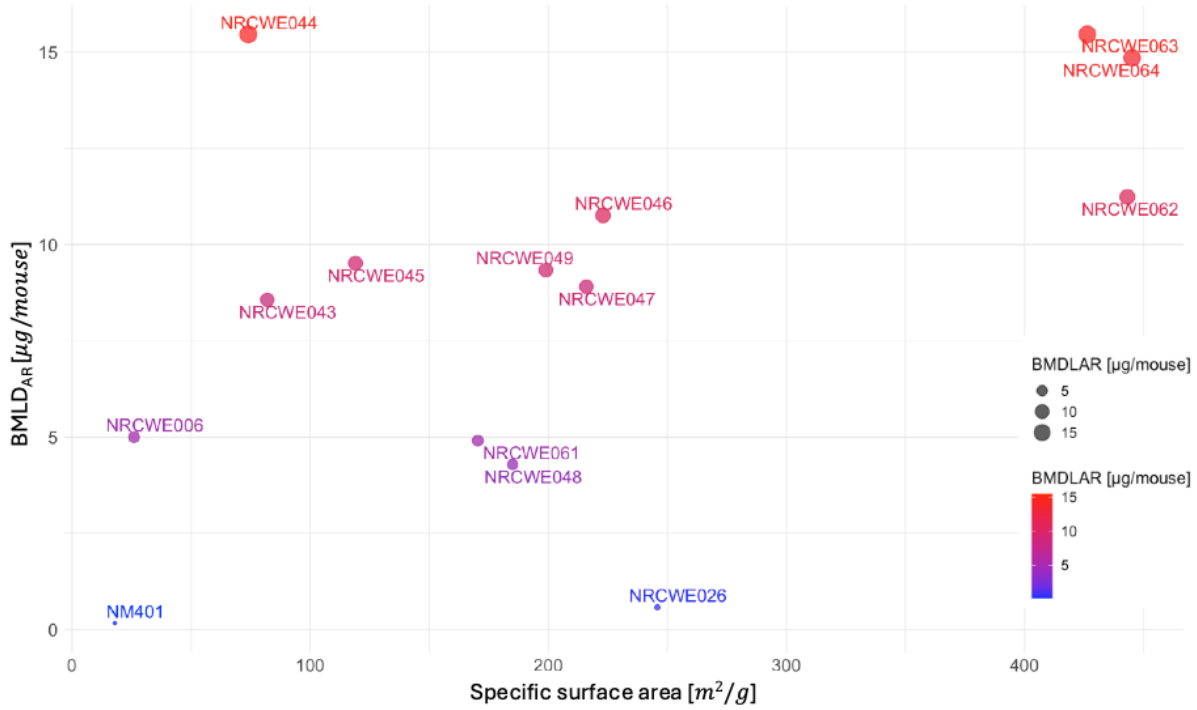

Figure 12. Exploring the impact of specific surface area characterizing multi-walled carbon nanotubes on $BMDL_{AR}$. The size and color of the dots correspond to $BMDL_{AR}$: the biggest red dots refer to the highest.

To better understand how aspect ratio and surface area jointly influence biological responses, I have additionally examined their combined effects. By plotting the studied MWCNTs in a two-dimensional space defined by aspect ratio vs. specific surface area, I was able to visualize potential synergistic effects. In this plot visualization (Figure 13),

each nanotube is represented by a dot whose size and color reflect its toxicity: larger green dots indicate less toxic materials (requiring higher doses), while smaller red dots indicate more toxic ones (requiring lower doses). An arrow marks the direction of increasing toxicity across the plot, highlighting the combined influence of both descriptors.

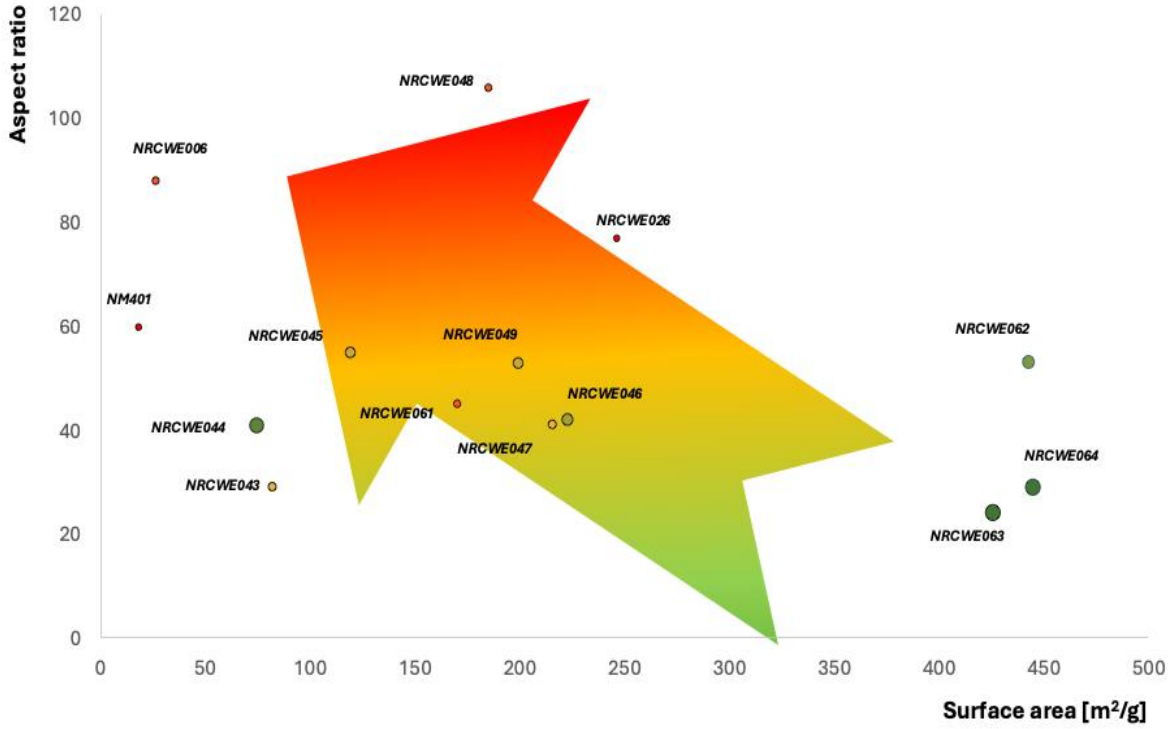

Figure 13. Exploring the impact of standardized aspect ratio and surface area characterizing multi-walled carbon nanotubes on $BMDL_{AR}$. The size and color of the dots correspond to $BMDL_{AR}$: the biggest green dots refer to the highest doses (less toxic), while the smallest red dots refer to the lowest doses (high toxic). Arrow presents the trend of increasing toxicity.

Nanotubes characterized by lower aspect ratios and higher specific surface areas generally exhibit reduced toxicity in relation to their ability to perturb the acute phase signaling pathway. For example, NRCWE064 and NRCWE063 required significantly higher doses to induce a measurable toxic response. In contrast, nanotubes with the highest aspect ratios, commonly referred to as high-aspect-ratio MWCNTs (e.g., NRCWE006, NRCWE048, and NRCWE026), were demonstrated to be significantly more toxic. These nanotubes required much lower doses to induce pathway perturbation, consistent with

previous studies suggesting that higher aspect ratios enhance the capacity of CNTs to penetrate cellular and tissue barriers, increasing their potential to penetration increases their potential to cause cellular damage and trigger inflammatory responses.

This study confirms that both the aspect ratio and specific surface area play roles in shaping the effects of MWCNTs on the acute phase response signaling. These properties are, therefore, important determinants of CNT-induced inflammation, which may contribute to the development of lung and cardiovascular pathologies, as outlined in AOP33 and AOP237. Inflammation and acute phase response represent early key events within these AOP, linking the inhalation of various engineered nanomaterials, including CNTs, to adverse outcomes such as fibrosis, atherosclerosis and cancer.[114–116]

However, it is important to note that the current findings do not explain all biological interactions that may occur following inhalation and the subsequent onset of pulmonary toxicity. Some nanotubes deviate from the observed trends, suggesting that additional factors may modulate the toxic response. These include structural rigidity, surface modifications and the presence of residual metal purities, and the formation of a protein corona.

The protein corona, which forms when nanoparticles interact with biological fluids, can alter their identity, biodistribution, and cellular uptake, thereby significantly altering their toxicological profiles.[71,117] The composition and dynamics of the protein corona depend on both the physicochemical properties of the nanomaterials (e,g., surface charge, functional groups, hydrophobicity) and the biological environment. Inhaled CNTs rapidly adsorb lung surfactant proteins and other serum proteins[104] potentially modifying surface features that drive cellular interactions. As such, inter-individual or material-specific variations in protein corona formation may help explain inconsistencies in pulmonary toxicity outcomes.

The rigidity of MWCNTs, particularly in high aspect ratio structures, has been linked with their ability to induce frustrated phagocytosis in macrophages, which can lead to chronic inflammation and granuloma formation. Surface chemistry and functionalization

also significantly influence CNT toxicity. Functional groups such as -COOH or -OH can enhance water solubility and improve dispersion, thereby modifying how these materials interact with cells. These modifications may also increase MWCNT reactivity with cellular components, exacerbating oxidative stress and inflammatory responses under certain conditions.[118]

Metal impurities are often retained from the synthesis process, further contribute to MWCNT toxicity. Transition metals such as iron, nickel, and cobalt, commonly used as catalysts, can persist even after purification and catalyze the formation of reactive oxygen species (ROS), thereby intensifying oxidative stress and promoting the release of pro-inflammatory cytokines.[104] For example, elements like manganese (Mn) and iron (Fe) have been associated with increased neutrophil influx, a hallmark of inflammation, shortly after exposure, while nickel (Ni) has been linked to a reduced inflammatory response over time. These observations suggest that the type and quantity of residual metal impurities can modulate the CNT toxicity, possibly by influencing ROS generation and associated biological pathways.

Additionally, the chirality of CNTs, a property for which data were not available in this study, may also play a role in determining their toxicological profiles. This limitation emphasizes the need for future investigations to evaluate the influence of the chirality of MWCNT-induced responses.

In conclusion, the toxicological behavior of MWCNTs is multifaceted, shaped by complex interactions among various physicochemical characteristics, including aspect ratio, surface area, rigidity, surface chemistry, metal impurities and potential chirality. Achieving a deeper mechanistic understanding of these interdependencies is crucial for the rational design of safer nanomaterials in industrial and biomedical applications. Thus, further research and investigations into the mechanistic pathways and biological interactions underlying the MWCNTs-induced inflammatory response are warranted.

In conclusion, this study employed a non-linear machine learning regression approach to develop an AOP-anchored Nano-QSAR model, aimed at investigating how the

structural characteristics of 14 MWCNTs influence lung inflammation at the tissue level. These results highlighted the critical role of aspect ratio and specific surface area as key drivers in initiating acute inflammation processes, which may subsequently progress to fibrosis and atherosclerosis through the acute phase response signaling pathway.

By integrating AOP concepts within the Nano-QSAR framework, this study provides mechanistic insights into the toxicological effects of nanomaterials, effectively linking structural properties with biological outcomes. These results not only deepen our understanding of MWCNT-induced pulmonary toxicity but also highlight the utility of AOP-informed models as new NAMs in nanomaterial hazard assessment. Ultimately, this work advances safer-by-design strategies and contributes to regulatory initiatives aimed at improving the risk assessment of ENMs.

4.2. Grouping-based on the Physicochemical Properties Drives Differences in Transcriptomic Responses Induced by Single- and Multiwalled Carbon Nanotubes Following Inhalation Exposure

4.2.1. SPECIFIC OBJECTIVES AND SUBJECT OF RESEARCH

In line with the second objective of this research (see section 2.3), the work presented in Section 4.2 aims to achieve the following:

OBJECTIVE 2.

To quantitatively compare S- and MWCNTs in terms of their structural properties and associated impact on the acute phase response signaling pathway, with the aim of identifying shared characteristics and gene expression profiles that may help explain their similar modes of action (MoA) related to pulmonary and cardiovascular pathologies.

4.2.2. EXPERIMENTAL DATA

To support this comparative analysis, the data set used in Section 4.1 was expanded to include a total of 21 CNTs, comprising both SWCNTs and MWCNTs (Table 7).[100,101,103–106] Specifically, seven SWCNTs (NRCWE-051 to NRCWE-057) and four MWCNTs (NRCWE-061 to NRCWE-064) were sourced from Timesnano (Chengdu Organic Chemicals Co. Ltd., China). An additional, seven MWCNTs (NRCWE-043 to NRCWE-049) were obtained from Cheaptubes (Brattleboro, VT, USA). NM-401 was provided by the European Joint Research Centre (JRC), Ispra, Italy; NRCWE-026 was sourced from Nanocyl (Sambreville, Belgium), and NRCWE-006 (Mistui-7) was generously provided by Mitsui, Tokyo, Japan.

Table 7. Physicochemical properties of single and multi-walled carbon nanotubes (S- and MWCNTs)

Physicochemical properties of S- and MWCNTs																	
Type	**Name**	**Aspect ratio**		**BET**	**Functionalization**				**Composition**				**Metal Content**				
		Length	**Diameter**		**Pristine**	**OH**	**COOH**	**NH_2**	**C**	**H**	**N**	**O**	**MgO**	**MnO**	**Fe_2O_3**	**CoO**	**NiO**
SWCNTs	NRCWE-051	0	1	442.6	1	0	0	0	90.2	0.12	0.08	1.8	0.04	0	1.63	1.08	0.06
	NRCWE-052	0	1	405.7	1	0	0	0	92.9	0.16	0.03	1.3	0.03	0.01	1.05	1.23	0.12
	NRCWE-053	0	1	367.8	0	1	0	0	88.2	0.18	0.24	3	0.02	0.02	0.85	3.82	0.1
	NRCWE-054	0	1	370.8	0	0	1	0	87.9	0.18	0.19	4.8	0.03	0	1.59	3.81	0.13
	NRCWE-055	0	1	453.1	1	0	0	0	91.9	0.2	0.08	2.5	0.03	0.03	4.39	1.33	0.05
	NRCWE-056	0	1	356.7	0	1	0	0	89.6	0.21	0.22	4.4	0.04	0.03	1.26	3.65	0.1
	NRCWE-057	0	1	281.6	0	0	1	0	83.1	0.37	0.22	9.6	0.18	0.04	2.2	2.74	0.14
MWCNTs	Mitsui7	5730	74	26	1	0	0	0	98.1	0.69	0.02	0.1	0.01	0	0.08	0	0
	NM-401	4048	67	18	1	0	0	0	98	0.69	0.01	0	0.01	0	0.05	0	0
	NRCWE-026	847	11	254	1	0	0	0	85.5	0.15	0.01	1.3	0	0	0.29	0.11	0
	NRCWE-043	771.3	55.6	82	1	0	0	0	96	0.69	0.04	0.2	0.01	0	0.01	0	1.2
	NRCWE-044	1330	32.7	74	1	0	0	0	96.1	0.79	0.02	0.2	0.02	0	0	0	1.04
	NRCWE-045	1553	30.2	119	1	0	0	0	91.6	0.69	0.04	0.6	0.02	0	1.17	0.25	1.34
	NRCWE-046	717.2	29.1	223	1	0	0	0	95.1	1.39	0.02	0.6	0.22	0.3	0.01	0.25	0
	NRCWE-047	532.5	22.6	216	1	0	0	0	96.1	1.09	0.02	0.3	0.22	0.3	0.01	0.25	0
	NRCWE-048	1604	17.9	185	1	0	0	0	95.3	1.79	0.04	0.6	0.19	0.28	0.01	0.24	0
	NRCWE-049	731.1	14.9	199	1	0	0	0	96	1.49	0.07	0.3	0.19	0.29	0	0.25	0
	NRCWE-061	730.85	16.42	170.4	0	0	0	1	96.5	0.22	0.65	0.7	0.01	0.01	0.59	0	1.97
	NRCWE-062	468	8.82	443.2	1	0	0	0	89.1	0.17	0.44	4.2	0.07	0	0.58	4.6	0.22
	NRCWE-063	345.35	14.18	426.4	0	1	0	0	88.2	0.14	0.38	4.3	0.07	0.02	1.95	5.88	0.49
	NRCWE-064	213.62	7.46	445.2	0	0	1	0	88.4	0.17	0.17	5.1	0.03	0.03	1.8	5.51	0.3

BET = specific surface area (m^2/g), C = carbon (% w/w), H = hydrogen (% w/w), N = nitrogen (% w/w), O = oxygen (% w/w)

The dataset included key physicochemical descriptors, such as aspect ratio (length and diameter), specific surface area (BET), surface functionalization (pristine, hydroxy (-OH), carboxyl (-COOH), amine (-NH_2)), chemical composition (C, H, N, O), metal impurities (Fe_2O_3, CoO, NiO, MgO, MnO). These parameters reflect the intrinsic properties of each nanomaterial and are hypothesized to influence their biological activity.

To link structural features with toxicological outcomes, previously published BMDL values were incorporated. These values, derived from transcriptomic dose–response analyses, quantify pathway-level activation of the acute phase response signaling pathway, aligned with relevant adverse outcome pathways (AOPs). As such, these BMDLs serve as transcriptomic indicators of toxicological potency. By integrating physicochemical and biological response data, this dataset enables a comparative mechanistic analysis aimed at identifying both shared and distinct structural features that influence acute phase signaling pathway across SWCNTs and MWCNTs.

4.2.3. METHODOLOGY USED

In this study, transcriptomic data analyses using advanced chemometrics methods such as unsupervised clustering and supervised machine learning, provide insights into the potential toxicity and biological impacts of CNTs. Hierarchical cluster analysis (HCA)[119,120], a multivariate method, is commonly used to visualize hierarchical clustering and grouping based on their physicochemical property similarities through heatmaps. Furthermore, the comparative analysis of the physicochemical properties of S- and MWCNTs and their inflammatory responses, a correlation matrix was constructed using Pearson's correlation method and represented through a radar plot. Additionally, principal component analysis (PCA)[120] was performed to explore the data structure by identifying similarities and dissimilarities among variables, object positions, grouping tendencies and outliers.

4.2.4. RESULTS AND DISCUSSION

To achieve the study objectives, a total of 21 single-walled and multi-walled carbon nanotubes (S- and MWCNTs) were analyzed following a standardized single-dose inhalation exposure (54 μg/ per mouse), with transcriptomic responses assessed on day 1 post-exposure. This consistent experimental design allowed us to focus on early biological responses reflective of acute toxicity.

The primary aim of this analysis was to elucidate the relationship between the physicochemical characteristics of CNTs and their toxicological potency, particularly the activation of the acute phase response (AR) pathway. Table 7 summarizes the key structural and compositional features of the studied CNTs, including aspect ratio, specific surface area, functional groups, elemental composition, and metal impurities. The results presented in this section are organized into two complementary parts: (1) a similarity-based investigation of structural and chemical consistency among the CNTs, and (2) a comparative mechanistic analysis of how these properties relate to transcriptomic responses and inflammatory signaling pathways.

Investigating Structural and Chemical Consistency in Carbon Nanotubes: A Similarity-based Perspective

To build on the earlier analysis of physicochemical influences on transcriptomic responses, this section explores the intrinsic structural and chemical similarities among CNTs. Using hierarchical cluster analysis (HCA) with heatmap visualization (Figure 14), I evaluated independent physicochemical properties such as specific surface area, elemental composition (C, H, N, O), and metal oxide content (MgO, MnO, Fe_2O_3, CoO, NiO) across the panel of 21 S- and MWCNTs. Unsupervised analysis identified six distinct similarity-based clusters, providing an integrated view of structural heterogeneity and potential shared features that may drive comparable biological outcomes.

Cluster 1: Hydroxyl (-OH) Functionalized S- and MWCNTs with Moderate Metal Content

This cluster includes both single- and multi-walled carbon nanotubes (NRCWE-063, NRCWE-053, and NRCWE-056) functionalized with hydroxyl (-OH) groups. These CNTs exhibit high specific surface areas, ranging from 356.7 to 426.4 m^2/g, and moderately elevated levels of metal oxides, particularly Fe_2O_3 and CoO. For instance, NRCWE-056 contains 4.42% oxygen, confirming successful hydroxylation. Hydroxyl functionalization enhances hydrophilicity and improves dispersion in aqueous environments, such as biological media. This facilitates cellular uptake and increases interactions with biomolecules. Additionally, the presence of transition metals like iron and cobalt can catalyze Fenton-like reactions, promoting the generation of reactive oxygen species (ROS). These ROS can damage cellular macromolecules and activate pro-inflammatory signaling cascades.[10,11,121] As such, CNTs in this cluster demonstrate elevated biological reactivity and a moderate to high toxicological potential.

Cluster 2: Carboxyl (-COOH) Functionalized S- and MWCNTs with High Oxidative Potential

Cluster 2 comprises carboxyl-functionalized CNTs (NRCWE-057, NRCWE-064, and NRCWE-054) with similarly high specific surface areas (e.g., 445.2 m^2/g for NRCWE-064) and moderate amounts of transition metals, including Fe_2O_3 and CoO. High oxygen content confirms extensive surface oxidation. Carboxyl groups impart a strongly acidic surface character, promoting electrostatic interactions with positively charged biomolecules such as cell membranes and serum proteins.[105,106] This enhances internalization and tissue penetration, potentially leading to greater intracellular disruption. Compared to hydroxylated CNTs, carboxylated CNTs exhibit higher polarity and acidity, which may drive more pronounced oxidative stress and inflammation.[102] Overall, this cluster is associated with a high level of biological reactivity and potential toxicity.

Cluster 3: **Pristine MWCNTs with High Metal Content and Low Functionalization**

This cluster includes unfunctionalized MWCNTs (NRCWE-046, -047, -048, -049), characterized by high carbon purity (>95%) and significant metal oxide content, particularly MgO and MnO. They possess moderate specific surface areas (199–223 m^2/g)

and minimal oxygen and nitrogen content. Although chemically inert due to a lack of functional groups, these CNTs are not biologically benign. Their hydrophobic nature and poor dispersion in biological media encourage agglomeration, which may impair phagocytic clearance and promote biopersistence. Furthermore, elevated levels of transition metals can sustain ROS production and provoke chronic low-grade inflammation. Hence, despite their low intrinsic surface reactivity, these CNTs may exert significant long-term toxic effects.

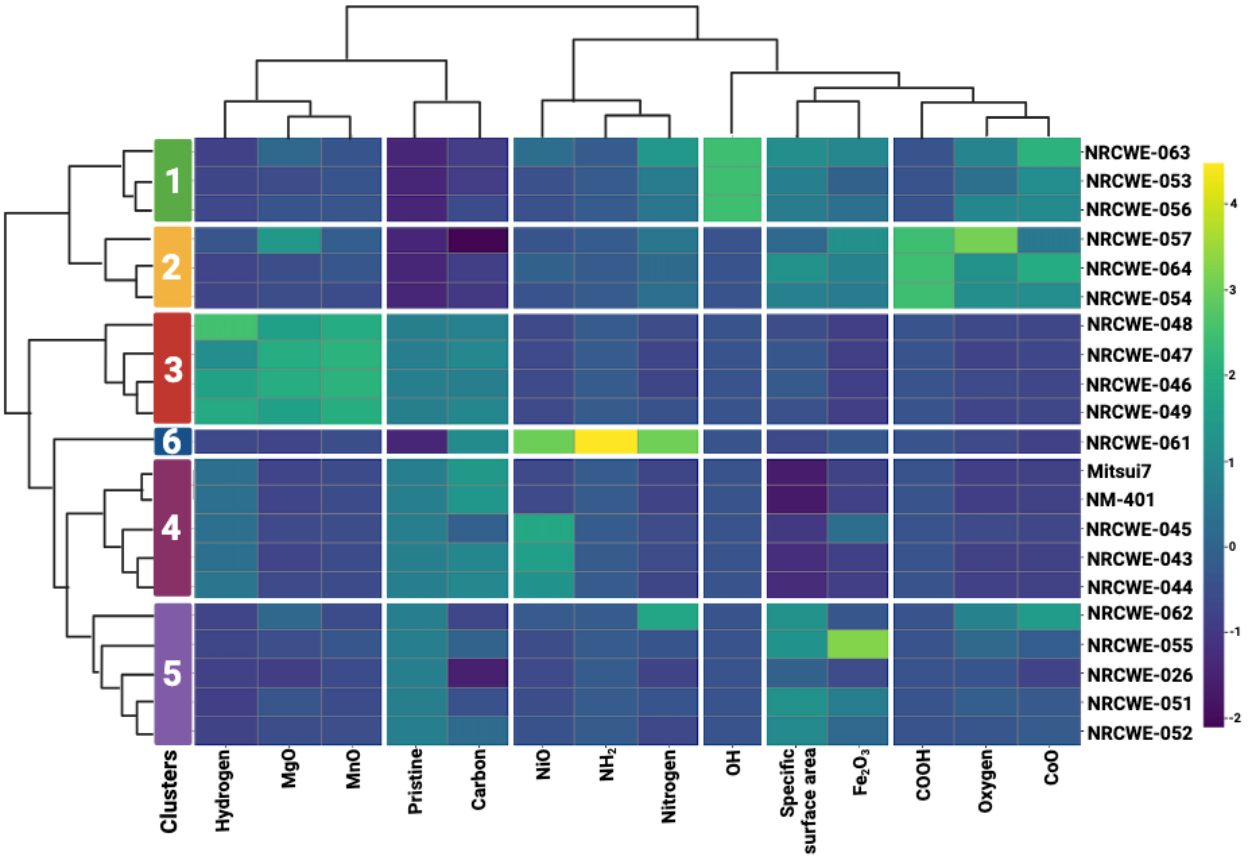

Figure 14. The heat map represents the impact of the physicochemical properties of S- and MWCNTs on their adverse responses between similarities and dissimilarities (Euclidean distance and Ward method for clustering).

Cluster 4: Pristine MWCNTs with low specific surface areas and metal contents

Cluster 4 comprises several well-characterized MWCNTs, including NRCWE-043, -044, -045, NM-401, and Mitsui-7. These materials are defined by high carbon purity (96–98%), large diameters, low specific surface areas (18–119 m^2/g), and negligible metal content.

The low reactivity of these CNTs results from their chemical inertness, yet their physical attributes confer a different kind of hazard. Their large diameters and structural rigidity hinder phagocytic uptake, often leading to frustrated phagocytosis and prolonged retention in pulmonary tissues. While chemical toxicity is low, their bio-persistence and mechanical interactions with alveolar structures may promote granuloma formation and fibrotic remodeling.[122] This underscores the importance of physical structure, not just surface chemistry, in evaluating CNT safety.

Cluster 5: Pristine S- and MWCNTs with high specific surface area and moderate metal content

This cluster includes both pristine single- and multi-walled CNTs (NRCWE-026, -051, -052, -055, -062) with high specific surface areas (>250 m^2/g) and moderate concentrations of metal oxides, especially Fe_2O_3 and CoO. Despite lacking chemical functionalization, their large surface areas enhance interactions with biological membranes and proteins. This can increase the likelihood of cellular uptake and immune activation. Transition metal impurities further elevate ROS production, contributing to oxidative stress (Soto et al., 2007). Notably, NRCWE-055, with a surface area of 453.1 m^2/g and 4.39% Fe_2O_3, has demonstrated robust inflammatory responses *in vivo* (Poulsen et al., 2015).[101] This cluster exemplifies how pristine CNTs can be toxic via physicochemical mechanisms unrelated to surface functional groups.

Cluster 6: Amine (-NH_2) functionalized MWCNT with moderate metal content

This cluster is uniquely represented by NRCWE-061, an MWCNT functionalized with amine (-NH_2) groups and containing 1.97% NiO. The amine functionalization imparts a positive surface charge, promoting strong electrostatic interactions with negatively charged biomolecules such as DNA, proteins, and cell membranes. These interactions can

significantly enhance cellular uptake and activate pro-inflammatory pathways. Moreover, the presence of nickel oxide, a known immunotoxicant, raises concerns about immune hypersensitivity and oxidative injury (Pacurari et al., 2008).[123] The combined effects of electrostatic reactivity and metal-driven immunotoxicity suggest that this CNT possesses high potential for immune modulation and pulmonary inflammation.

The six identified clusters of carbon nanotubes (CNTs) reflect distinct physicochemical profiles that influence their biological interactions and toxicological outcomes. Clusters 1 and 2, comprising hydroxyl- and carboxyl-functionalized CNTs respectively, exhibit high surface reactivity and enhanced aqueous dispersibility, contributing to increased cellular uptake and a strong potential for oxidative stress and inflammation. In contrast, Cluster 3 includes pristine MWCNTs with high metal content but low surface functionalization; while chemically inert, these CNTs are toxic due to poor clearance and sustained ROS generation from metal contaminants. Cluster 4 represents pristine MWCNTs with low surface area and minimal metal content; their large diameter and rigidity reduce phagocytic uptake, leading to frustrated phagocytosis and bio-persistence that can disrupt lung architecture and promote fibrotic responses. Cluster 5 encompasses pristine SWCNTs and MWCNTs with high surface area and moderate metal content; despite lacking functional groups, their large reactive surface and embedded metals can still induce significant toxicity through oxidative mechanisms. Finally, Cluster 6, characterized by amine functionalized MWCNTs, presents a unique immunogenic profile due to the positively charged surface and presence of nickel oxide, a known immunotoxicant. Collectively, these clusters underscore the importance of integrating both chemical and structural features when assessing the safety profiles of engineered nanomaterials.

Comparative Analysis of the Physicochemical Properties of S- and MWCNTs and Their Transcriptomics-based Inflammatory

The cluster-based analysis of SWCNTs and MWCNTs previously revealed how variations in physicochemical properties drive distinct toxicological behaviors, particularly

oxidative stress, inflammation, and fibrosis. While these groupings based on properties offer valuable insights, they cannot fully capture the intricate biological responses that occur at the molecular level. Inflammation and immune activation, for instance, often stem from more complex interactions than can be explained by morphology or surface chemistry alone. To delve deeper into the biological mechanisms underlying these responses, I employed two complementary statistical techniques: Pearson correlation analysis and PCA.

Pearson correlation was used to examine linear relationships between selected physicochemical parameters, such as specific surface area, elemental composition (C, H, N, O), and metal oxide impurities (MgO, MnO, Fe_2O_3, CoO, NiO) and adverse pulmonary outcomes measured by benchmark dose lower confidence limits for acute responses ($BMDL_{AR}$).[102] To ensure consistency and data quality, I excluded variables like CNT length (due to missing data for SWCNTs), diameter (uniform across SWCNT samples), and surface functional groups (due to their binary categorization). The resulting correlation matrix (Figure 15) offers a visual summary of these associations and helps identify key drivers of CNT-induced toxicity.

In SWCNTs, the analysis uncovered strong positive correlations between the acute phase response and the presence of manganese oxide (MnO), as well as elevated hydrogen and oxygen content. In contrast, specific surface area was negatively correlated, suggesting that more dispersible or less aggregated particles might trigger milder inflammatory responses. Among these factors, MnO stood out with the strongest correlation, indicating its significant role in triggering immune activation. This is consistent with earlier clustering results (Figure 14), where Mn-rich SWCNTs like NRCWE-051 and NRCWE-052 showed pronounced inflammatory and oxidative stress signatures. These materials not only contained more MnO but also exhibited higher levels of hydrogen and oxygen, supporting the idea that a combination of metal impurities and surface reactivity amplifies toxicity through oxidative mechanisms.

In MWCNTs, the patterns diverged slightly but remained centered around metal-driven toxicity. Strong positive correlations emerged between the acute phase response and contents of Fe_2O_3, CoO, and oxygen. These results imply that redox-active metal impurities

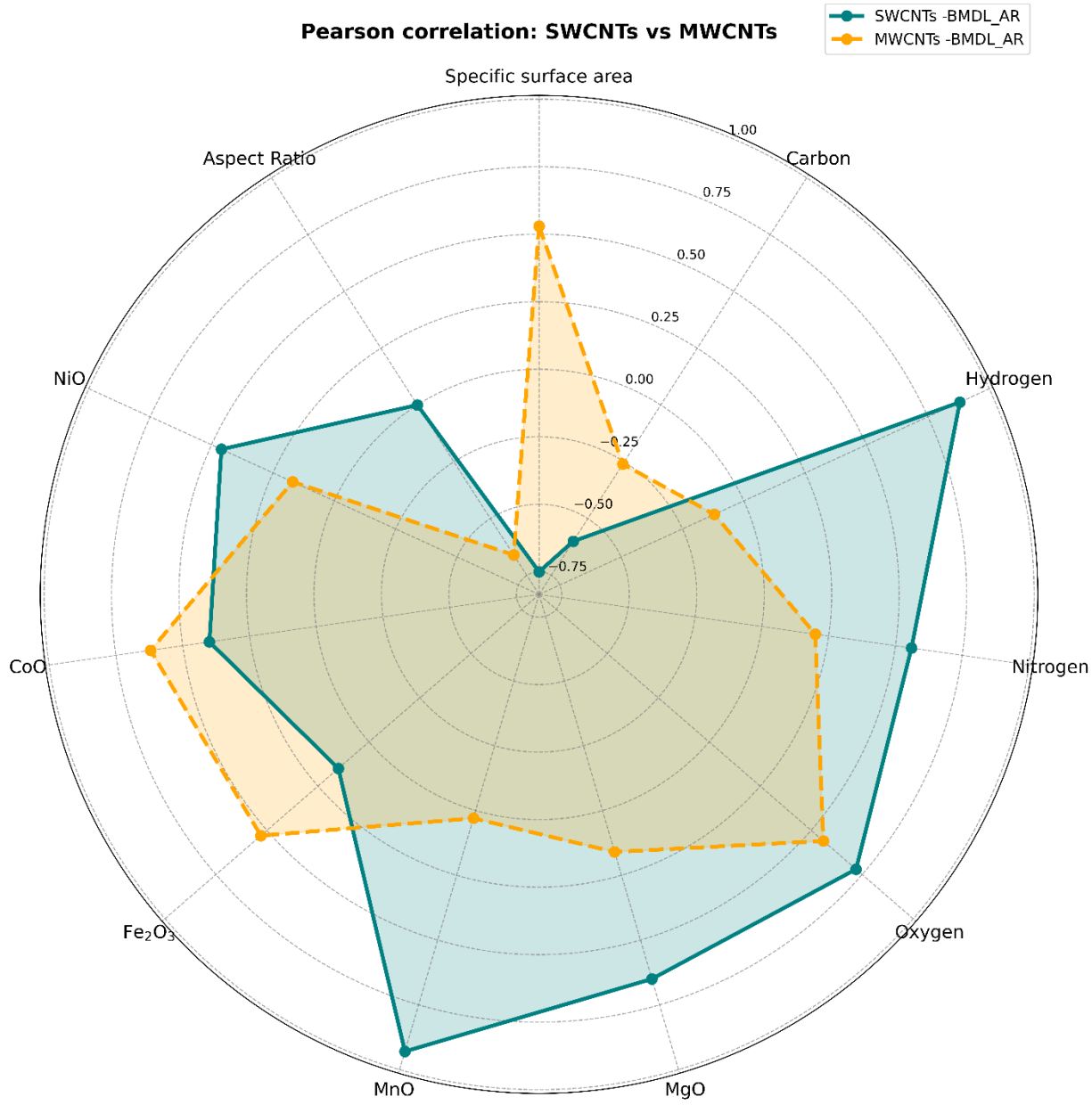

Figure 15. The radar plot provides a visual representation of the Pearson correlation coefficients (r) for specific physicochemical properties of S- and MWCNTs, with acute-phase signaling response ($BMDL_{AR}$).

and surface properties contribute significantly to the inflammatory potential of MWCNTs. Notably, the aspect ratio demonstrated a strong negative correlation with inflammation, meaning that shorter, thicker MWCNTs may provoke stronger immune responses.[124–126] This could be due to increased uptake by macrophages or reduced clearance from the lungs. When plotted in a two-dimensional space defined by aspect ratio and specific surface area, MWCNT samples displayed patterns suggesting that these two properties interact synergistically to modulate toxicity.[73]

This observation was reinforced by findings discussed earlier in Section 4.1, where samples like NRCWE-062 and NRCWE-063, marked by high Fe_2O_3 and CoO levels and relatively low aspect ratios, were grouped into clusters with elevated inflammatory and fibrotic profiles. The consistency between correlation analysis and clustering patterns strengthens the case that both composition and morphology shape transcriptomic responses in exposed lung tissue.

These findings are consistent with recent literature. For example, Danielsen et al. (2024)[104] identified similar correlations using Pearson analysis across CNT types. For SWCNTs, specific surface area and oxygen content were found to cluster together, highlighting their combined impact on toxicity. For MWCNTs, distinct clusters emerged, one grouping specific surface area, diameter, length, and cobalt, and another composed of manganese and magnesium. Their biological data echoed our findings, where specific surface area was the best predictor of neutrophil influx in SWCNTs, while diameter served as the strongest predictor for MWCNTs. Notably, metal contents such as Mg and Fe were linked to increased neutrophil activity post-exposure, while nickel showed a type-specific effect reducing inflammation in MWCNTs but increasing it in SWCNTs. Additional support comes from Gandhi et al. (2022)[127], who emphasized the role of MnO in pulmonary toxicity, although its precise molecular mechanism remains unresolved. Similarly, Hadrup et al. (2020)[128] demonstrated that Fe_2O_3 exposure can lead to respiratory and cardiovascular damage in vivo, adding further weight to the role of metal oxides in CNT toxicity.

Together, the correlation analyses presented in Figure 15 help delineate both shared and unique determinants of inflammation between CNT types. In SWCNTs, metal oxide content, particularly MnO along with elevated hydrogen and oxygen levels, strongly correlates with acute phase signaling. These elements likely initiate oxidative stress pathways, triggering immune responses. The clustering of Mn-rich SWCNTs in high-toxicity groups supports this view and emphasizes the role of elemental impurities in early molecular events. MWCNTs, on the other hand, appear to follow a dual mechanism. While metal oxides like Fe_2O_3 and CoO remain central to their inflammatory potential, physical morphology especially a low aspect ratio emerges as a crucial factor. Short, thick MWCNTs may interact more readily with immune cells, enhancing their biological impact. This geometric influence appears to operate both independently and in synergy with surface area, shaping the overall transcriptomic profile observed post-exposure.

summary, although both CNT types are influenced by surface chemistry and metal content, SWCNT-induced toxicity seems to be more chemically driven, particularly by MnO and oxidative elements. In contrast, MWCNT toxicity arises from a combination of chemical impurities and physical features. These distinctions highlight the need for tailored safety evaluations that consider CNT-type-specific traits when assessing inhalation risks. The agreement between our correlation analysis and clustering data strengthens the validity of these insights and offers a reliable framework for predicting CNT-induced lung responses.

Building on the Pearson correlation analysis, which indicated associations between specific physicochemical properties of carbon nanotubes (CNTs) and their biological effects, I further explored these patterns using Principal Component Analysis (PCA), the dataset was expanded to include previously underutilized but mechanistically relevant variables such as specific surface area, surface functionalization types (Pristine, –OH, –COOH, $–NH_2$), elemental composition (C, H, N, O), and metal oxide content (e.g., MgO, MnO, Fe_2O_3, CoO, NiO). No external data were added; the aim was to better be capturing the intrinsic variability of SWCNTs and MWCNTs relevant to pulmonary toxicity.

PCA was employed to reduce dimensionality and uncover multivariate patterns that relate CNT physicochemical structure to transcriptomic responses ($BMDL_{AR}$ values). The resulting PCA biplots (Figures 16a and 16b) demonstrate a clear separation between SWCNTs and MWCNTs along the first two principal components (PC1 and PC2), which together account for 61.49% of the total variance. A color gradient corresponding to $BMDL_{AR}$ values overlays the plots, revealing trends in toxicity that are structural differentiation. The scree plot (Figure 16c) confirms that PC1 and PC2 are most informative dimensions, as determined by the Malinowski rule with absolute values $\geq \pm 0.7$. These groupings indicate that distinct physicochemical profiles are predictive of divergent biological responses.

PC1 captures the greatest variance and reflects a gradient of surface reactivity and metal content. Positive PC1 loadings are associated with high CoO (0.867), oxygen content (0.855), specific surface area (0.747), Fe_2O_3 (0.679), and COOH groups (0.564), features more common in MWCNTs. Moderate contributions from –OH (0.485) and nitrogen (0.577) further characterize this cluster. In contrast, negative PC1 scores are driven by high carbon (–0.827), hydrogen (–0.808), and pristine surfaces (–0.791), traits more typical of SWCNTs. Thus, PC1 effectively distinguishes CNTs with higher surface reactivity and impurity content from more chemically inert forms. PC2 explains additional variance and is primarily shaped by NiO (0.832) and NH_2 functionalization (0.756), with moderate contributions from nitrogen (0.477) and carbon (0.291). This suggests PC2 captures variations associated with nickel presence and amine chemistry. Negative loadings include MgO (–0.673), MnO (–0.575), hydrogen (–0.360), and COOH (–0.281), indicating a compositional axis reflecting reduced amine modification and distinct metal content.
Together, PC1 and PC2 define distinct structural subtypes that support mechanistic interpretations of biological effects.

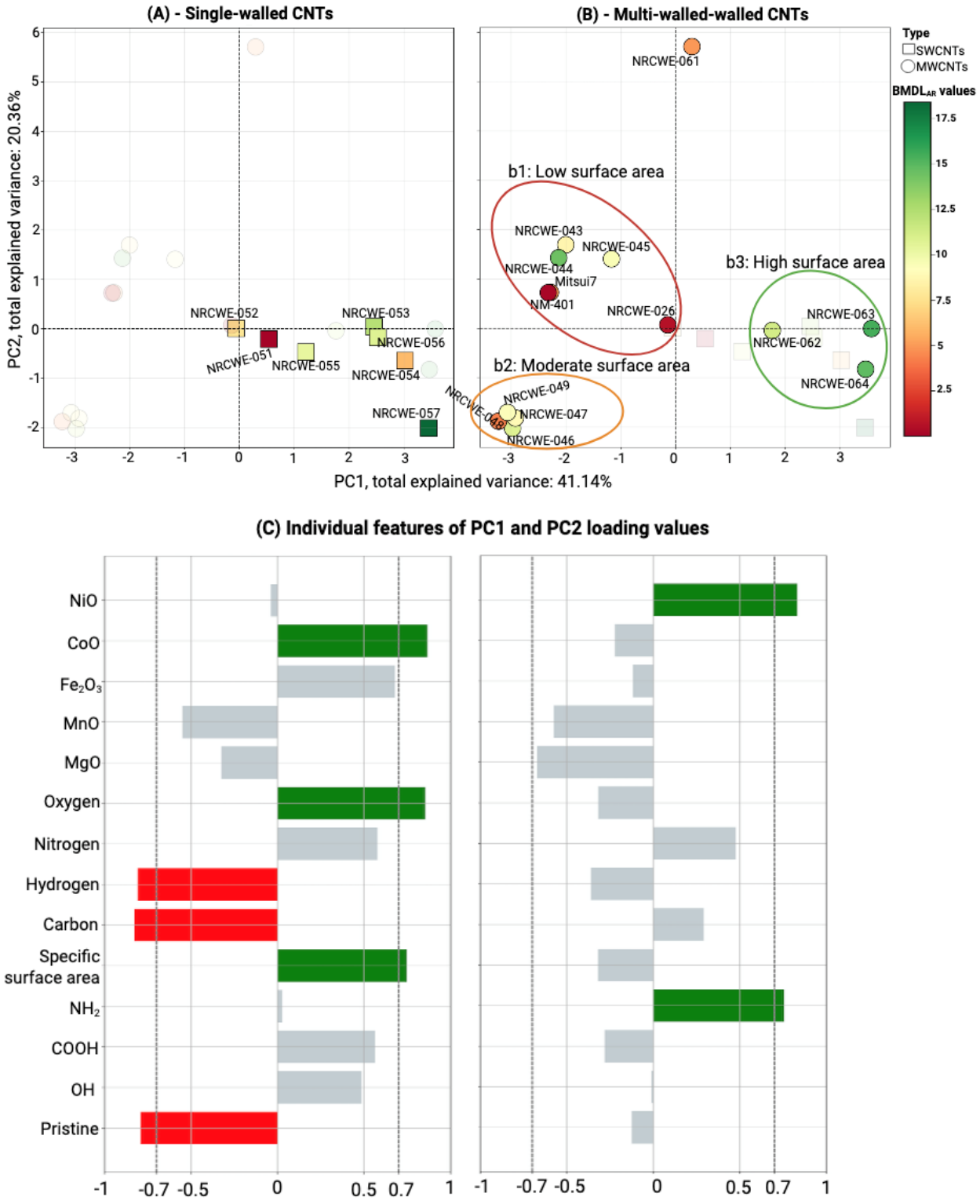

Figure 16. This figure illustrates the PCA analysis of the first two principal components (PCs) for acute-phase response signaling pathways; both (a and b) implies the points are scaled and colored according to the acute phase signaling response pathway BMDL range values, with SWCNTs

represented by squares and MWCNTs by circles; (c) the panel shows the features displayed by Malinowski rule the cut-off loading values $\geq \pm 0.7$ on the first two PCs.

Interpretation by CNT Type:

Single-Walled Carbon Nanotubes

Among SWCNTs, six CNTs, NRCWE-057, -054, -056, -053, -055, and -051, score positively on PC1. These particles share high specific surface areas and surface functionalization (e.g., –OH, –COOH), correlating with strong transcriptomic activation in acute-phase signaling, consistent with prior HCA and correlation analyses. For example, NRCWE-057 (SWCNT–COOH) has one of the highest PC1 scores and the highest $BMDL_{AR}$ value (lowest toxicity), supporting the protective role of hydrophilic functionalization.[104,106] An exception is NRCWE-051 (SWCNT–pristine), which also loads positively on PC1 despite lacking surface groups. Its strong transcriptomic potency (low $BMDL_{AR}$) likely stems from high surface area and a previously reported low aspect ratio, which enhances cellular uptake and oxidative stress potential. NRCWE-052 is the only SWCNT with a negative PC1 score, representing a low-surface-area, minimally functionalized form, and shows moderate transcriptomic activation.

Variation along PC2 is more subtle. NRCWE-057 exhibits a distinctly negative PC2 score, suggesting unique transcriptomic effects influenced by its surface chemistry. In contrast, NRCWE-053, -054, and -056 cluster near the PC1-PC2 origin, indicating moderate biological responses, likely driven by mechanisms beyond surface reactivity, such as immunomodulation or redox effects.

Toxicity Trends for SWCNTs

- SWCNTs with positive PC1 scores (functionalized, high surface area) generally show high $BMDL_{AR}$ values (low toxicity)
- NRCWE-051 is an exception: pristine, high surface area, but highly toxic (low $BMDL_{AR}$), illustrating the importance of physical structure

- NRCWE-052 (negative PC1) shows moderate toxicity, suggesting limited biological interaction due to lower surface activity

These findings highlight surface functionalization and area as key modulators of SWCNT toxicity.

Multi-Walled Carbon Nanotubes

Among MWCNTs, several long, rigid, pristine CNTs, Mitsui-7, NM-401, NRCWE-043, -044, -045, and -026, cluster on the negative PC1 side (group 1b). Characterized by low surface areas and high aspect ratios, these materials are associated with bio-persistence and asbestos-like toxicity.[129–132] Their low $BMDL_{AR}$ values reflect potent activation of fibrotic and inflammatory pathways. NRCWE-026, although grouped here, has a less negative PC1 score, likely due to a relatively higher surface area, contributing to acute-phase gene activation. Group 2b includes functionalized, metal-rich MWCNTs (NRCWE-046 to -049), with the most negative PC1 and PC2 values. Despite functionalization, these CNTs exhibit enhanced transcriptomic reactivity, potentially due to high MnO and MgO content and intermediate surface areas. Notably, NRCWE-048, despite its thick morphology and low surface area, shows high transcriptomic potency, suggesting that metal impurities and geometry can override conventional surface area effects.[133] Group 3b comprises functionalized MWCNTs, NRCWE-061 ($–NH_2$), -062 (pristine), -063 (–OH), and -064 (–COOH), which load positively on PC1 and exhibit high surface area and metal oxide content (e.g., CoO, Fe_2O_3). These materials show moderate-to-low toxicity and cluster due to shared surface characteristics. NRCWE-061 stands out with high PC1 and the most positive PC2 score, indicating selective pathway activation (e.g., cytokine signaling rather than inflammation).[104,106]

Similarly, NRCWE-043 to -045, while negatively loaded on PC1, have moderate PC2 values, suggesting additional biological effects such as immune cell recruitment or ECM remodeling, potentially better captured by PC2.

Toxicity Trends for MWCNTs

Group 1b (negative PC1): Long, rigid, pristine MWCNTs with high toxicity (low $BMDL_{AR}$), consistent with asbestos-like behavior

Group 2b (negative PC1 and PC2): Functionalized, metal-rich MWCNTs with moderate-to-high toxicity

Group 3b (positive PC1): Functionalized MWCNTs with elevated surface area and moderate $BMDL_{AR}$ values, indicating lower toxicity and more biocompatible profiles

In summary, PC1 and PC2 together form a two-dimensional map that explains key aspects of CNT-induced transcriptomic responses. PC1 distinguishes materials based on surface reactivity and contamination, while PC2 captures secondary variation due to composition and functionalization. Although aspect ratio was not included in the PCA input, known values from prior work support the biological interpretations.

To meet evolving regulatory demands for nanomaterials safety assessment within frameworks such as REACH, OECD grouping guidance, and NGRA, the application of Integrated Approaches to Testing and Assessment (IATA) has become essential. IATA leverages multiple data sources and methodologies in a weight-of-evidence (WoE) manner to support robust, mechanism-informed grouping and read-across strategies, thereby minimizing unnecessary testing and advancing regulatory acceptance.

In this study, I employed complementary computational approaches within an IATA framework, including HCA, Pearson correlation and PCA, to categorize 21 S- and MWCNTs. These methods collectively integrate physicochemical similarity and biological response data, providing a strong scientific basis for data-driven grouping aligned with regulatory principles of structural and toxicodynamic similarity. The six clusters identified through HCA revealed systematic and biologically relevant groupings, informed by specific surface area/surface modification (-OH, -COOH, -NH2), metal-oxide compositions (such as MnO, MgO, Fe2O3, CoO and NiO). These features were not only distinct across clusters but also mechanistically meaningful; this mechanistic coherence may fulfil OECD criteria for read-across, such as structural similarity, shared mode of

action (MoA) and common toxicological outcomes. Pearson correlation analysis further refined the mechanistic understanding by quantitatively linking physicochemical properties with transcriptomic endpoints, particularly the acute phase response. Strong associations were observed with metal oxide content, especially CoO and Fe2O3. These findings support mechanism-based grouping and facilitate the integration of AOP-informed Nano-QSAR models.

PCA was employed to capture the dominant axes of variation (PC1 and PC2) in physicochemical properties. PC1 clearly distinguished S- and MWCNTs based on transition metal enrichment, while PC2 reflected differences in surface area and functionalization. These dimensions correspond to molecular initiating events (MIEs) that may trigger chronic pulmonary pathologies such as fibrosis and cancer, as outlined in AOP 33 and AOP 237, and were found to align closely with both correlation analysis and HCA clustering results.

Considering together, this integrative, mechanism-informed approach within the IATA framework supports hazard-based grouping, informs tiered testing strategies, and enables the rational prioritization of CNTs for further evaluation. This framework aligns with Safe-by-Design (SbD) principles and the European Commisions vision for sustainable nanomaterial innovation and digital safety assessment. Ultimately, it bridges regulatory needs with mechanistic insight through the application of NAMs and AOP-based frameworks.

4.3. Transcriptomics-based and AOP-informed Metal Impurities in Carbon Nanotubes: Towards the Global Nano-QSAR Models

4.3.1. SPECIFIC OBJECTIVES AND SUBJECT OF RESEARCH

In line with the third objective of this research (see section 2.4), the following specific aim was presented in section 4.3

OBJECTIVE 3.

To investigate the role of metal impurities in CNTs as potential contributors to transcriptomic disturbances that drive inflammation and fibrosis mechanisms following inhalation exposure. This objective aims to develop a global AOP-informed Nano-QSAR model that quantitatively links specific metal contaminants in CNTs to gene expression changes, particularly within the acute phase response signaling pathway. The model will focus on early upstream key events (KEs) associated with pro-inflammatory responses and enable the prediction of lung and cardiovascular pathologies induced by metal-containing CNTs.

4.3.2. EXPERIMENTAL DATA

The dataset used in this study comprised 21 S- and MWCNTs, previously described in Section 4.2. It included key physicochemical properties such as specific surface area and concentrations of selected metal impurities (Fe_2O_3 and CoO), alongside biological data in the form of differentially expressed genes (DEGs). These data were derived from transcriptomic dose–response analyses ($BMDL_{AR}$) within the acute phase response signaling pathway (see Table 8).[33,100–106]

This integrated dataset served as the foundation for developing global quantitative structure–activity relationship (QSAR) models. These models aimed to predict CNT-

induced biological effects based on their chemical and transcriptomic profiles. To enhance the mechanistic interpretability of the models, the biological responses were further represented using principal component scores (PC1 and PC2), capturing the variance associated with DEG expression patterns.

Table 8. Structural properties of S- and MWCNTs and their endpoints.

Experimental data									
CNTs	**Physicochemical properties of S- and MWCNTs**						**Endpoints**		
	Surface area [m2/g]	**MgO**	**MnO**	**Fe2O3**	**CoO**	**NiO**	**$BMDL_{AR}$ [μg/mouse]**	**PC1**	**PC2**
NRCWE-051	442.6	0.04	0.00	1.63	1.08	0.06	0.00	5.23	1.28
NRCWE-052	405.7	0.03	0.01	1.05	1.23	0.12	7.69	-4.80	-1.30
NRCWE-053	367.8	0.02	0.02	0.85	3.82	0.10	12.22	-6.29	0.80
NRCWE-054	370.8	0.03	0.00	1.59	3.81	0.13	5.98	0.30	-0.32
NRCWE-055	453.1	0.03	0.03	4.39	1.33	0.05	10.29	-3.86	0.42
NRCWE-056	356.7	0.04	0.03	1.26	3.65	0.10	10.72	-5.26	0.97
NRCWE-057	281.6	0.18	0.04	2.20	2.74	0.14	18.39	-5.21	-0.87
Mitsui7	26.0	0.01	0.00	0.08	0.00	0.00	5.00	1.47	7.93
NM-401	18.0	0.01	0.00	0.05	0.00	0.00	0.17	4.42	4.49
NRCWE-026	254.0	0.00	0.00	0.29	0.11	0.00	0.58	4.82	12.56
NRCWE-043	82.0	0.01	0.00	0.01	0.00	1.20	8.57	4.08	-4.20
NRCWE-044	74.0	0.02	0.00	0.00	0.00	1.04	14.46	1.18	-2.52
NRCWE-045	119.0	0.02	0.00	1.17	0.25	1.34	9.52	5.52	-4.09
NRCWE-046	223.0	0.22	0.30	0.01	0.25	0.00	10.76	2.55	-2.26
NRCWE-047	216.0	0.22	0.30	0.01	0.25	0.00	8.91	2.59	-3.86
NRCWE-048	185.0	0.19	0.28	0.01	0.24	0.00	4.29	9.69	-2.58
NRCWE-049	199.0	0.19	0.29	0.00	0.25	0.00	9.34	6.97	-4.29
NRCWE-061	170.4	0.01	0.01	0.59	0.00	1.97	4.91	-2.38	1.83
NRCWE-062	443.2	0.07	0.00	0.58	4.60	0.22	11.24	-3.19	-1.81
NRCWE-063	426.4	0.07	0.02	1.95	5.88	0.49	15.46	-9.65	2.24
NRCWE-064	445.2	0.03	0.03	1.80	5.51	0.30	14.85	-8.19	-4.39

4.3.3. METHODS USED

To develop predictive global QSAR models that link the physicochemical descriptors of S- and MWCNTs with transcriptomic responses, specifically differentially expressed genes (DEGs) and $BMDL_{AR}$ values from the acute phase response signaling pathway. I employed a suite of ensemble regression techniques such as Random Forest (RF), Gradient Boosting (GB), Extreme Gradient Boosting (XGB), and Decision Tree (DT) algorithms from the Scikit-learn library.[93,134]

Among these methods, Random Forest was selected as the primary modeling approach due to its robustness in capturing complex, non-linear relationships between input features and biological responses. This approach is particularly suited for modeling interactions between metal impurities, surface properties, and transcriptomic alterations related to pro-inflammatory key events (KEs), which are implicated in chronic outcomes such as fibrosis, cardiovascular, and cancer diseases. The other ensemble methods (GB, XGB, and DT) were used for comparison to assess model stability and performance across different algorithms. For all ensemble models, the number of estimators was set to 500 (i.e., n_estimators=500).

The input features (X) consisted of physicochemical properties, such as specific surface area and concentrations of Fe_2O_3 and CoO extracted from the literature and Section 4.2 and detailed in Table 8. The target variable (y) was the pathway-level $BMDL_{AR}$ value, representing the transcriptomic potency associated with the acute phase response. To build the model, I first ranked the dataset in ascending order based on the $BMDL_{AR}$ values. The ranked data were then split into a training set (80%) and a validation set (20%) using a stratified, ratio-based approach.[108] Seventeen CNTs were assigned to the training set, while four were used for model validation. This manual split ensured that both sets reflected the diversity and range of the full dataset, thereby supporting robust model training and evaluation.

To further assess the generalizability of the models, I conducted additional validation using an independent test set. Specifically, I randomly removed seven data

points (approximately 20% of the full dataset) prior to model training. These excluded points served as an unseen test set to evaluate model performance on completely new data. This approach minimized overfitting and confirmed that the trained models could reliably predict biological outcomes for CNTs not used during model development.

Table 9. The detailed splitting for the training and test sets of the ten global Nano-QSAR models

S- and MWCNTs	Splitting									
	Model-1	Model-2	Model-3	Model-4	Model-5	Model-6	Model-7	Model-8	Model-9	Model-10
NRCWE-051	T	T	T	T	T	T	T	T	T	T
NM-401	T	T	T	T	T	T	T	T	T	T
NRCWE-026	T	T	T	T	T	T	T	T	T	T
NRCWE-048	T	T	T	T	T	T	T	T	T	T
NRCWE-061	V	V	V	V	V	V	V	V	V	V
Mitsui7	T	V	T	T	T	T	T	T	T	T
NRCWE-054	T	T	T	T	T	T	T	T	T	T
NRCWE-052	V	T	T	T	T	T	T	T	T	T
NRCWE-043	T	T	T	T	T	T	V	T	T	T
NRCWE-047	V	V	V	V	V	V	V	V	T	V
NRCWE-049	T	T	T	T	V	T	T	T	T	T
NRCWE-045	T	T	T	T	T	T	T	T	T	T
NRCWE-055	T	T	V	T	T	T	T	T	V	T
NRCWE-056	T	T	T	V	T	T	T	V	T	T
NRCWE-046	T	T	T	T	T	T	T	T	V	T
NRCWE-062	T	T	T	T	T	V	T	T	T	T
NRCWE-053	T	T	T	T	T	T	T	T	T	V
NRCWE-044	T	T	T	T	T	T	T	T	T	T
NRCWE-064	T	T	T	T	T	T	T	V	T	T
NRCWE-063	V	V	V	V	V	V	V	T	V	V
NRCWE-057	T	T	T	T	T	T	T	T	T	T

4.3.4. RESULTS AND DISCUSSIONS

The section presents the results of modeling efforts aimed at elucidating the relationships between residual metal content in CNTs and the transcriptomic signatures of acute phase response toxicity, as measured by BMDL values. Specifically, the study was divided into two key objectives:

Development of a Global AOP-Informed Nano-QSAR Model

This model quantitatively links the physicochemical properties of S- and MWCNTs to the $BMDL_{AR}$ values derived from the acute phase response signaling pathway. The goal was to assess how variations in CNT surface characteristics and metal impurities contribute to transcriptomic potency associated with inflammation.

Clustering Based on Structure–Activity Relationships

In this part, S- and MWCNTs were grouped according to their principal component (PC1/PC2) scores, which represent the magnitude of differentially expressed genes (DEGs) in the acute phase response pathway. These scores were then correlated with physicochemical descriptors to uncover mechanistic insights and support structure-based categorization.

Together, these complementary analyses provide a predictive and mechanistic understanding of CNT-induced transcriptomic responses, highlighting the role of surface properties and metal contaminants in driving pro-inflammatory signaling, as discussed below:

Global AOP-informed Nano-QSAR model

This section focuses on the development of a predictive global AOP-informed Nano-QSAR model, aimed at quantitatively linking the physicochemical properties of S- and MWCNTs to the acute phase response signaling pathway ($BMDL_{AR}$). To build this model, I utilized the physicochemical profiles of 21 CNTs, as summarized in Table 9. These profiles included specific surface area (m^2/g) and concentrations of metal impurities such as Fe_2O_3, CoO, NiO, MgO, and MnO. All physicochemical characteristics were

obtained from experimentally validated sources (Section 4.2), ensuring the reliability of the input descriptors.

By correlating these measured properties with $BMDL_{AR}$ values, the model aimed to uncover the key features driving transcriptomic-level inflammatory responses following CNT inhalation exposure. This modeling approach supports the broader goal of integrating mechanistic insights with predictive toxicology in the context of adverse outcome pathways (AOPs).

The selection of predictive features for the Nano-QSAR model development on previous findings (Section 4.1), which highlighted the significance of descriptors such as aspect ratio and specific surface area in driving CNT-induced lung inflammation. However, this study specifically aimed to investigate the role of residual metals in modulating acute phase responses. To address this, I incorporated two additional descriptors, iron (Fe_2O_3) and cobalt (CoO) content, based on prior Sections 4.2, where these metals showed a strong correlation with acute phase response markers.

The resulting model used Random Forest (RF) regression to quantitatively link three key physicochemical descriptors, such as specific surface area, iron, and cobalt concentrations associated with the acute phase response signaling pathway (BMDL values). These features were selected as the most predictive variables for estimating lung inflammation outcomes following CNT exposure.

To ensure robustness, I evaluated the model's quality and predictive performance using multiple metrics. In addition to the RF model, I applied Gradient Boosting (GBoost), XGBoost, and Decision Tree (DT) regression methods to determine whether alternative ensemble approaches could enhance predictive accuracy or offer further insights. However, since neither GBoost nor XGBoost outperformed the RF model, the latter was selected as the primary modeling framework for subsequent analysis.

In the next step, I developed ten individual global Nano-QSAR models, each using different training and test set compositions, as summarized in Table 8. All models were evaluated based on key statistical metrics to ensure robustness and predictive reliability.

They demonstrated consistently high performance, with goodness-of-fit values (R^2) ranging from 0.83 to 0.855. Predictive power was further supported by external-validated performance metrics (Q^2F1 = 0.78–0.93, Q^2F2 = 0.72–0.93, Q^2F3 = 0.83–0.95 and CCC = 0.89–0.97). The root mean square errors for training and test sets were low ($RMSE_C$ = 1.97–2.09, $RMSE_{EXT}$ = 1.1–2.06), confirming the models accuracy and generalizability across different data splits.

Table 10. The detailed statistics of the obtained RF-based predicted ten global Nano-QSAR models.

No.	Model calibration		Model validation				
	R2	**$RMSE_C$**	**Q^2F_1**	**Q^2F_2**	**Q^2F_3**	**CCC**	**$RMSE_{EXT}$**
Model-1	0.85	1.98	0.90	0.90	0.94	0.94	1.23
Model-2	0.83	2.09	0.93	0.93	0.95	0.97	1.11
Model-3	0.84	2.03	0.92	0.91	0.95	0.95	1.11
Model-4	0.84	2.03	0.89	0.87	0.93	0.95	1.37
Model-5	0.85	2.00	0.87	0.86	0.93	0.92	1.40
Model-6	0.85	1.99	0.89	0.86	0.92	0.94	1.41
Model-7	0.85	2.03	0.87	0.86	0.92	0.94	1.42
Model-8	0.86	1.97	0.85	0.83	0.92	0.93	1.47
Model-9	0.85	1.98	0.85	0.81	0.90	0.94	1.62
Model-10	0.84	2.03	0.78	0.72	0.83	0.89	2.06

To further validate model robustness, I followed a classical cross-validation strategy using small external datasets, consistent with the method described in Section 4.1. This approach minimized overfitting and helped assess model generalizability.

From these ten models, I selected the best-performing one based on a combination of internal and external validation metrics, along with the visual inspection of scatter plots comparing experimental and predicted BMDL values (Figure 17a). This evaluation followed OECD Principle 4, which emphasizes appropriate measures of goodness-of-fit, robustness, and predictability. The selected model met these criteria, with training and

validation data points closely clustered around the trend line, indicating strong predictive accuracy. The detailed results, including experimental versus predicted values, are presented in Table 11.

Table 11. The best global Nano-QSAR model experimental versus predicted BMDL values

S- and MWCNTs	Specific surface area	Fe_2O_3	CoO	Experimental $BMDL_{AR}$	Predicted $BMDL_{AR}$	Set
NRCWE-051	442.6	1.625	1.082	0.00	3.26	T
NM-401	18.0	0.05	0	0.17	2.89	T
NRCWE-026	254.0	0.29	0.110	0.58	3.08	T
NRCWE-048	185.0	0.007	0.240	4.29	6.44	T
Mitsui7	170.4	0.591	0.001	5.00	4.75	T
NRCWE-054	26.0	0.08	0	5.98	8.27	T
NRCWE-043	370.8	1.593	3.809	8.57	8.11	T
NRCWE-049	405.7	1.046	1.232	9.34	9.84	T
NRCWE-045	82.0	0.008	0.001	9.52	8.32	T
NRCWE-055	216.0	0.007	0.250	10.29	9.91	T
NRCWE-056	199.0	0.004	0.250	10.72	10.09	T
NRCWE-046	119.0	1.17	0.250	10.76	9.38	T
NRCWE-062	453.1	4.386	1.330	11.24	10.50	T
NRCWE-053	356.7	1.259	3.648	12.22	11.10	T
NRCWE-044	223.0	0.008	0.250	14.46	11.87	T
NRCWE-064	443.2	0.578	4.603	14.85	12.53	T
NRCWE-057	367.8	0.846	3.821	18.39	14.61	T
NRCWE-061	74.0	0.004	0.002	4.91	4.98	V
NRCWE-052	445.2	1.796	5.514	7.69	7.99	V
NRCWE-047	426.4	1.949	5.875	8.91	9.06	V
NRCWE-063	281.6	2.197	2.741	15.46	13.03	V

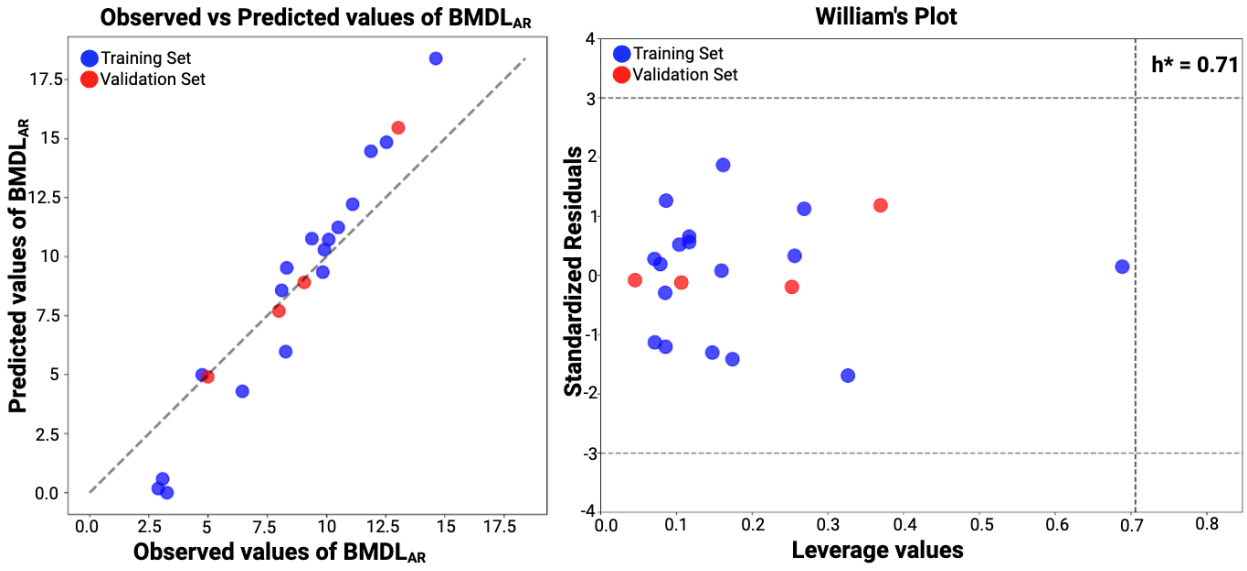

Figure 17. (a) The plot experimentally observed versus predicted $BMDL_{AR}$ values for training and validation compounds for a global Nano-QSAR model; (b) William's plot: dot-and-dash lines represent ± 3 standard deviation units, dash line represents the critical value (h* = 0.71).

Another important aspect of model validation, as outlined by OECD Principle 3, is defining the applicability domain (AD), the theoretical chemical space within which model predictions are considered reliable. To evaluate this, I applied the Williams plot approach to the best-performing global AOP-informed Nano-QSAR model (Figure 17b). The plot displays standardized residuals against leverage values for each data point from both the training and validation sets. The results showed that all data points fell within the acceptable ±3 standard deviation threshold of residuals, forming a tight distribution around the mean. This pattern indicates that the residuals follow a normal distribution and confirms that the model predictions are both stable and reliable. Furthermore, no data points were identified as outliers or influential points, which further supports the robustness of the model.

The well-defined applicability domain confirms that the model can be used confidently to predict lung inflammation outcomes related to acute phase response signaling ($BMDL_{AR}$ values) for S- and MWCNTs within the studied descriptor space. This

step reinforces the model's credibility and highlights its potential utility for supporting nanomaterial safety assessments.

Mechanistic Grouping S- and MWCNTs Based on Structure-Activity Relationships and Acute Phase Transcriptomic Profiles

To further explore the biological mechanisms underlying CNT-induced inflammation, I conducted a principal component analysis (PCA) on differentially expressed genes (DEGs) associated with the acute phase response signaling pathway (Figure 19). This step aimed to identify distinct transcriptional signatures and uncover how structural variations among CNTs influence gene expression patterns.

The PCA included all 21 CNT-exposed samples (both S- and MWCNTs), focusing on genes that exhibited notable fold changes in either direction. The first two principal components (PC1 and PC2) accounted for approximately 40% of the total variance in the gene expression dataset, capturing the dominant trends in the transcriptional response. The PCA results revealed a clear separation of CNTs along Principal Component 1 (PC1), enabling their classification into two mechanistically distinct groups (Figure 19). The PCA plot shows that CNTs with negative PC1 scores (Group 1), including NRCWE-063, NRCWE-064, NRCWE-053, NRCWE-056, NRCWE-057, NRCWE-052, NRCWE-055, NRCWE-062, and NRCWE-06, were characterized by high levels of transition metal impurities and moderate to high specific surface area. In contrast, CNTs with positive PC1 scores (Group 2), such as NRCWE-048, NRCWE-049, NRCWE-045, NRCWE-043, NRCWE-047, NRCWE-046, NRCWE-044, and NRCWE-054, exhibited low metal content and were generally defined by higher aspect ratios (see section 4.1). These physicochemical distinctions were strongly reflected in their transcriptional profiles, indicating that structural variations in CNTs play a key role in driving pathway-specific gene expression changes.

Among the two components, PC1 emerged as the dominant side of variation, capturing the major differences in gene expression that correlated with transition metal content (particularly Fe_2O_3 and CoO) and specific surface area, both of which have been

known to contribute to acute proinflammatory responses (see Section 4.2). While PC2 accounted for a smaller proportion of variance (15%), it provided additional mechanistic insights. This PC appeared to capture the influence of high aspect ratios and very low metal contamination. CNTs with high positive PC2 scores, such as NRCWE-026, Mitsui-7, and NM-401 (refer to Section 4.1), shared these features. Despite their low metal content, these materials were associated with robust transcriptional activity, potentially due to mechanisms such as prolonged cellular uptake, biopersistence, lysosomal membrane destabilization, and frustrated phagocytosis.

To further explore the underlying drivers of transcriptional variance, the "Malinowski rule" has been used for the gene loading values (absolute values highlighted by $\geq \pm 0.7$) on PC1 and PC2. This analysis revealed 18 genes on PC1, including MAPK3, SOCS3, SAA1, MYD88, IL1B, MAP2K2, NFKB2, SOCS1, IL33, NOLC1, CP, ITIH4, IL6, CFB, NFKBIE, NGFR, and AKT2. These genes are well-established mediators of inflammatory and fibrotic responses, commonly reported in animal models of CNT exposure. Their strong contributions to PC1 suggest that they play central roles in the lung's transcriptional response to CNTs.

To gain further insight into the structure–activity relationships, to quantitatively relate the structural features of CNTs to the observed transcriptional signatures captured by PC1.

Table 12. The best PC1-based Nano-QSAR model experimental versus predicted BMDL values

CNTs	Specific surface area	Fe2O3	CoO	Experimental $BMDL_{AR}$	PC1 predicted	Set
NRCWE-063	426.4	1.949	5.875	-9.65	-6.94	T
NRCWE-053	367.8	0.846	3.821	-6.29	-4.86	T
NRCWE-056	356.7	1.259	3.648	-5.26	-4.68	T
NRCWE-057	281.6	2.197	2.741	-5.21	-4.25	T
NRCWE-052	405.7	1.046	1.232	-4.80	-2.15	T
NRCWE-062	443.2	0.578	4.603	-3.19	-3.97	T
NRCWE-061	170.4	0.591	0.001	-2.38	0.23	T
NRCWE-054	370.8	1.593	3.809	0.30	-1.77	T
NRCWE-044	74.0	0.004	0.002	1.18	2.42	T
NRCWE-046	223.0	0.008	0.250	2.55	3.07	T
NRCWE-047	216.0	0.007	0.250	2.59	3.91	T
NRCWE-043	82.0	0.008	0.001	4.08	3.27	T
NM-401	18.0	0.05	0	4.42	3.63	T
NRCWE-026	254.0	0.29	0.110	4.82	4.01	T
NRCWE-051	442.6	1.625	1.082	5.23	2.36	T
NRCWE-045	119.0	1.17	0.250	5.52	3.57	T
NRCWE-048	185.0	0.007	0.240	9.69	6.99	T
NRCWE-064	445.2	1.796	5.514	-8.19	-6.81	V
NRCWE-055	453.1	4.386	1.330	-3.86	-2.02	V
Mitsui7	26.0	0.08	0	1.47	3.63	V
NRCWE-049	199.0	0.004	0.250	6.97	4.84	V

For this purpose, ten Nano-QSAR models were developed using the Random Forest (RF) algorithm, incorporating Fe_2O_3 and CoO content along with specific surface area as key input descriptors. Among these, the best-performing model demonstrated strong predictive power and generalizability, as detailed in Table 12. The model demonstrated robust statistical performance metrics with R^2 of 0.88 and a root mean square error of calibration **(**$RMSE_C$) of 1.82. In external validation, the model maintained excellent

predictivity, achieving a Q^2_{EXT} of 0.90 and root mean square error of predicted (RMSE$_{EXT}$) of 1.84. These results confirm the model reliability in both training and validation sets and highlight its strong capability to predict the transcriptional activity of CNTs not included in model development (Figure 18a). This optimized model offers a robust framework for linking the physicochemical properties of CNTs to their transcriptional biological activity.

Furthermore, I evaluated the applicability domain (AD) of the developed model to assess its predictive reliability for compounds with both similar and/or dissimilar structural features in the training and validation sets. Notably, one outlier (NRCWE-055) was identified within the validation set of S- and MWCNTs (Figure 18b). While this CNT exhibited a leverage value (h_i) greater than the threshold (h^*) value and within acceptable limits. Such compounds are known as good high-leverage points; they may lie outside the model's core domain (interpolation region) but still contribute to model stability and prediction quality (Jaworska et al., 2005).[135] According to Jaworska et al., compounds with h_i > h* and standardized residuals within ±3 standard deviations can support the model and make it predictive for new compounds, including those that are slightly different from the training set.

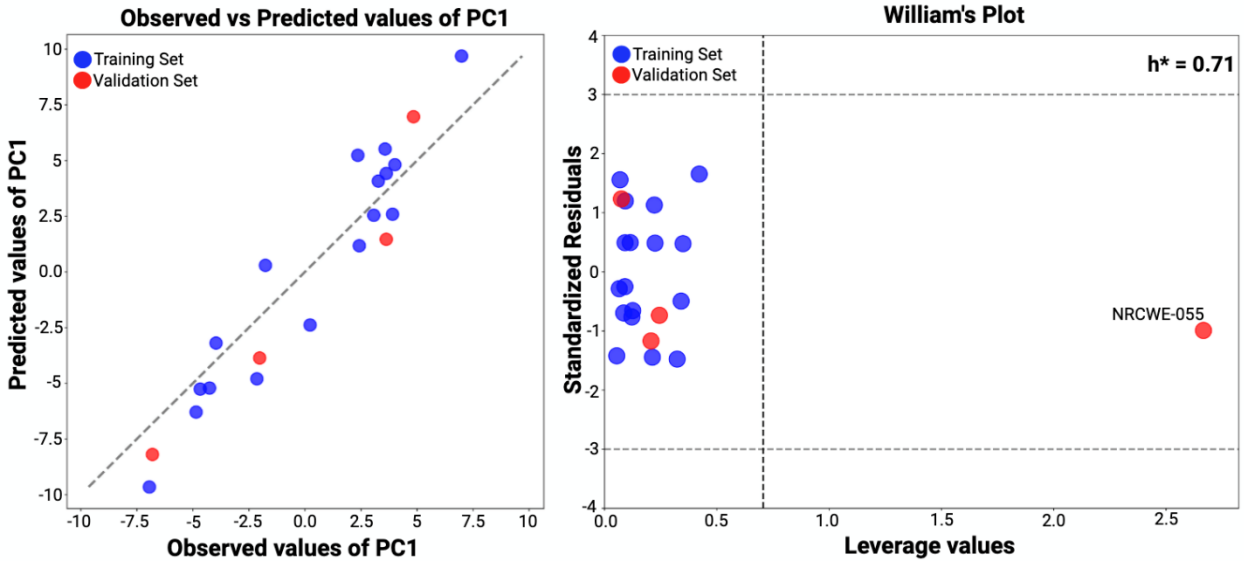

Figure 18. (a) The plot experimentally observed versus predicted PC1 values for training and validation compounds for a global Nano-QSAR model; (b) William's plot: dot-and-dash lines represent ± 3 standard deviation units, dash line represents the critical value (h* = 0.71).

One should be aware that the current model does not predict perturbation of individual genes, since PC1 represents a linear combination of multiple gene expressions. However, given that alterations in a single gene expression are insufficient to trigger pathway-level responses. In fact, such developing models solely on individual genes may be misleading. Instead, predictive models should aim to capture coordinated alterations across sets of genes or entire biological pathways.

Building on this rationale, previous studies have demonstrated the value of transcriptomics-informed predictive models within AOP frameworks. For instance, Jagiello et al. (2021)[73] developed AOP-guided structure–activity relationship models to predict MWCNT-induced pulmonary pathology, focusing on the agranulocyte adhesion and diapedesis pathway. More recently, Merugu et al. (2025)[136] proposed a novel AOP incorporating acute inflammation mechanisms to assess MWCNT-induced lung fibrosis and atherosclerosis. Likewise, Muratov et al. (2025)[137] constructed over 600 transcriptomics-based models to predict pulmonary toxicity of titanium dioxide nanoparticles.

These studies underscore a shift from modeling individual gene perturbations to capturing coordinated pathway-level changes. Consistent with this, our PCA-driven Nano-QSAR approach demonstrates that a small set of physicochemical descriptors, particularly metal content and specific surface area can robustly predict PC1-based transcriptomic profiles.

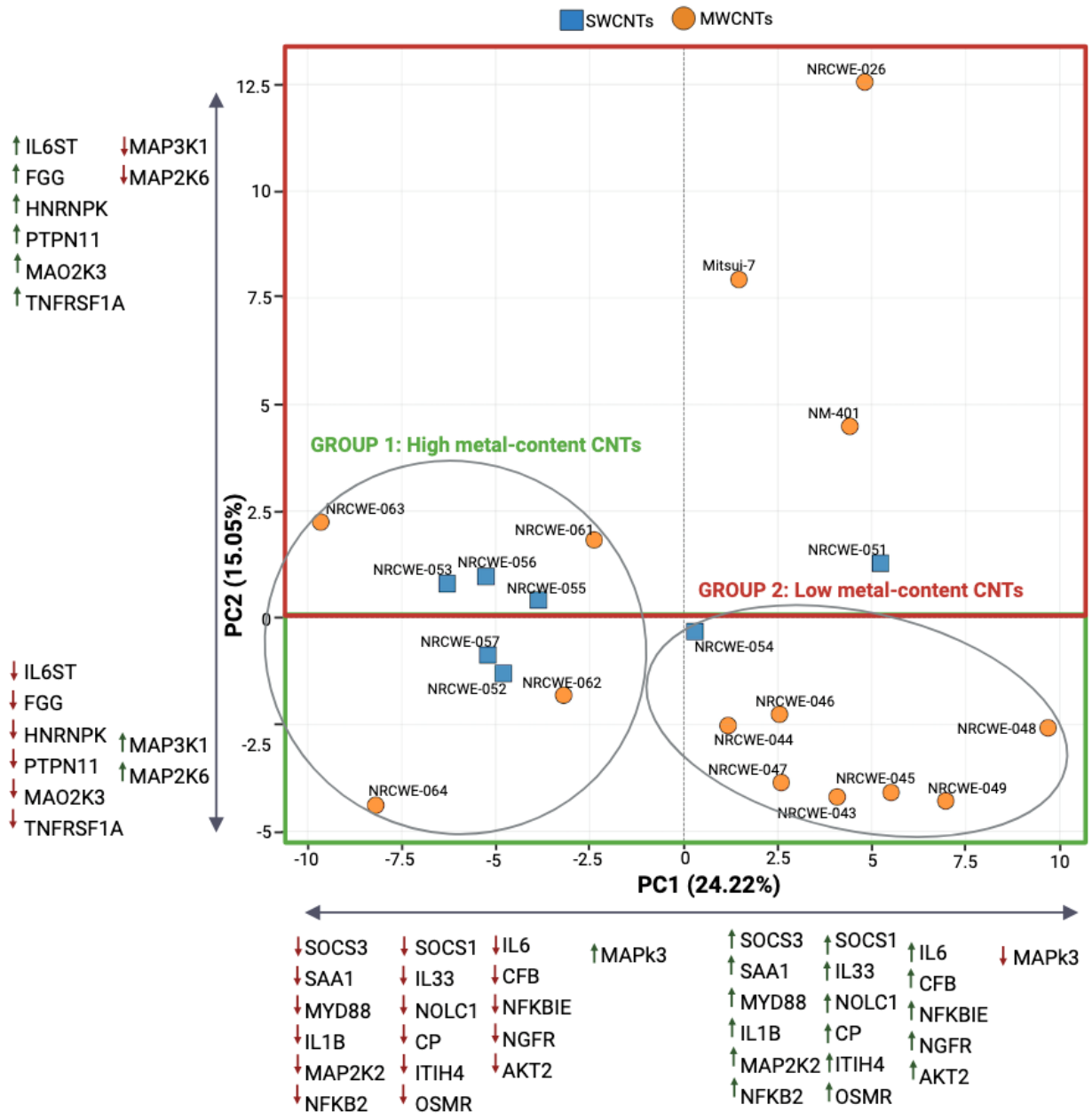

Figure 19. Score plot illustrating the grouping of S- and MWCNTs in the space of gene expressions associated with the acute phase response signaling pathway. In the parentheses, information about the percentage of variance explained by each PC is provided. Genes associated with PC1 and PC2 are listed (according to the Malinowski rule, absolute loading values $\geq \pm 0.7$). The arrow directions show up- or down-regulation of genes in a given direction of particular PC (arrows up – genes up-regulation; arrows down – genes down-regulation).

To gain a deeper understanding of these transcriptional patterns, I focused on individual CNTs in the expression profiles of genes with the highest PC1 loadings. These findings indicate that S- and MWCNTs elicit distinct regulatory effects on key gene families such as MAPK**,** SOCS, and acute phase response genes, with residual metal content being a primary influencing factor.

For example, MAPK3 (ERK1), a key mediator of signaling in response to oxidative stress and inflammatory stimuli, was upregulated in metal-rich CNTs with moderate to high surface area (e.g., NRCWE-063, NRCWE-064, NRCWE-053), suggesting activation via metal-catalyzed ROS or receptor-ligand signaling.[138,139] This aligns with previous studies by Poulsen et al.[100,101,133]*,* Halappanavar et al.[105,106] and Danielsen et al.[104]*,* which links MAPK pathway activation to CNT-induced inflammation. Similarly, Pacurari et al.[123] reported metal-rich SWCNTs trigger MAPK cascades and ROS-mediated damage. Moreover, our results are in line with alternative studies that have explored transcriptomic responses *in vivo* and DNA methylation changes *in vitro*, further supporting the epigenetic and transcriptional relevance of metal impurities in CNTs.[140–142]

Overall, these findings suggest that the central role of MAPK signaling is in regulating innate immune responses, inflammatory signaling and cell survival pathways following CNT exposure. Conversely, CNTs with low metal content, such as NRCWE-048, NRCWE-049, and NRCWE-045, were associated with downregulated pro-inflammatory genes including SOCS3, SAA1, MYD88, and IL1B (Figure 19), which are implicated in fibrogenic outcomes and have been well-characterized in animal models.[100,104,105] Notably, serum amyloid A (SAA1), a key marker of the acute phase response, has been identified both as a predictor of systemic inflammation in animal studies and as a top-ranked biomarker in machine learning-based models.[104,137]

For examining PC2 loadings revealed genes like IL6ST, FGG, HNRNPK, and TNFRSF1A (positive PC2) and MAP2K6, AP3K1 (negative PC2), which play regulatory roles in inflammation. CNTs with high PC2 scores (e.g., NRCWE-026, Mitsui-7, NM-401) share low metal content, high aspect ratio**,** rigidity, and biopersistence, structural traits that

may influence upstream regulators of inflammation via distinct interactions in the airway vs. alveolar regions.[138,139,143,144]

Although our Nano-QSAR models targeted intermediate KEs, the results identified several key genes, MAPK3 and SAA1, that could refine the molecular initiating events (MIEs) in AOP 33. Currently, MIE definitions are vague, often described broadly as CNT cell membrane interactions. These findings provide a molecular basis to sharpen those definitions. Thus, beyond offering a methodology to apply AOP frameworks using transcriptomic pathways as endpoints in Nano-QSAR, this study also demonstrates how such models can inform upstream KEs or redefine MIEs. Additionally, the clear differences in gene expression profiles associated with specific surface area vs. aspect ratio in S- and MWCNTs (Figure 19) further emphasize the mechanistic role of physicochemical properties. In conclusion, this study demonstrated the applicability of a previously developed transcriptomic-based, AOP-informed Nano-QSAR model to quantify how the structural properties of S- and MWCNTs influence lung tissue inflammatory responses at the transcriptomic pathway level. By integrating physicochemical descriptors with gene expression data, the model identified specific surface area and the presence of impurities (Fe2O3 and CoO) as critical predictors of early biological events triggering the acute phase response signaling pathway.

Importantly, although all CNTs in the dataset were capable of eliciting acute and chronic inflammatory responses, those with higher metal content and surface area showed greater transcriptional activation of key inflammatory mediators. This suggests that interference with upstream regulatory molecules, potentially through competitive binding or ROS-mediated signaling, may hinder immune resolution. Such dysregulation can promote persistent tissue injury, contributing to long-term adverse outcomes including fibrosis, atherosclerosis, and cancer.

While this analysis focused specifically on S- and MWCNTs, the acute phase response pathway is known to be modulated by a wide range of nanomaterials. This highlights the broader applicability of the Nano-QSAR model presented here for predicting biological

responses across diverse nanomaterial types. Moreover, several transcriptional biomarkers identified in this study, such as MAPK3, SAA1, and SOCS3 may serve as valuable endpoints for developing or refining high-throughput in vitro bioassays to assess the inflammogenic potential of CNTs.

Overall, these findings reinforce the utility of integrating Nano-QSAR and AOP frameworks to develop mechanistically anchored, predictive models for nanotoxicology. Such approaches contribute to a more realistic, pathway-level understanding of nanomaterial-induced health risks and support their inclusion in next-generation risk assessment (NGRA) workflows.

5. CONCLUSION AND FUTURE PERSPECTIVES

This dissertation has highlighted the rapid advancement and widespread application of carbon nanotubes (CNTs), which turn in presents significant challenges in assessing their potential risks to human health and the environment. To address these challenges, this research investigated how data-driven, mechanistically anchored Nano-QSAR models can improve the prediction and grouping of CNTs based on their potential to induce pulmonary toxicity. By integrating cheminformatics, high-throughput transcriptomics, and pathway-based modeling, the study examined how key physicochemical properties such as aspect ratio, specific surface area (BET), surface modifications, and metal impurities are mechanistically linked to early molecular events in the acute phase response (AR) signaling pathway. The ultimate goal was to support the development of safer nanomaterials and advance mechanism-based risk assessment strategies in line with next-generation toxicology and evolving regulatory frameworks.

The first part of this work focused on applying a previously developed AOP-anchored Nano-QSAR approach to develop transcriptomic responses triggered by the inhalation exposure to MWCNTs. Particular attention was given to the acute phase responses (AR) signaling pathway, which plays a crucial role in neutrophil influx and initiates the acute immune response. This process, characterized by the recruitment of pro-inflammatory cells into the lungs, can ultimately lead to lung fibrosis (as outlined in AOP 33) and atherosclerosis (as per AOP 237) pathologies. To link the structural properties of a set of MWCNTs with transcriptional benchmark dose level ($BMDL_{AR}$) responses of genes associated with this pathway, the Kernel-weighted Local Polynomial Regression (KwLPR) algorithm was employed. The results emphasized the critical role of the aspect ratio and specific surface area of MWCNTs in triggering acute inflammation and, subsequently, driving long-term pathologies through the inflammation-mediated mechanisms. This newly developed data-driven model (transcriptomic-based, AOP-informed Nano-QSAR) potentially serves as an in silico new approach methodology (NAM) to support the MWCNTs safety assessment based on the weight of evidence.

In the second part of this dissertation, the research was extended to include single-walled carbon nanotubes (SWCNTs), enabling a comparative analysis with MWCNTs. This comparative approach aimed to deepen the mechanistic understanding of the molecular-level toxicity in both CNT types, which is essential for precise safety evaluation and effective risk mitigation. The study investigated grouping-based comparative analysis of physicochemical properties of CNTs and their pulmonary effects, particularly those linked to the acute phase response (AR) pathway, assessed at the transcriptomic level. By integrating transcriptomic endpoints with advanced chemometric analyses, the consequence, key drivers of downstream lung pathologies such as inflammation and fibrosis, were identified.

For MWCNTs, structural features such as aspect ratio, specific surface area, surface functionalization (e.g., –OH, –COOH, $–NH_2$) and metal impurities (iron and cobalt) were strongly linked to transcriptomic perturbations and fibrogenic responses. In contrast, for SWCNTs, although surface area and functionalization were robust predictors of toxicity, the relationships appeared more complex and did not follow the linear trends. Metal impurities, particularly manganese and magnesium, emerged as prominent drivers of toxicity in SWCNTs. These findings suggest that SWCNTs may require distinct mechanistic modelling approaches. Further, the complexities observed in SWCNTs could be partly attributed to data limitations, such as the insufficient information on their length and diameter.

In the third part of this dissertation, the previously developed AOP-informed Nano-QSAR model was employed using a random forest (RF) algorithm to quantify the impact of the structural properties of both S- and MWCNTs on the transcriptional benchmark dose level ($BMDL_{AR}$) responses within the acute phase response (AR) signaling pathway. The results highlighted that the specific surface area, Fe2O3 and CoO content as major predictors of the early biological events that initiate the inflammatory processes, ultimately leading to lung fibrosis (as outlined in AOP 33) and atherosclerosis (as per AOP 237) pathologies. By employing the grouping strategy, this extended Nano-QSAR framework

enabled predicted key events (KEs) across nanotubes based on their modeled physicochemical profiles.

In conclusion, these results support the integration of Nano-QSAR and Nano-AOP modeling approaches for both S- and MWCNTs. This integration can contribute to the refinement of AOP33 and its broader applicability, enhancing the mechanistic understanding and regulatory assessment of nanomaterial-induced toxicity.

This dissertation presents several key strengths that contribute to its novelty and scientific value. It is among the first studies to combine transcriptomic pathway analysis with cheminformatics in a way that directly aligns with regulatory decision-making. The thoughtful selection and application of machine learning methods, including regression, classification, and clustering, enabled each modeling task to address specific scientific objectives. By focusing on molecular pathway-level responses rather than traditional apical endpoints, this work provides mechanistic insights into nanomaterial toxicity, advancing beyond descriptive toxicology. Moreover, the emphasis on impurity profiling offers a new and often underexplored dimension to ENMs assessment. This aspect contributes to a more complete understanding of how metal impurities, such as iron, cobalt, manganese, magnesium and nickel, may influence biological outcomes.

However, the research is not without limitations. The dataset, particularly for SWCNTs, was relatively limited, which may constrain the generalizability of some findings. Additionally, the study focused on acute-phase response data from single-dose exposures, which does not fully capture the complexity of chronic or low-dose, real-world exposure scenarios. Future work should aim to expand datasets to include a wider array of nanomaterials, exposure durations and dose levels. Integrating emerging *in vitro* and *in silico* systems, such as organ-on-chip systems and physiologically based pharmacokinetic (PBPK), will be essential to improving cross-species extrapolation and enhancing human relevance. Furthermore, the incorporation of multi-omics data (e.g., proteomics and metabolomics) can enrich the mechanistic modelling landscape, paving the way toward

systems toxicology approaches. Such integration would allow the development of more holistic, dynamic models of nanomaterial-induced adverse outcomes.

In summary, this dissertation offers a rational, mechanism-informed prediction of nanomaterial toxicity. By integrating AOPs and transcriptomic pathway data into computational modeling, it demonstrates the potential of *in silico* tools to support hazard identification, grouping, and read-across for CNTs and similar materials. The work not only contributes meaningfully to the scientific foundation of nanotoxicology but also supports the advancement of regulatory science, aligning with ethical, mechanistically grounded and efficient safety assessment strategies. Ultimately, it supports the broader vision of Safe-and-Sustainable-by-Design (SSbD) innovation in nanotechnology, an essential step toward sustainable and responsible development of advanced materials.

6. REFERENCES

(1) Iijima, S.; Ichihashi, T. Single-Shell Carbon Nanotubes of 1-Nm Diameter. *Nature* **1993**, *363* (6430), 603–605. https://doi.org/10.1038/363603a0.

(2) Kalbáč, M.; Kavan, L.; Dunsch, L. In Situ Raman Spectroelectrochemistry as a Tool for the Differentiation of Inner Tubes of Double-Wall Carbon Nanotubes and Thin Single-Wall Carbon Nanotubes. *Anal Chem* **2007**, *79* (23), 9074–9081. https://doi.org/10.1021/ac071205u.

(3) Shen, C.; Brozena, A. H.; Wang, Y. Double-Walled Carbon Nanotubes: Challenges and Opportunities. *Nanoscale* **2011**, *3* (2), 503–518. https://doi.org/10.1039/C0NR00620C.

(4) Morrot-Woisard, I.; Nguyen, E. K.; Vukadinovic, N.; Boero, M. Structural, Electronic and Dielectric Properties of Carbon Nanotubes Interacting with Co Nanoclusters. *Carbon Trends* **2024**, *17*, 100410. https://doi.org/10.1016/j.cartre.2024.100410.

(5) Qin, L.-C. Determination of the Chiral Indices (n,m) of Carbon Nanotubes by Electron Diffraction. *Phys. Chem. Chem. Phys.* **2007**, *9* (1), 31–48. https://doi.org/10.1039/B614121H.

(6) Domun, N.; Hadavinia, H.; Zhang, T.; Sainsbury, T.; Liaghat, G. H.; Vahid, S. Improving the Fracture Toughness and the Strength of Epoxy Using Nanomaterials – a Review of the Current Status. *Nanoscale* **2015**, *7* (23), 10294–10329. https://doi.org/10.1039/C5NR01354B.

(7) Yue, S.-Y.; Ouyang, T.; Hu, M. Diameter Dependence of Lattice Thermal Conductivity of Single-Walled Carbon Nanotubes: Study from Ab Initio. *Sci Rep* **2015**, *5* (1), 15440. https://doi.org/10.1038/srep15440.

(8) Bandaru, P. R. Electrical Properties and Applications of Carbon Nanotube Structures. *J Nanosci Nanotechnol* **2007**, *7* (4), 1239–1267. https://doi.org/10.1166/jnn.2007.307.

(9) Lasky, J. A.; Coin, P. G.; Lindroos, P. M.; Ostrowski, L. E.; Brody, A. R.; Bonner, J. C. Chrysotile Asbestos Stimulates Platelet-Derived Growth Factor-

AA Production by Rat Lung Fibroblasts in Vitro: Evidence for an Autocrine Loop. *Am J Respir Cell Mol Biol* **1995**, *12* (2), 162–170. https://doi.org/10.1165/ajrcmb.12.2.7865215.

(10) Wang, P.; Wang, Y.; Nie, X.; Braïni, C.; Bai, R.; Chen, C. Multiwall Carbon Nanotubes Directly Promote Fibroblast-Myofibroblast and Epithelial-Mesenchymal Transitions through the Activation of the TGF-β/Smad Signaling Pathway. *Small* **2015**, *11* (4), 446–455. https://doi.org/10.1002/smll.201303588.

(11) Vietti, G.; Ibouraadaten, S.; Palmai-Pallag, M.; Yakoub, Y.; Bailly, C.; Fenoglio, I.; Marbaix, E.; Lison, D.; van den Brule, S. Towards Predicting the Lung Fibrogenic Activity of Nanomaterials: Experimental Validation of an in Vitro Fibroblast Proliferation Assay. *Part Fibre Toxicol* **2013**, *10* (1), 52. https://doi.org/10.1186/1743-8977-10-52.

(12) Donaldson, K.; Poland, C. A.; Murphy, F. A.; MacFarlane, M.; Chernova, T.; Schinwald, A. Pulmonary Toxicity of Carbon Nanotubes and Asbestos — Similarities and Differences. *Adv Drug Deliv Rev* **2013**, *65* (15), 2078–2086. https://doi.org/10.1016/j.addr.2013.07.014.

(13) Poland, C. A.; Duffin, R.; Kinloch, I.; Maynard, A.; Wallace, W. A. H.; Seaton, A.; Stone, V.; Brown, S.; MacNee, W.; Donaldson, K. Carbon Nanotubes Introduced into the Abdominal Cavity of Mice Show Asbestos-like Pathogenicity in a Pilot Study. *Nat Nanotechnol* **2008**, *3* (7), 423–428. https://doi.org/10.1038/nnano.2008.111.

(14) Huang, Y.; Wu, J.; Hwang, K. C. Thickness of Graphene and Single-Wall Carbon Nanotubes. *Phys Rev B* **2006**, *74* (24), 245413. https://doi.org/10.1103/PhysRevB.74.245413.

(15) Mallakpour, S.; Soltanian, S. Surface Functionalization of Carbon Nanotubes: Fabrication and Applications. *RSC Adv* **2016**, *6* (111), 109916–109935. https://doi.org/10.1039/C6RA24522F.

(16) Zhou, L.; Forman, H. J.; Ge, Y.; Lunec, J. Multi-Walled Carbon Nanotubes: A Cytotoxicity Study in Relation to Functionalization, Dose and Dispersion. *Toxicology in Vitro* **2017**, *42*, 292–298. https://doi.org/10.1016/j.tiv.2017.04.027.

(17) Benko, A.; Duch, J.; Gajewska, M.; Marzec, M.; Bernasik, A.; Nocuń, M.; Piskorz, W.; Kotarba, A. Covalently Bonded Surface Functional Groups on Carbon Nanotubes: From Molecular Modeling to Practical Applications. *Nanoscale* **2021**, *13* (22), 10152–10166. https://doi.org/10.1039/D0NR09057C.

(18) Ge, C.; Li, Y.; Yin, J.-J.; Liu, Y.; Wang, L.; Zhao, Y.; Chen, C. The Contributions of Metal Impurities and Tube Structure to the Toxicity of Carbon Nanotube Materials. *NPG Asia Mater* **2012**, *4* (12), e32–e32. https://doi.org/10.1038/am.2012.60.

(19) Thiruvengadam, M.; Rajakumar, G.; Swetha, V.; Ansari, M.; Alghamdi, S.; Almehmadi, M.; Halawi, M.; Kungumadevi, L.; Raja, V.; Sabura Sarbudeen, S.; Madhavan, S.; Rebezov, M.; Ali Shariati, M.; Sviderskiy, A.; Bogonosov, K. Recent Insights and Multifactorial Applications of Carbon Nanotubes. *Micromachines (Basel)* **2021**, *12* (12), 1502. https://doi.org/10.3390/mi12121502.

(20) Hughes, K. J.; Iyer, K. A.; Bird, R. E.; Ivanov, J.; Banerjee, S.; Georges, G.; Zhou, Q. A. Review of Carbon Nanotube Research and Development: Materials and Emerging Applications. *ACS Appl Nano Mater* **2024**, *7* (16), 18695–18713. https://doi.org/10.1021/acsanm.4c02721.

(21) Jariwala, D.; Sangwan, V. K.; Lauhon, L. J.; Marks, T. J.; Hersam, M. C. Carbon Nanomaterials for Electronics, Optoelectronics, Photovoltaics, and Sensing. *Chem. Soc. Rev.* **2013**, *42* (7), 2824–2860. https://doi.org/10.1039/C2CS35335K.

(22) He, H.; Pham-Huy, L. A.; Dramou, P.; Xiao, D.; Zuo, P.; Pham-Huy, C. Carbon Nanotubes: Applications in Pharmacy and Medicine. *Biomed Res Int* **2013**, *2013*, 1–12. https://doi.org/10.1155/2013/578290.

(23) Syduzzaman, M.; Islam Saad, M. S.; Piam, M. F.; Talukdar, T. A.; Shobdo, T. T.; Pritha, N. M. Carbon Nanotubes: Structure, Properties and Applications in the Aerospace Industry. *Results in Materials* **2025**, *25*, 100654. https://doi.org/10.1016/j.rinma.2024.100654.

(24) Rathinavel, S.; Priyadharshini, K.; Panda, D. A Review on Carbon Nanotube: An Overview of Synthesis, Properties, Functionalization, Characterization, and the Application. *Materials Science and Engineering: B* **2021**, *268*, 115095. https://doi.org/10.1016/j.mseb.2021.115095.

(25) grandviewresearch.com. [Accessed on: 07.06.2025]

(26) researchandmarkets.com. [Accessed on: 07.06.2025]

(27) theinsightpartners.com. [Accessed on: 07.06.2025]

(28) marketsandmarkets.com. [Accessed on: 07.06.2025]

(29) Dong, J.; Ma, Q. Advances in Mechanisms and Signaling Pathways of Carbon Nanotube Toxicity. *Nanotoxicology* **2015**, *9* (5), 658–676. https://doi.org/10.3109/17435390.2015.1009187.

(30) Saleemi, M. A.; Hosseini Fouladi, M.; Yong, P. V. C.; Chinna, K.; Palanisamy, N. K.; Wong, E. H. Toxicity of Carbon Nanotubes: Molecular Mechanisms, Signaling Cascades, and Remedies in Biomedical Applications. *Chem Res Toxicol* **2021**, *34* (1), 24–46. https://doi.org/10.1021/acs.chemrestox.0c00172.

(31) Snyder, R. J.; Verhein, K. C.; Vellers, H. L.; Burkholder, A. B.; Garantziotis, S.; Kleeberger, S. R. Multi-Walled Carbon Nanotubes Upregulate Mitochondrial Gene Expression and Trigger Mitochondrial Dysfunction in Primary Human Bronchial Epithelial Cells. *Nanotoxicology* **2019**, *13* (10), 1344–1361. https://doi.org/10.1080/17435390.2019.1655107.

(32) Shvedova, A. A.; Pietroiusti, A.; Fadeel, B.; Kagan, V. E. Mechanisms of Carbon Nanotube-Induced Toxicity: Focus on Oxidative Stress. *Toxicol Appl Pharmacol* **2012**, *261* (2), 121–133. https://doi.org/10.1016/j.taap.2012.03.023.

(33) Dong, J.; Porter, D. W.; Batteli, L. A.; Wolfarth, M. G.; Richardson, D. L.; Ma, Q. Pathologic and Molecular Profiling of Rapid-Onset Fibrosis and Inflammation Induced by Multi-Walled Carbon Nanotubes. *Arch Toxicol* **2015**, *89* (4), 621–633. https://doi.org/10.1007/s00204-014-1428-y.

(34) Fadeel, B.; Kagan, V. E. Apoptosis and Macrophage Clearance of Neutrophils: Regulation by Reactive Oxygen Species. *Redox Report* **2003**, *8* (3), 143–150. https://doi.org/10.1179/135100003225001511.

(35) Poulsen, S. S.; Jackson, P.; Kling, K.; Knudsen, K. B.; Skaug, V.; Kyjovska, Z. O.; Thomsen, B. L.; Clausen, P. A.; Atluri, R.; Berthing, T.; Bengtson, S.; Wolff, H.; Jensen, K. A.; Wallin, H.; Vogel, U. Multi-Walled Carbon Nanotube Physicochemical Properties Predict Pulmonary Inflammation and Genotoxicity. *Nanotoxicology* **2016**, *10* (9), 1263–1275. https://doi.org/10.1080/17435390.2016.1202351.

(36) Aschberger, K.; Asturiol, D.; Lamon, L.; Richarz, A.; Gerloff, K.; Worth, A. Grouping of Multi-Walled Carbon Nanotubes to Read-across Genotoxicity: A Case Study to Evaluate the Applicability of Regulatory Guidance. *Computational Toxicology* **2019**, *9*, 22–35. https://doi.org/10.1016/j.comtox.2018.10.001.

(37) Shvedova, A. A.; Pietroiusti, A.; Fadeel, B.; Kagan, V. E. Mechanisms of Carbon Nanotube-Induced Toxicity: Focus on Oxidative Stress. *Toxicol Appl Pharmacol* **2012**, *261* (2), 121–133. https://doi.org/10.1016/j.taap.2012.03.023.

(38) Ghosh, M.; Chakraborty, A.; Bandyopadhyay, M.; Mukherjee, A. Multi-Walled Carbon Nanotubes (MWCNT): Induction of DNA Damage in Plant

and Mammalian Cells. *J Hazard Mater* **2011**, *197*, 327–336. https://doi.org/10.1016/j.jhazmat.2011.09.090.

(39) Poulsen, S. S.; Saber, A. T.; Mortensen, A.; Szarek, J.; Wu, D.; Williams, A.; Andersen, O.; Jacobsen, N. R.; Yauk, C. L.; Wallin, H.; Halappanavar, S.; Vogel, U. Changes in Cholesterol Homeostasis and Acute Phase Response Link Pulmonary Exposure to Multi-Walled Carbon Nanotubes to Risk of Cardiovascular Disease. *Toxicol Appl Pharmacol* **2015**, *283* (3), 210–222. https://doi.org/10.1016/j.taap.2015.01.011.

(40) Dong, J.; Ma, Q. Advances in Mechanisms and Signaling Pathways of Carbon Nanotube Toxicity. *Nanotoxicology* **2015**, *9* (5), 658–676. https://doi.org/10.3109/17435390.2015.1009187.

(41) Dong, J.; Ma, Q. Osteopontin Enhances Multi-Walled Carbon Nanotube-Triggered Lung Fibrosis by Promoting TGF-B1 Activation and Myofibroblast Differentiation. *Part Fibre Toxicol* **2017**, *14* (1). https://doi.org/10.1186/s12989-017-0198-0.

(42) Dong, J.; Ma, Q. Suppression of Basal and Carbon Nanotube-Induced Oxidative Stress, Inflammation and Fibrosis in Mouse Lungs by Nrf2. *Nanotoxicology* **2016**, *10* (6), 699–709. https://doi.org/10.3109/17435390.2015.1110758.

(43) Duke, K. S.; Bonner, J. C. Mechanisms of Carbon Nanotube-Induced Pulmonary Fibrosis: A Physicochemical Characteristic Perspective. *Wiley Interdiscip Rev Nanomed Nanobiotechnol* **2018**, *10* (3). https://doi.org/10.1002/WNAN.1498.

(44) Dong, J.; Ma, Q. TIMP1 Promotes Multi-Walled Carbon Nanotube-Induced Lung Fibrosis by Stimulating Fibroblast Activation and Proliferation. *Nanotoxicology* **2017**, *11* (1), 41–51. https://doi.org/10.1080/17435390.2016.1262919.

(45) Dong, J.; Ma, Q. In Vivo Activation and Pro-Fibrotic Function of NF-KB in Fibroblastic Cells During Pulmonary Inflammation and Fibrosis Induced by Carbon Nanotubes. *Front Pharmacol* **2019**, *10*. https://doi.org/10.3389/fphar.2019.01140.

(46) Dong, J.; Ma, Q. Macrophage Polarization and Activation at the Interface of Multi-Walled Carbon Nanotube-Induced Pulmonary Inflammation and Fibrosis. *Nanotoxicology* **2018**, *12* (2), 153–168. https://doi.org/10.1080/17435390.2018.1425501.

(47) Dong, J.; Ma, Q. Integration of Inflammation, Fibrosis, and Cancer Induced by Carbon Nanotubes. *Nanotoxicology* **2019**, *13* (9), 1244–1274. https://doi.org/10.1080/17435390.2019.1651920.

(48) Saleh, D. M.; Alexander, W. T.; Numano, T.; Ahmed, O. H. M.; Gunasekaran, S.; Alexander, D. B.; Abdelgied, M.; El-Gazzar, A. M.; Takase, H.; Xu, J.; Naiki-Ito, A.; Takahashi, S.; Hirose, A.; Ohnishi, M.; Kanno, J.; Tsuda, H. Comparative Carcinogenicity Study of a Thick, Straight-Type and a Thin, Tangled-Type Multi-Walled Carbon Nanotube Administered by Intra-Tracheal Instillation in the Rat. *Part Fibre Toxicol* **2020**, *17* (1), 48. https://doi.org/10.1186/s12989-020-00382-y.

(49) Gaté, L.; Knudsen, K. B.; Seidel, C.; Berthing, T.; Chézeau, L.; Jacobsen, N. R.; Valentino, S.; Wallin, H.; Bau, S.; Wolff, H.; Sébillaud, S.; Lorcin, M.; Grossmann, S.; Viton, S.; Nunge, H.; Darne, C.; Vogel, U.; Cosnier, F. Pulmonary Toxicity of Two Different Multi-Walled Carbon Nanotubes in Rat: Comparison between Intratracheal Instillation and Inhalation Exposure. *Toxicol Appl Pharmacol* **2019**, *375*, 17–31. https://doi.org/10.1016/j.taap.2019.05.001.

(50) Rahman, L.; Jacobsen, N. R.; Aziz, S. A.; Wu, D.; Williams, A.; Yauk, C. L.; White, P.; Wallin, H.; Vogel, U.; Halappanavar, S. Multi-Walled Carbon Nanotube-Induced Genotoxic, Inflammatory and pro-Fibrotic Responses in

Mice: Investigating the Mechanisms of Pulmonary Carcinogenesis. *Mutation Research/Genetic Toxicology and Environmental Mutagenesis* **2017**, *823*, 28–44. https://doi.org/10.1016/j.mrgentox.2017.08.005.

(51) Dong, J. Signaling Pathways Implicated in Carbon Nanotube-Induced Lung Inflammation. *Front Immunol* **2020**, *11*. https://doi.org/10.3389/fimmu.2020.552613.

(52) Rabbit, R. R.; Hartung, aka T. Advice for Bad Toxicologists. *NAM Journal* **2025**, *1*, 100002. https://doi.org/10.1016/j.namjnl.2024.100002.

(53) Halappanavar, S.; Nymark, P.; Krug, H. F.; Clift, M. J. D.; Rothen-Rutishauser, B.; Vogel, U. Non-Animal Strategies for Toxicity Assessment of Nanoscale Materials: Role of Adverse Outcome Pathways in the Selection of Endpoints. *Small* **2021**, *17* (15). https://doi.org/10.1002/smll.202007628.

(54) *The Use of Alternatives to Testing on Animals for the REACH Regulation*; ECHA, 2023.

(55) Berggren, E.; Worth, A. P. Towards a Future Regulatory Framework for Chemicals in the European Union – Chemicals 2.0. *Regulatory Toxicology and Pharmacology* **2023**, *142*, 105431. https://doi.org/10.1016/j.yrtph.2023.105431.

(56) Manful, M. E.; Ahmed, L.; Barry-Ryan, C. New Approach Methodologies (NAMs) for Safety Testing of Complex Food Matrices: A Review of Status, Considerations, and Regulatory Adoption. *Trends Food Sci Technol* **2023**, *142*, 104191. https://doi.org/10.1016/j.tifs.2023.104191.

(57) Sewell, F.; Alexander-White, C.; Brescia, S.; Currie, R. A.; Roberts, R.; Roper, C.; Vickers, C.; Westmoreland, C.; Kimber, I. New Approach Methodologies (NAMs): Identifying and Overcoming Hurdles to Accelerated Adoption. *Toxicol Res (Camb)* **2024**, *13* (2). https://doi.org/10.1093/toxres/tfae044.

(58) Jagiello, K.; Sosnowska, A.; Stępnik, M.; Gromelski, M.; Płonka, K. *Nano-Specific Alternative Methods in Human Hazard/Safety Assessment under*

Different EU Regulations, Considering the Animal Testing Bans Already in Place for Cosmetics and Their Ingredients Final Report, **2023.**

(59) Carramusa, L.; Mune, W.; Hunt, N.; Browne, L.; Osborne, O.; Potter, C. New Approach Methodologies (NAMs) to Support Regulatory Decisions for Chemical Safety. *FSA Research and Evidence* **2024**. https://doi.org/10.46756/001c.122591.

(60) Hristozov, D.; Badetti, E.; Bigini, P.; Brunelli, A.; Dekkers, S.; Diomede, L.; Doak, S. H.; Fransman, W.; Gajewicz-Skretna, A.; Giubilato, E.; Gómez-Cuadrado, L.; Grafström, R.; Gutleb, A. C.; Halappanavar, S.; Hischier, R.; Hunt, N.; Katsumiti, A.; Kermanizadeh, A.; Marcomini, A.; Moschini, E.; Oomen, A.; Pizzol, L.; Rumbo, C.; Schmid, O.; Shandilya, N.; Stone, V.; Stoycheva, S.; Stoeger, T.; Merino, B. S.; Tran, L.; Tsiliki, G.; Vogel, U. B.; Wohlleben, W.; Zabeo, A. Next Generation Risk Assessment Approaches for Advanced Nanomaterials: Current Status and Future Perspectives. *NanoImpact* **2024**, *35*, 100523. https://doi.org/10.1016/j.impact.2024.100523.

(61) Carmichael, P. Ready for Regulatory Use: NAMs and NGRA for Chemical Safety Assurance. *ALTEX* **2022**. https://doi.org/10.14573/altex.2204281.

(62) *Guidance Document on Integrated Approaches to Testing and Assessment (IATA) for Serious Eye Damage and Eye Irritation, Third Edition*; OECD Series on Testing and Assessment; OECD Publishing, 2024. https://doi.org/10.1787/cdb440be-en.

(63) Murphy, F. How to Formulate Hypotheses and IATA to Support Grouping and Read-across of Nanoforms. *ALTEX* **2022**. https://doi.org/10.14573/altex.2203241.

(64) Jeliazkova, N.; Bleeker, E.; Cross, R.; Haase, A.; Janer, G.; Peijnenburg, W.; Pink, M.; Rauscher, H.; Svendsen, C.; Tsiliki, G.; Zabeo, A.; Hristozov, D.; Stone, V.; Wohlleben, W. How Can We Justify Grouping of Nanoforms for

Hazard Assessment? Concepts and Tools to Quantify Similarity. *NanoImpact* **2022**, *25*, 100366. https://doi.org/10.1016/j.impact.2021.100366.

(65) Gerloff, K.; Landesmann, B.; Worth, A.; Munn, S.; Palosaari, T.; Whelan, M. The Adverse Outcome Pathway Approach in Nanotoxicology. *Computational Toxicology* **2017**, *1*, 3–11. https://doi.org/10.1016/j.comtox.2016.07.001.

(66) Nymark, P.; Clerbaux, L.-A.; Amorim, M.-J.; Andronis, C.; de Bernardi, F.; Bezemer, G. F. G.; Coecke, S.; Gavins, F. N. E.; Jacobson, D.; Lekka, E.; Margiotta-Casaluci, L.; Martens, M.; Mayasich, S. A.; Mortensen, H. M.; Kim, Y. J.; Sachana, M.; Tanabe, S.; Virvilis, V.; Edwards, S. W.; Halappanavar, S. Building an Adverse Outcome Pathway Network for COVID-19. *Frontiers in Systems Biology* **2024**, *4*. https://doi.org/10.3389/fsysb.2024.1384481.

(67) Nymark, P.; Bakker, M.; Dekkers, S.; Franken, R.; Fransman, W.; García-Bilbao, A.; Greco, D.; Gulumian, M.; Hadrup, N.; Halappanavar, S.; Hongisto, V.; Hougaard, K. S.; Jensen, K. A.; Kohonen, P.; Koivisto, A. J.; Dal Maso, M.; Oosterwijk, T.; Poikkimäki, M.; Rodriguez-Llopis, I.; Stierum, R.; Sørli, J. B.; Grafström, R. Toward Rigorous Materials Production: New Approach Methodologies Have Extensive Potential to Improve Current Safety Assessment Practices. *Small* **2020**, *16* (6). https://doi.org/10.1002/smll.201904749.

(68) https://aopwiki.org. [Accessed on: 07.06.2025]

(69) Rahman, L.; Williams, A.; Gelda, K.; Nikota, J.; Wu, D.; Vogel, U.; Halappanavar, S. 21st Century Tools for Nanotoxicology: Transcriptomic Biomarker Panel and Precision-Cut Lung Slice Organ Mimic System for the Assessment of Nanomaterial-Induced Lung Fibrosis. *Small* **2020**, *16* (36). https://doi.org/10.1002/smll.202000272.

(70) Halappanavar, S.; van den Brule, S.; Nymark, P.; Gaté, L.; Seidel, C.; Valentino, S.; Zhernovkov, V.; Høgh Danielsen, P.; De Vizcaya, A.; Wolff, H.; Stöger, T.; Boyadziev, A.; Poulsen, S. S.; Sørli, J. B.; Vogel, U. Adverse

Outcome Pathways as a Tool for the Design of Testing Strategies to Support the Safety Assessment of Emerging Advanced Materials at the Nanoscale. *Part Fibre Toxicol* **2020**, *17* (1), 16. https://doi.org/10.1186/s12989-020-00344-4.

(71) Bajard, L.; Adamovsky, O.; Audouze, K.; Baken, K.; Barouki, R.; Beltman, J. B.; Beronius, A.; Bonefeld-Jørgensen, E. C.; Cano-Sancho, G.; de Baat, M. L.; Di Tillio, F.; Fernández, M. F.; FitzGerald, R. E.; Gundacker, C.; Hernández, A. F.; Hilscherova, K.; Karakitsios, S.; Kuchovska, E.; Long, M.; Luijten, M.; Majid, S.; Marx-Stoelting, P.; Mustieles, V.; Negi, C. K.; Sarigiannis, D.; Scholz, S.; Sovadinova, I.; Stierum, R.; Tanabe, S.; Tollefsen, K. E.; van den Brand, A. D.; Vogs, C.; Wielsøe, M.; Wittwehr, C.; Blaha, L. Application of AOPs to Assist Regulatory Assessment of Chemical Risks – Case Studies, Needs and Recommendations. *Environ Res* **2023**, *217*, 114650. https://doi.org/10.1016/j.envres.2022.114650.

(72) Puzyn, T.; Leszczynska, D.; Leszczynski, J. Toward the Development of "Nano-QSARs": Advances and Challenges. *Small* **2009**, *5* (22), 2494–2509. https://doi.org/10.1002/smll.200900179.

(73) Wyrzykowska, E.; Mikolajczyk, A.; Lynch, I.; Jeliazkova, N.; Kochev, N.; Sarimveis, H.; Doganis, P.; Karatzas, P.; Afantitis, A.; Melagraki, G.; Serra, A.; Greco, D.; Subbotina, J.; Lobaskin, V.; Bañares, M. A.; Valsami-Jones, E.; Jagiello, K.; Puzyn, T. Representing and Describing Nanomaterials in Predictive Nanoinformatics. *Nat Nanotechnol* **2022**, *17* (9), 924–932. https://doi.org/10.1038/s41565-022-01173-6.

(74) Mancardi, G.; Mikolajczyk, A.; Annapoorani, V. K.; Bahl, A.; Blekos, K.; Burk, J.; Çetin, Y. A.; Chairetakis, K.; Dutta, S.; Escorihuela, L.; Jagiello, K.; Singhal, A.; van der Pol, R.; Bañares, M. A.; Buchete, N.-V.; Calatayud, M.; Dumit, V. I.; Gardini, D.; Jeliazkova, N.; Haase, A.; Marcoulaki, E.; Martorell, B.; Puzyn, T.; Agur Sevink, G. J.; Simeone, F. C.; Tämm, K.; Chiavazzo, E.

A Computational View on Nanomaterial Intrinsic and Extrinsic Features for Nanosafety and Sustainability. *Materials Today* **2023**, *67*, 344–370. https://doi.org/10.1016/j.mattod.2023.05.029.

(75) Jagiello, K.; Halappanavar, S.; Rybińska-Fryca, A.; Willliams, A.; Vogel, U.; Puzyn, T. Transcriptomics-Based and AOP-Informed Structure–Activity Relationships to Predict Pulmonary Pathology Induced by Multiwalled Carbon Nanotubes. *Small* **2021**, *17* (15). https://doi.org/10.1002/smll.202003465.

(76) Gadaleta, D.; Garcia de Lomana, M.; Serrano-Candelas, E.; Ortega-Vallbona, R.; Gozalbes, R.; Roncaglioni, A.; Benfenati, E. Quantitative Structure–Activity Relationships of Chemical Bioactivity toward Proteins Associated with Molecular Initiating Events of Organ-Specific Toxicity. *J Cheminform* **2024**, *16* (1), 122. https://doi.org/10.1186/s13321-024-00917-x.

(77) Puzyn, T.; Mostrag-Szlichtyng, A.; Gajewicz, A.; Skrzyński, M.; Worth, A. P. Investigating the Influence of Data Splitting on the Predictive Ability of QSAR/QSPR Models. *Struct Chem* **2011**, *22* (4), 795–804. https://doi.org/10.1007/s11224-011-9757-4.

(78) Gramatica, P. Origin of the OECD Principles for QSAR Validation and Their Role in Changing the QSAR Paradigm Worldwide: An Historical Overview. *J Chemom* **2025**, *39* (3). https://doi.org/10.1002/cem.70014.

(79) Gorodenkoff. *(Q)SAR Assessment Framework: Guidance for the Regulatory Assessment of (Quantitative) Structure Activity Relationship Models and Predictions, Second Edition Series on Testing and Assessment No. 405*; 2024.

(80) Sosnowska, A.; Bulawska, N.; Kowalska, D.; Puzyn, T. Towards Higher Scientific Validity and Regulatory Acceptance of Predictive Models for PFAS. *Green Chemistry* **2023**, *25* (4), 1261–1275. https://doi.org/10.1039/D2GC04341F.

(81) Cherkasov, A.; Muratov, E. N.; Fourches, D.; Varnek, A.; Baskin, I. I.; Cronin, M.; Dearden, J.; Gramatica, P.; Martin, Y. C.; Todeschini, R.; Consonni, V.;

Kuz'min, V. E.; Cramer, R.; Benigni, R.; Yang, C.; Rathman, J.; Terfloth, L.; Gasteiger, J.; Richard, A.; Tropsha, A. QSAR Modeling: Where Have You Been? Where Are You Going To? *J Med Chem* **2014**, *57* (12), 4977–5010. https://doi.org/10.1021/jm4004285.

(82) Tropsha, A. Best Practices for QSAR Model Development, Validation, and Exploitation. *Mol Inform* **2010**, *29* (6–7), 476–488. https://doi.org/10.1002/minf.201000061.

(83) Fourches, D.; Muratov, E.; Tropsha, A. Trust, But Verify: On the Importance of Chemical Structure Curation in Cheminformatics and QSAR Modeling Research. *J Chem Inf Model* **2010**, *50* (7), 1189–1204. https://doi.org/10.1021/ci100176x.

(84) Gramatica, P. Principles of QSAR Modeling. *International Journal of Quantitative Structure-Property Relationships* **2020**, *5* (3), 61–97. https://doi.org/10.4018/IJQSPR.20200701.oa1.

(85) Papa, E.; Villa, F.; Gramatica, P. Statistically Validated QSARs, Based on Theoretical Descriptors, for Modeling Aquatic Toxicity of Organic Chemicals in *Pimephales p Romelas* (Fathead Minnow). *J Chem Inf Model* **2005**, *45* (5), 1256–1266. https://doi.org/10.1021/ci050212l.

(86) Roy, K.; Das, R. N.; Ambure, P.; Aher, R. B. Be Aware of Error Measures. Further Studies on Validation of Predictive QSAR Models. *Chemometrics and Intelligent Laboratory Systems* **2016**, *152*, 18–33. https://doi.org/10.1016/j.chemolab.2016.01.008.

(87) Chirico, N.; Gramatica, P. Real External Predictivity of QSAR Models: How To Evaluate It? Comparison of Different Validation Criteria and Proposal of Using the Concordance Correlation Coefficient. *J Chem Inf Model* **2011**, *51* (9), 2320–2335. https://doi.org/10.1021/ci200211n.

(88) Gramatica, P. Principles of QSAR Models Validation: Internal and External. *QSAR Comb Sci* **2007**, *26* (5), 694–701. https://doi.org/10.1002/qsar.200610151.

(89) Tropsha, A.; Gramatica, P.; Gombar, V. K. The Importance of Being Earnest: Validation Is the Absolute Essential for Successful Application and Interpretation of QSPR Models. *QSAR Comb Sci* **2003**, *22* (1), 69–77. https://doi.org/10.1002/qsar.200390007.

(90) Numpy. https://numpy.org. [Accessed on: 07.06.2025]

(91) R. https://www.r-Project.org. [Accessed on: 07.06.2025]

(92) Python. https://python.org. [Accessed on: 07.06.2025]

(93) Seaborn. https://seaborn.pydata.org. [Accessed on: 07.06.2025]

(94) Matplotlib. https://matplotlib.org. [Accessed on: 07.06.2025]

(95) Scikit-Learn. https://scikit-learn.org/stable. [Accessed on: 07.06.2025]

(96) Scipy. https://www.scipy.org. [Accessed on: 07.06.2025]

(97) Stats. https://cran.r-project.org. [Accessed on: 07.06.2025]

(98) Dplyr. https://cran.r-project.org. [Accessed on: 07.06.2025]

(99) Reshape2. https://cran.r-project.org. [Accessed on: 07.06.2025]

(100) ggplot2. https://ggplot2.tidyverse.org. [Accessed on: 07.06.2025]

(101) Caret. https://cran.r-project.org. [Accessed on: 07.06.2025]

(102) Søs Poulsen, S.; Jacobsen, N. R.; Labib, S.; Wu, D.; Husain, M.; Williams, A.; Bøgelund, J. P.; Andersen, O.; Købler, C.; Mølhave, K.; Kyjovska, Z. O.; Saber, A. T.; Wallin, H.; Yauk, C. L.; Vogel, U.; Halappanavar, S. Transcriptomic Analysis Reveals Novel Mechanistic Insight into Murine Biological Responses to Multi-Walled Carbon Nanotubes in Lungs and Cultured Lung Epithelial Cells. *PLoS One* **2013**, *8* (11), e80452. https://doi.org/10.1371/journal.pone.0080452.

(103) Poulsen, S. S.; Saber, A. T.; Mortensen, A.; Szarek, J.; Wu, D.; Williams, A.; Andersen, O.; Jacobsen, N. R.; Yauk, C. L.; Wallin, H.; Halappanavar, S.;

Vogel, U. Changes in Cholesterol Homeostasis and Acute Phase Response Link Pulmonary Exposure to Multi-Walled Carbon Nanotubes to Risk of Cardiovascular Disease. *Toxicol Appl Pharmacol* **2015**, *283* (3), 210–222. https://doi.org/10.1016/j.taap.2015.01.011.

(104) Jackson, P.; Kling, K.; Jensen, K. A.; Clausen, P. A.; Madsen, A. M.; Wallin, H.; Vogel, U. Characterization of Genotoxic Response to 15 Multiwalled Carbon Nanotubes with Variable Physicochemical Properties Including Surface Functionalizations in the <scp>FE</Scp> 1-Muta(<scp>TM</Scp>) Mouse Lung Epithelial Cell Line. *Environ Mol Mutagen* **2015**, *56* (2), 183–203. https://doi.org/10.1002/em.21922.

(105) Knudsen, K. B.; Berthing, T.; Jackson, P.; Poulsen, S. S.; Mortensen, A.; Jacobsen, N. R.; Skaug, V.; Szarek, J.; Hougaard, K. S.; Wolff, H.; Wallin, H.; Vogel, U. Physicochemical Predictors of Multi-Walled Carbon Nanotube–Induced Pulmonary Histopathology and Toxicity One Year after Pulmonary Deposition of 11 Different Multi-Walled Carbon Nanotubes in Mice. *Basic Clin Pharmacol Toxicol* **2019**, *124* (2), 211–227. https://doi.org/10.1111/bcpt.13119.

(106) Danielsen, P. H.; Poulsen, S. S.; Knudsen, K. B.; Clausen, P. A.; Jensen, K. A.; Wallin, H.; Vogel, U. Physicochemical Properties of 26 Carbon Nanotubes as Predictors for Pulmonary Inflammation and Acute Phase Response in Mice Following Intratracheal Lung Exposure. *Environ Toxicol Pharmacol* **2024**, *107*, 104413. https://doi.org/10.1016/j.etap.2024.104413.

(107) Halappanavar, S.; Rahman, L.; Nikota, J.; Poulsen, S. S.; Ding, Y.; Jackson, P.; Wallin, H.; Schmid, O.; Vogel, U.; Williams, A. Ranking of Nanomaterial Potency to Induce Pathway Perturbations Associated with Lung Responses. *NanoImpact* **2019**, *14*, 100158. https://doi.org/10.1016/j.impact.2019.100158.

(108) Solorio-Rodriguez, S. A.; Williams, A.; Poulsen, S. S.; Knudsen, K. B.; Jensen, K. A.; Clausen, P. A.; Danielsen, P. H.; Wallin, H.; Vogel, U.;

Halappanavar, S. Single-Walled vs. Multi-Walled Carbon Nanotubes: Influence of Physico-Chemical Properties on Toxicogenomics Responses in Mouse Lungs. *Nanomaterials* **2023**, *13* (6), 1059. https://doi.org/10.3390/nano13061059.

(109) Gajewicz-Skretna, A.; Kar, S.; Piotrowska, M.; Leszczynski, J. The Kernel-Weighted Local Polynomial Regression (KwLPR) Approach: An Efficient, Novel Tool for Development of QSAR/QSAAR Toxicity Extrapolation Models. *J Cheminform* **2021**, *13* (1), 9. https://doi.org/10.1186/s13321-021-00484-5.

(110) Puzyn, T.; Rasulev, B.; Gajewicz, A.; Hu, X.; Dasari, T. P.; Michalkova, A.; Hwang, H.-M.; Toropov, A.; Leszczynska, D.; Leszczynski, J. Using Nano-QSAR to Predict the Cytotoxicity of Metal Oxide Nanoparticles. *Nat Nanotechnol* **2011**, *6* (3), 175–178. https://doi.org/10.1038/nnano.2011.10.

(111) Dubey, R.; Dutta, D.; Sarkar, A.; Chattopadhyay, P. Functionalized Carbon Nanotubes: Synthesis, Properties and Applications in Water Purification, Drug Delivery, and Material and Biomedical Sciences. *Nanoscale Adv* **2021**, *3* (20), 5722–5744. https://doi.org/10.1039/D1NA00293G.

(112) Gajewicz, A. How to Judge Whether QSAR/Read-across Predictions Can Be Trusted: A Novel Approach for Establishing a Model's Applicability Domain. *Environ Sci Nano* **2018**, *5* (2), 408–421. https://doi.org/10.1039/C7EN00774D.

(113) Bickel, P.; Diggle, P.; Fienberg, S.; Krickeberg, K.; Olkin, I.; Wermuth, N.; Zeger, S. *Springer Series in Statistics*.

(114) Lee, D.-K.; Jeon, S.; Han, Y.; Kim, S.-H.; Lee, S.; Yu, I. J.; Song, K. S.; Kang, A.; Yun, W. S.; Kang, S.-M.; Huh, Y. S.; Cho, W.-S. Threshold Rigidity Values for the Asbestos-like Pathogenicity of High-Aspect-Ratio Carbon Nanotubes in a Mouse Pleural Inflammation Model. *ACS Nano* **2018**, *12* (11), 10867–10879. https://doi.org/10.1021/acsnano.8b03604.

(115) Gupta, S. S.; Singh, K. P.; Gupta, S.; Dusinska, M.; Rahman, Q. Do Carbon Nanotubes and Asbestos Fibers Exhibit Common Toxicity Mechanisms? *Nanomaterials* **2022**, *12* (10), 1708. https://doi.org/10.3390/nano12101708.

(116) Halappanavar, S.; van den Brule, S.; Nymark, P.; Gaté, L.; Seidel, C.; Valentino, S.; Zhernovkov, V.; Høgh Danielsen, P.; De Vizcaya, A.; Wolff, H.; Stöger, T.; Boyadziev, A.; Poulsen, S. S.; Sørli, J. B.; Vogel, U. Adverse Outcome Pathways as a Tool for the Design of Testing Strategies to Support the Safety Assessment of Emerging Advanced Materials at the Nanoscale. *Part Fibre Toxicol* **2020**, *17* (1), 16. https://doi.org/10.1186/s12989-020-00344-4.

(117) Nikota, J.; Banville, A.; Goodwin, L. R.; Wu, D.; Williams, A.; Yauk, C. L.; Wallin, H.; Vogel, U.; Halappanavar, S. Stat-6 Signaling Pathway and Not Interleukin-1 Mediates Multi-Walled Carbon Nanotube-Induced Lung Fibrosis in Mice: Insights from an Adverse Outcome Pathway Framework. *Part Fibre Toxicol* **2017**, *14* (1), 37. https://doi.org/10.1186/s12989-017-0218-0.

(118) Murphy, F.; Dekkers, S.; Braakhuis, H.; Ma-Hock, L.; Johnston, H.; Janer, G.; di Cristo, L.; Sabella, S.; Jacobsen, N. R.; Oomen, A. G.; Haase, A.; Fernandes, T.; Stone, V. An Integrated Approach to Testing and Assessment of High Aspect Ratio Nanomaterials and Its Application for Grouping Based on a Common Mesothelioma Hazard. *NanoImpact* **2021**, *22*, 100314. https://doi.org/10.1016/j.impact.2021.100314.

(119) Sengottiyan, S.; Mikolajczyk, A.; Jagiełło, K.; Swirog, M.; Puzyn, T. Core, Coating, or Corona? The Importance of Considering Protein Coronas in Nano-QSPR Modeling of Zeta Potential. *ACS Nano* **2023**, *17* (3), 1989–1997. https://doi.org/10.1021/acsnano.2c06977.

(120) Saleemi, M. A.; Hosseini Fouladi, M.; Yong, P. V. C.; Chinna, K.; Palanisamy, N. K.; Wong, E. H. Toxicity of Carbon Nanotubes: Molecular Mechanisms,

Signaling Cascades, and Remedies in Biomedical Applications. *Chem Res Toxicol* **2021**, *34* (1), 24–46. https://doi.org/10.1021/acs.chemrestox.0c00172.

(121) Granato, D.; Santos, J. S.; Escher, G. B.; Ferreira, B. L.; Maggio, R. M. Use of Principal Component Analysis (PCA) and Hierarchical Cluster Analysis (HCA) for Multivariate Association between Bioactive Compounds and Functional Properties in Foods: A Critical Perspective. *Trends Food Sci Technol* **2018**, *72*, 83–90. https://doi.org/10.1016/j.tifs.2017.12.006.

(122) Bro, R.; Smilde, A. K. Principal Component Analysis. *Anal. Methods* **2014**, *6* (9), 2812–2831. https://doi.org/10.1039/C3AY41907J.

(123) Shvedova, A. A.; Kisin, E. R.; Mercer, R.; Murray, A. R.; Johnson, V. J.; Potapovich, A. I.; Tyurina, Y. Y.; Gorelik, O.; Arepalli, S.; Schwegler-Berry, D.; Hubbs, A. F.; Antonini, J.; Evans, D. E.; Ku, B.-K.; Ramsey, D.; Maynard, A.; Kagan, V. E.; Castranova, V.; Baron, P. Unusual Inflammatory and Fibrogenic Pulmonary Responses to Single-Walled Carbon Nanotubes in Mice. *American Journal of Physiology-Lung Cellular and Molecular Physiology* **2005**, *289* (5), L698–L708. https://doi.org/10.1152/ajplung.00084.2005.

(124) Donaldson, K.; Murphy, F. A.; Duffin, R.; Poland, C. A. Asbestos, Carbon Nanotubes and the Pleural Mesothelium: A Review and the Hypothesis Regarding the Role of Long Fibre Retention in the Parietal Pleura, Inflammation and Mesothelioma. *Part Fibre Toxicol* **2010**, *7* (1), 5. https://doi.org/10.1186/1743-8977-7-5.

(125) Pacurari, M.; Yin, X. J.; Zhao, J.; Ding, M.; Leonard, S. S.; Schwegler-Berry, D.; Ducatman, B. S.; Sbarra, D.; Hoover, M. D.; Castranova, V.; Vallyathan, V. Raw Single-Wall Carbon Nanotubes Induce Oxidative Stress and Activate MAPKs, AP-1, NF-KB, and Akt in Normal and Malignant Human Mesothelial Cells. *Environ Health Perspect* **2008**, *116* (9), 1211–1217. https://doi.org/10.1289/ehp.10924.

(126) Sharma, M.; Nikota, J.; Halappanavar, S.; Castranova, V.; Rothen-Rutishauser, B.; Clippinger, A. J. Predicting Pulmonary Fibrosis in Humans after Exposure to Multi-Walled Carbon Nanotubes (MWCNTs). *Arch Toxicol* **2016**, *90* (7), 1605–1622. https://doi.org/10.1007/s00204-016-1742-7.

(127) Kasai, T.; Umeda, Y.; Ohnishi, M.; Kondo, H.; Takeuchi, T.; Aiso, S.; Nishizawa, T.; Matsumoto, M.; Fukushima, S. Thirteen-Week Study of Toxicity of Fiber-like Multi-Walled Carbon Nanotubes with Whole-Body Inhalation Exposure in Rats. *Nanotoxicology* **2015**, *9* (4), 413–422. https://doi.org/10.3109/17435390.2014.933903.

(128) Poulsen, S. S.; Knudsen, K. B.; Jackson, P.; Weydahl, I. E. K.; Saber, A. T.; Wallin, H.; Vogel, U. Multi-Walled Carbon Nanotube-Physicochemical Properties Predict the Systemic Acute Phase Response Following Pulmonary Exposure in Mice. *PLoS One* **2017**, *12* (4), e0174167. https://doi.org/10.1371/journal.pone.0174167.

(129) Gandhi, D.; Rudrashetti, A. P.; Rajasekaran, S. The Impact of Environmental and Occupational Exposures of Manganese on Pulmonary, Hepatic, and Renal Functions. *Journal of Applied Toxicology* **2022**, *42* (1), 103–129. https://doi.org/10.1002/jat.4214.

(130) Hadrup, N.; Zhernovkov, V.; Jacobsen, N. R.; Voss, C.; Strunz, M.; Ansari, M.; Schiller, H. B.; Halappanavar, S.; Poulsen, S. S.; Kholodenko, B.; Stoeger, T.; Saber, A. T.; Vogel, U. Acute Phase Response as a Biological Mechanism-of-Action of (Nano)Particle-Induced Cardiovascular Disease. *Small* **2020**, *16* (21). https://doi.org/10.1002/smll.201907476.

(131) Nagai, H.; Okazaki, Y.; Chew, S. H.; Misawa, N.; Yamashita, Y.; Akatsuka, S.; Ishihara, T.; Yamashita, K.; Yoshikawa, Y.; Yasui, H.; Jiang, L.; Ohara, H.; Takahashi, T.; Ichihara, G.; Kostarelos, K.; Miyata, Y.; Shinohara, H.; Toyokuni, S. Diameter and Rigidity of Multiwalled Carbon Nanotubes Are Critical Factors in Mesothelial Injury and Carcinogenesis. *Proceedings of the*

National Academy of Sciences **2011**, *108* (49). https://doi.org/10.1073/pnas.1110013108.

(132) Fraser, K.; Hubbs, A.; Yanamala, N.; Mercer, R. R.; Stueckle, T. A.; Jensen, J.; Eye, T.; Battelli, L.; Clingerman, S.; Fluharty, K.; Dodd, T.; Casuccio, G.; Bunker, K.; Lersch, T. L.; Kashon, M. L.; Orandle, M.; Dahm, M.; Schubauer-Berigan, M. K.; Kodali, V.; Erdely, A. Histopathology of the Broad Class of Carbon Nanotubes and Nanofibers Used or Produced in U.S. Facilities in a Murine Model. *Part Fibre Toxicol* **2021**, *18* (1), 47. https://doi.org/10.1186/s12989-021-00440-z.

(133) Murphy, F.; Dekkers, S.; Braakhuis, H.; Ma-Hock, L.; Johnston, H.; Janer, G.; di Cristo, L.; Sabella, S.; Jacobsen, N. R.; Oomen, A. G.; Haase, A.; Fernandes, T.; Stone, V. An Integrated Approach to Testing and Assessment of High Aspect Ratio Nanomaterials and Its Application for Grouping Based on a Common Mesothelioma Hazard. *NanoImpact* **2021**, *22*, 100314. https://doi.org/10.1016/j.impact.2021.100314.

(134) Murphy, F.; Jacobsen, N. R.; Di Ianni, E.; Johnston, H.; Braakhuis, H.; Peijnenburg, W.; Oomen, A.; Fernandes, T.; Stone, V. Grouping MWCNTs Based on Their Similar Potential to Cause Pulmonary Hazard after Inhalation: A Case-Study. *Part Fibre Toxicol* **2022**, *19* (1), 50. https://doi.org/10.1186/s12989-022-00487-6.

(135) Poulsen, S. S.; Saber, A. T.; Williams, A.; Andersen, O.; Køobler, C.; Atluri, R.; Pozzebon, M. E.; Mucelli, S. P.; Simion, M.; Rickerby, D.; Mortensen, A.; Jackson, P.; Kyjovska, Z. O.; Mølhave, K.; Jacobsen, N. R.; Jensen, K. A.; Yauk, C. L.; Wallin, H.; Halappanavar, S.; Vogel, U. MWCNTs of Different Physicochemical Properties Cause Similar Inflammatory Responses, but Differences in Transcriptional and Histological Markers of Fibrosis in Mouse Lungs. *Toxicol Appl Pharmacol* **2015**, *284* (1), 16–32. https://doi.org/10.1016/j.taap.2014.12.011.

(136) Egwim, C. N.; Alaka, H.; Toriola-Coker, L. O.; Balogun, H.; Sunmola, F. Applied Artificial Intelligence for Predicting Construction Projects Delay. *Machine Learning with Applications* **2021**, *6*, 100166. https://doi.org/10.1016/j.mlwa.2021.100166.

(137) Jaworska, J.; Nikolova-Jeliazkova, N.; Aldenberg, T. QSAR Applicability Domain Estimation by Projection of the Training Set in Descriptor Space: A Review. *Alternatives to Laboratory Animals* **2005**, *33* (5), 445–459. https://doi.org/10.1177/026119290503300508.

(138) Merugu, S.; Jagiello, K.; Gajewicz-Skretna, A.; Halappanavar, S.; Willliams, A.; Vogel, U.; Puzyn, T. The Impact of Carbon Nanotube Properties on Lung Pathologies and Atherosclerosis Through Acute Inflammation: A New AOP-Anchored *in Silico* NAM. *Small* **2025**, *21* (14). https://doi.org/10.1002/smll.202501185.

(139) Muratov, V.; Jagiello, K.; Mikolajczyk, A.; Danielsen, P. H.; Halappanavar, S.; Vogel, U.; Puzyn, T. The Role of Machine Learning in Predicting Titanium Dioxide Nanoparticles Induced Pulmonary Pathology Using Transcriptomic Biomarkers. *J Hazard Mater* **2025**, *493*, 138240. https://doi.org/10.1016/j.jhazmat.2025.138240.

(140) Dong, J.; Porter, D. W.; Batteli, L. A.; Wolfarth, M. G.; Richardson, D. L.; Ma, Q. Pathologic and Molecular Profiling of Rapid-Onset Fibrosis and Inflammation Induced by Multi-Walled Carbon Nanotubes. *Arch Toxicol* **2015**, *89* (4), 621–633. https://doi.org/10.1007/s00204-014-1428-y.

(141) Nikota, J.; Banville, A.; Goodwin, L. R.; Wu, D.; Williams, A.; Yauk, C. L.; Wallin, H.; Vogel, U.; Halappanavar, S. Stat-6 Signaling Pathway and Not Interleukin-1 Mediates Multi-Walled Carbon Nanotube-Induced Lung Fibrosis in Mice: Insights from an Adverse Outcome Pathway Framework. *Part Fibre Toxicol* **2017**, *14* (1), 37. https://doi.org/10.1186/s12989-017-0218-0.

(142) Kinaret, P.; Marwah, V.; Fortino, V.; Ilves, M.; Wolff, H.; Ruokolainen, L.; Auvinen, P.; Savolainen, K.; Alenius, H.; Greco, D. Network Analysis Reveals Similar Transcriptomic Responses to Intrinsic Properties of Carbon Nanomaterials *in Vitro* and *in Vivo*. *ACS Nano* **2017**, *11* (4), 3786–3796. https://doi.org/10.1021/acsnano.6b08650.

(143) Öner, D.; Moisse, M.; Ghosh, M.; Duca, R. C.; Poels, K.; Luyts, K.; Putzeys, E.; Cokic, S. M.; Van Landuyt, K.; Vanoirbeek, J.; Lambrechts, D.; Godderis, L.; Hoet, P. H. M. Epigenetic Effects of Carbon Nanotubes in Human Monocytic Cells. *Mutagenesis* **2017**, *32* (1), 181–191. https://doi.org/10.1093/mutage/gew053.

(144) Scala, G.; Kinaret, P.; Marwah, V.; Sund, J.; Fortino, V.; Greco, D. Multi-Omics Analysis of Ten Carbon Nanomaterials Effects Highlights Cell Type Specific Patterns of Molecular Regulation and Adaptation. *NanoImpact* **2018**, *11*, 99–108. https://doi.org/10.1016/j.impact.2018.05.003.

(145) Saarimäki, L. A.; Kinaret, P. A. S.; Scala, G.; del Giudice, G.; Federico, A.; Serra, A.; Greco, D. Toxicogenomics Analysis of Dynamic Dose-Response in Macrophages Highlights Molecular Alterations Relevant for Multi-Walled Carbon Nanotube-Induced Lung Fibrosis. *NanoImpact* **2020**, *20*, 100274. https://doi.org/10.1016/j.impact.2020.100274.

(146) Labib, S.; Williams, A.; Yauk, C. L.; Nikota, J. K.; Wallin, H.; Vogel, U.; Halappanavar, S. Nano-Risk Science: Application of Toxicogenomics in an Adverse Outcome Pathway Framework for Risk Assessment of Multi-Walled Carbon Nanotubes. *Part Fibre Toxicol* **2015**, *13* (1), 15. https://doi.org/10.1186/s12989-016-0125-9.

7. SUPPLEMENT

LIST OF SCIENTIFIC ACHIEVEMENTS

Research papers published during the course of the PhD dissertation

2025 **Sattibabu Merugu**, Karolina Jagiello, Agnieszka Gajewicz-Skretna, Sabina Halappanavar, Andrew Willliams, Ulla Vogel, and Tomasz Puzyn: The Impact of Carbon Nanotube Properties on Lung Pathologies and Atherosclerosis Through Acute Inflammation: a New AOP-Anchored in Silico NAM. *Small* ***2025***, 2501185.https://doi.org/10.1002/small.202501185

Total impact factor = 13.2

Total MNiSW points = 200

Other research publications

2019 M. Elizabeth Sobhia, Keta Ghosh, Ajeet Singh, Komal Sul, Monica Singh, Ravi Kumar, Sandeep, **Sattibabu Merugu***, and Sunil Chand Donempudi. "A Multi-Perspective Review on Dengue Research: *Curr. Drug Targets*. ***2019***, 1550-1562. https://doi:10.2174/1389450120666190724145937

2016 Lagu Surendra Babu, **M. Sattibabu***, Ch. Suresh, K. Phani Kumar: Evaluation of Anti-Convulsant Activity of Aqueous Extract of Argyria Nervosa against Induced by Mes and Ptz Methods in Mice. *IOSR-JPBS*. ***2016***, *Volume 11*. https://doi: 10.9790/3008-1113455020192016

Oral presentations

2025 **Tomasz Puzyn,** Michal Kalapus, Ewelina Wyrzykowska, Maciej Stepnik, **Sattibabu Merugu*,** Karolina Jagiello, "In AI we trust? Towards the increasing acceptance of AI-based QSAR models in the risk assessment of nanomaterials", SOT 64th Annual Meeting & ToxExpo in Orlando, Florida, 16-23.03.2025

2024 **Sattibabu Merugu**, Karolina Jagiello, Agnieszka Gajewicz-Skretna, Sabina Halappanavar, Andrew Williams, Ulla Vogel, and Tomasz Puzyn, "An AOP-informed Nano-QSAR Model to understand the impact of carbon nanotubes

structural properties on lung inflammation: The Step Towards in silico-based NAMs to be Applied in SbD", OpenTox Summer School 2024, 26-30.08.2024 (online)

Poster presentations

2025 **K. Jagiello**, S. Halappanavar, U. Vogel, A. Williams, **S. Merugu*,** and T. Puzyn, "Transcriptomic-based and AOP-guided QSAR Models as in silico New Approach Methods for Predicting Lung and Cardiovascular Toxicity of Nanomaterials", SOT 64th Annual Meeting & ToxExpo in Orlando, Florida from 16-23.03.2025

2024 **Sattibabu Merugu**, Karolina Jagiello, Agnieszka Gajewicz-Skretna, Sabina Halappanavar, Andrew Willliams, Ulla Vogel, and Tomasz Puzyn, "An AOP-Informed Nano-QSAR Model to Understand the Impact of Carbon Nanotubes Structural Properties on Lung Inflammation: The Step Towards in Silico-based NAM to be Applied in SSbD", 10th S3C Summer School on Sustainable Chemistry Development by Leuphana University, Luneburg, Germany, 08-12.07.2024

2024 **Sattibabu Merugu**, Karolina Jagiello, Agnieszka Gajewicz-Skretna, Sabina Halappanavar, Andrew Williams, Ulla Vogel, and Tomasz Puzyn, "Nanosafety Assessment through AOP-Anchored Consensus Nano-QSAR Model: Insights into MWCNT-Induced Lung Toxicity", NanoTox2024, Venice, Italy, 23-25.09.2024

2022 **Sattibabu Merugu**, Karolina Jagiello and Tomasz Puzyn, "Can Interactions Between Carbon Nanotubes and Proteins Act as an MIE to AOP 173?", the 9th edition of Modelling & Design of Molecular materials (MDMM2022), Gdansk, Poland, 19-25.09.2022

*highlighted the contribution of the presented presentations